

# UC San Diego

## UC San Diego Electronic Theses and Dissertations

### Title

Unraveling the Personalized Nature of Olfaction

### Permalink

<https://escholarship.org/uc/item/8fh923ph>

### Author

Koblesky, Norah Kathryn

### Publication Date

2021

Peer reviewed|Thesis/dissertation

UNIVERSITY OF CALIFORNIA SAN DIEGO

Unraveling the Personalized Nature of Olfaction

A dissertation submitted in partial satisfaction of the  
requirements for the Degree Doctor of Philosophy

in

Neurosciences

by

Norah K. Koblesky

Committee in charge:

Professor Lisa Stowers, Chair  
Professor Nick Spitzer, Co-Chair  
Professor Ron Evans  
Professor Jing Wang  
Professor Kun Zhang

2021

Copyright

Norah K. Koblesky, 2021

All Rights Reserved

The dissertation of Norah K. Koblesky is approved, and it is acceptable in quality and form for publication on microfilm and electronically.

University of California San Diego

2021



## **DEDICATION**

To all of the people who feel the chaotic pull of abnormal internal states –  
may we learn from you and help future generations flourish.

## TABLE OF CONTENTS

DISSERTATION APPROVAL PAGE.....	iii
DEDICATION .....	iv
TABLE OF CONTENTS .....	v
LIST OF FIGURES AND TABLES .....	vii
LIST OF ABBREVIATIONS.....	x
ACKNOWLEDGEMENTS .....	xi
VITA .....	xii
ABSTRACT OF THE DISSERTATION .....	xiv
CHAPTER 1 – Heterogeneity in the Signal Transduction Cascade of the VNO .....	1
INTRODUCTION.....	1
RESULTS .....	10
1.1        PLC $\beta$ 2 is not the sole signal transducer in the VNO.....	11
1.2        VSNs express many PLC subtypes .....	15
1.3        PLC subtypes are potential signal transducers .....	16
1.4        PLC subtypes are not functionally redundant .....	20
1.5        Multiple signal transduction cascades exist in the VNO.....	22
1.6        The VNO signals through multiple distinct transduction cascades.....	27
1.7        PLC subtypes may not explain remaining VSN activity.....	30
1.8        The VNO expresses hormone recognition machinery.....	34
1.9        Intra-stimuli VSN activity varies between animals.....	35
DISCUSSION .....	37
MATERIALS AND METHODS.....	47
CHAPTER 2 - Sources of Variation in Innate Olfactory Valence Tests.....	75
INTRODUCTION.....	75
RESULTS .....	78
2.1        Olfactory valence sign and strength varies with test and apparatus.....	78
2.2        Olfactory valence temporal dynamics varies with test and apparatus.....	83
2.3        Other mouse tracking parameters do not explain mouse valence variability.....	86

2.4 Spatial bias relationship with odor preference varies between assays .....88

2.5 Raw investigation time does not reflect inter-odor differences or preference  
conclusions .....92

DISCUSSION .....96

MATERIALS AND METHODS .....100

## LIST OF FIGURES AND TABLES

Figure 1.1. GPCR-driven sensory modalities follow a similar, receptor-driven logic.....	1
Figure 1.2. Anatomy of the vomeronasal organ.....	3
Figure 1.3. The <i>EGR1</i> immediate early gene functions as a clean and reliable measure of activity in the VNO and can be assayed using small-molecule FISH.....	4
Figure 1.4. The inherent spatial organization of the vomeronasal organ.....	6
Figure 1.5. The hypothesize signal transduction cascade of the mouse peripheral vomeronasal system.....	7
Figure 1.6. Phospholipase C is a diverse family of signal transducers.....	9
Figure 1.7. Generating cell masks for depicting smFISH data.....	12
Figure 1.8. Most VSNs do not express <i>PLCβ2</i> .....	12
Figure 1.9. Most VSNs do not use a <i>PLCβ2</i> -dependent signal transduction cascade.....	13
Figure 1.10. VSNs express many <i>PLC</i> subtypes.....	15
Figure 1.11. VSNs don't express every <i>PLC</i> subtype.....	15
Figure 1.12. VSNs express no dominant signal transducer.....	16
Figure 1.13. The VNO's <i>PLC</i> expression is consistent across sex and state.....	17
Figure 1.14. Signal transducer heterogeneity is largely absent in non-pheromonal chemical senses.....	17
Figure 1.15. <i>PLCs</i> show little overlap in scRNAseq VSN data.....	19
Figure 1.16. <i>PLCs</i> show little overlap in multiplexed FISH VSN data.....	19
Figure 1.17. <i>PLCs</i> fall into distinct abundance classes .....	21
Figure 1.18. <i>PLCs</i> exhibit spatial, cell-type-specific patterning.....	22
Figure 1.19. Stimuli have unique <i>PLC</i> subtype co-expression patterns.....	24
Figure 1.20. <i>PLCβ3</i> mutation reduces VNO activity.....	26

Figure 1.21. PLC $\beta$ 3 phenotype is not due to technical, developmental, or population ratio concerns.....	26
Figure 1.22. PLC $\beta$ 3 is not the main vomeronasal signal transducer.....	27
Figure 1.23. PLC $\beta$ 4 mutation reduces VNO activity.....	29
Figure 1.24. PLC $\beta$ 4 phenotype is not due to technical or population ratio concerns.....	29
Figure 1.25. PLC $\epsilon$ 1 mutation does not affect S.A.E. Mix-mediated VNO activity.....	31
Figure 1.26. PLC $\epsilon$ 1 phenotype is not due to technical, developmental, population ratio, or overlap concerns.....	31
Figure 1.27. Removal of the PLC $\gamma$ 1 catalytic domain does not affect ferret bedding-mediated VNO activity.....	33
Figure 1.28. PLC $\gamma$ 1 phenotype is not due to technical, developmental, or population ratio concerns.....	33
Figure 1.29. The VNO expresses multiple types of hormone receptors.....	35
Figure 1.30. VSN activity varies between individuals.....	36
Figure 1.31. Probe dilution can be done to remove noise yet retain signal.....	51
Figure 1.32. PLC Probe controls.....	52
Figure 1.33. Morphology can be used to identify VSNs.....	54
Figure 1.34. Most data captured within 1 $\mu$ M from cell nucleus.....	54
Figure 1.35. Diameters of vomeronasal sensory neurons in IMARIS.....	55
Figure 1.36. Controls for VSN-specific PLC PCR.....	57
Figure 2.1. Tests used for innate olfactory valence comparison.....	79
Table 2.1. Odorant used in innate olfactory valence comparison .....	80
Figure 2.2. Innate olfactory valence results and conclusions change across apparatuses. ....	82
Figure 2.3. Innate olfactory valence temporal dynamics changes across apparatuses.....	85
Figure 2.4. Behavioral variability in olfactory valence unexplained by tracking-derived parameters.....	87

Figure 2.5. Relationship between spatial bias and odor valence varies between  
assays.....91

Figure 2.6. Raw time does not reflect behavioral differences of innate olfactory valence assays  
.....95

## LIST OF ABBREVIATIONS

2-MB – 2-Methylbuturic Acid

2-PE – 2-Phenylethanol

ADCY – Adenylyl Cyclase

DAG – Diacylglycerol

FISH – Fluorescent *In Situ* Hybridization

GNAI2 – Guanine Nucleotide-Binding Protein G(I) Subunit Alpha-2

GNAO1 – Guanine Nucleotide-Binding Protein G(o) Subunit Alpha

GPCR – G-protein Coupled-Receptor

IEG – Immediate-Early Gene

IP<sub>3</sub> – Inositol 1,4,5-Trisphosphate

ISO – Isopentylamine

MOE – Main Olfactory Epithelium

OMP – Olfactory Marker Protein

PIP<sub>2</sub> – Phosphatidylinositol 4,5-Bisphosphate

PLC – Phospholipase C

PROBES – Poking-Registered Olfactory Behavior Evaluation System

RTK – Receptor Tyrosine Kinase

scRNAseq – single cell RNA sequencing

TMT – 2,5-dihydro-2,4,5-Trimethylthiazoline

TRPC2 – Transient Receptor Potential Cation Channel, Subfamily C, Member 2

VNO – Vomeronasal Organ

VR – Vomeronasal Receptor

VSNs – Vomeronasal Sensory Neurons

## ACKNOWLEDGEMENTS

First of all, thank you to Lisa Stowers, my mentor and PhD advisor. You taught me to think big with my scientific questions, to convey my science effectively, and to stay excited and curious no matter my experimental results. Thank you to everyone in the Stowers Lab; you have been like a family for the past six years – I could not have done it without your support.

Particularly, I would like to thank: Jingyi Chen and Sourish Mukhopadhyay, who talked me through many a bad science day; Holli Keaton, for being a great lab administrator; Jason Keller, for teaching me how to navigate the lab; and Kushagra Patel, who took up the enormous IMARIS quantification burden and so kept me sane. I would also like to thank past lab members Tomohiro Tanaka and Sandeepa Dey – without your excellent research Chapter 1 of this thesis would not be possible.

I would like to thank everyone in Dorris Neuroscience Center for creating such a great community for research. From scientific advice to friendly chats to letting me borrow many a reagent, the contribution of DNC was invaluable. Thanks particularly to Denyse Huff for helping me manage a dozen mouse lines at once, and to Kathy Spencer for being helpful in everything and keeping the 40x objective oil-free. And finally, thank you to the many mice who inspired and drove this research.

I would also like to thank my generous thesis committee, for your support throughout my thesis project's many twists and turns. In particular, I would like to thank Dr. Ron Evans, for being my biggest advocate and reminding me to balance curiosity with practicality. I would also like to thank the many scientists that contributed datasets, mouse lines, or advice, including: Dr. Alan Smrcka, Dr. Florian Heidel, Dr. Hiro Matsunami, Dr. Ivan Rodriguez, Dr. Frank Zufall, Dr. Ben Cravatt, Dr. Ron Yu, Dr. Qiang Qiu, and Dr. Cory Root.



Thank you to the wonderful UCSD Neuroscience Graduate Program for providing me with a top-notch education and an opportunity to shine. I'd especially like to thank my wonderful cohort, which is full of the brightest, kindest, and coolest people I've ever met – I couldn't have asked for a better group of people to share this journey with.

Finally, thank you to my amazing family and friends, who all make me a better scientist. Thank you to my science sister Sierra for our many late nights in lab, full of deep science discussions and vending machine snacks. Thank you to my partner Marich, for your endless interest, humor, and patience throughout the long trek to a PhD. Thank you to my brother Theo, for inspiring me to become the second Dr. Koblesky – you are the smartest scientist I know. And thank you to my magical mother Laurie, who taught me so much about strength, courage, and shooting for the stars.

Chapter 1, in part, is a reprint of material that is currently being prepared for publication. Koblesky, Norah; Patel, Kushagra; Fodoulian, Léon; Rodriguez, Ivan, Stowers, Lisa. “The Vomeronasal System Signals through Multiple Stimuli-Specific Signal Transduction Cascades”. The dissertation author was the primary investigator and author of this paper.

Chapter 1, in part, contains unpublished material. Koblesky, Norah; Smrcka, Alan; Heidel, Florian; Matsunami, Hiroaki; Chien, Mingshan; Stowers, Lisa. Chapter 1. “The Vomeronasal System Signals through Multiple Stimuli-Specific Signal Transduction Cascades”. The dissertation author was the primary investigator and author of this paper.

Chapter 2, in part, is a reprint of material that is currently being prepared for publication. Koblesky, Norah; Taylor, Sandy; Gutierrez, Zachary; Stowers, Lisa. “Sources of Variation in Innate Olfactory Valence Tests”. The dissertation author was the primary investigator and author of this paper.

## VITA

- 2010 – 2014 Bachelor of Science, Biology, University of Iowa
- 2010 – 2014 Bachelor of Arts, Psychology, University of Iowa
- 2014 – 2021 Doctor of Philosophy, Neurosciences, University of California San Diego

## PUBLICATIONS

**Koblesky, NK**, Stowers, L. (2019). Animal Behavior: Honesty Can Kill. *Current biology : CB*, 29(7), R259–R261.

Anderson RM, Birnie AK, **Koblesky NK**, Romig-Martin SA, Radley JJ. (2014). Adrenocortical status predicts the degree of age-related deficits in prefrontal structural plasticity and working memory. *J Neurosci.*, 34(25), 8387-97.

Molumby MJ, Anderson RM, Newbold DJ, **Koblesky NK**, Garrett AM, Schreiner D, Radley JJ, Weiner JA. (2017).  $\gamma$ -Protocadherins Interact with Neuroligin-1 and Negatively Regulate Dendritic Spine Morphogenesis. *Cell Rep.*, 18(11), 2702-2714.

## ABSTRACTS

**Koblesky NK**, Fodouliau, L, Rodriguez I, Stowers L. (2019). Signal Transducer Heterogeneity of the Peripheral Pheromone System. *Association of Chemical Sciences (ACChemS) Conference*, Bonita Springs, FL.

**Koblesky NK**, Fodouliau, L, Rodriguez I, Stowers L. (2019). Signal Transducer Heterogeneity of the Peripheral Pheromone System. *Keystone Symposium - Mammalian Sensory Systems*, Seattle, WA.

**ABSTRACT OF THE DISSERTATION**

Unraveling the Personalized Nature of Olfaction

by

Norah K. Koblesky

Doctor of Philosophy in Neurosciences

University of California San Diego, 2021

Professor Lisa Stowers, Chair

Professor Nick Spitzer, Co-Chair

One's perception of the world is personal. Different people can experience the same sensory stimulus in myriad ways, and the same person can experience the same sensory stimulus differently across time. What factors cause sensory experiences to differ? While daunting, identifying the sources of individualized perception is essential to understanding how the brain functions – to truly understand a circuit, one must understand how inputs are processed. Olfaction, which is essential for many complex mouse behaviors and influenced by both experience and state, is a prime candidate for the study of such variation. While olfactory variation is known to exist, the biological, historical, or technical factors it stems from are not. Here, we find two sources of olfactory variation, one biological and one technical. In the first chapter, we find that pheromone-evoked activity is mediated not by one signal transduction cascade but several. None of the discovered signal transduction cascades are dominant, indicating that signaling heterogeneity is an integral feature in the vomeronasal system. These signal transduction cascades are stimulus-specific, hinting at a substantial utility. The discovery of multiple signaling pathways in the vomeronasal system identifies a new source for biological variation in olfaction. In the second chapter of this thesis, we find that the assay and apparatus used for innate olfactory valence tests affect results' strengths, timing, and conclusions, indicating that current unstandardized assays introduce substantial technical variation to data. We also show that raw data from these assays are unimpressive, often requiring transformation to become significant. Analysis of tests' raw data reveals that mice are initially attracted to all stimuli and aversive reactions take minutes to manifest – these data suggest that the currently-used position-as-reaction measure is flawed and needs to be replaced. Uncovering these sources of biological and technical variation poises the neuroscience community to understand how animals make sense of the world around them.

# CHAPTER 1 – Heterogeneity in the Signal Transduction Cascade of the VNO

## INTRODUCTION

Guanine nucleotide-binding protein (G-protein)-based sensory systems may detect disparate stimuli, but they use a similar signaling framework. Sensory cells across various modalities detect stimuli using many G-protein-coupled receptors (GPCRs) and amplify signals through one primary signal transduction cascade<sup>1</sup> (Figure 1.1). Knockout studies have verified that sensory cells within one GPCR-driven modality use predominately through one signal transducer<sup>2-7</sup>. While reports of specialized neuron types using unique molecular pathways exist<sup>3,8-10</sup>, these cells make up a fraction of the total sensory neuron pool, indicating that this is the exception and not the rule. The consistency of this sensory signaling model's use suggests a major benefit. Presumably this model allows for receptors to capture disparate information from the environment and perform the same transformation on the incoming signal, thus allowing it to be easily interpretable when it reaches the brain.

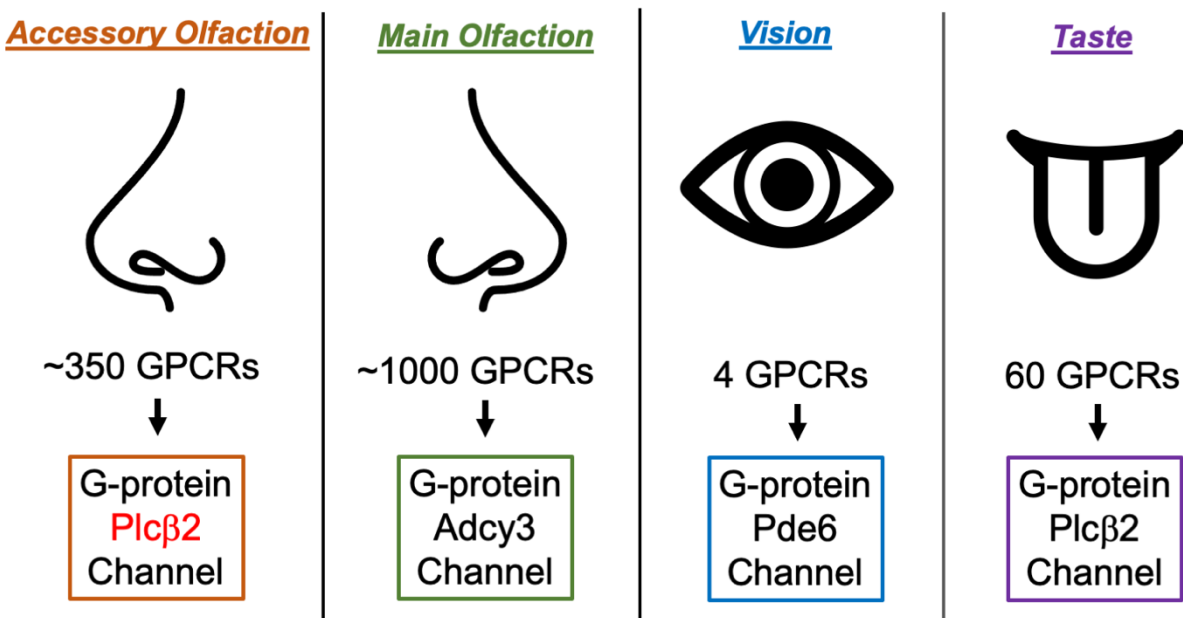


**Figure 1.1. GPCR-driven sensory modalities follow a similar, receptor-driven logic.** The hypothesized sensory logic for accessory olfaction<sup>11-13</sup>, main olfaction<sup>2,3</sup>, vision<sup>4-6</sup> and bitter/umami/sweet taste<sup>7</sup>. All listed modalities function similarly, with many GPCRs on sensory cells responding to external sensory cues and funneling resulting activity into one primary signal transduction cascade. Note that, unlike other modalities, the pheromone system's signal transducer has not been confirmed via knockout experiments.

The mouse olfactory systems, which include the main olfactory system (MOE) and the vomeronasal system (VNO)<sup>1</sup>, have long been thought to signal within the same framework. Rodents rely heavily on olfaction to sense and respond to the many volatile and involatile compounds in the environment, making them an ideal model organism for study of this sense<sup>14</sup>. The MOE allows mice to sense volatile odorants and navigate towards or away from important odor sources such as food<sup>15,16</sup>. In contrast, the VNO allows mice to sense pheromones (conspecific signals) and kairomones (predator signals) and respond with innate and stereotyped behaviors<sup>17,18</sup>. While there is functional overlap between the two subsystems<sup>19</sup>, the VNO uniquely senses involatile compounds<sup>17,20</sup> and is particularly important for social behaviors<sup>14</sup>. The two olfactory subsystems also send axonal projections to largely different downstream brain locations<sup>21</sup>; the MOE sends projections to the main olfactory bulb (MOB) and forebrain cortical regions, while the VNO sends projections to the accessory olfactory bulb (AOB) and midbrain regions. Despite the VNO's importance in animal behavior, it is less-well studied than its MOE counterpart.

The architecture of the peripheral vomeronasal organ, however, is well-characterized. The pair of cylindrical organs sit underneath the soft palette, running parallel with the jaw, and form mucus-filled tubes that contain the vomeronasal sensory neurons (VSNs)<sup>22-23</sup>. The sensory epithelium forms a crescent shape, with immature cells (iVSNs) at its points, mature OMP-expressing cells (mVSNs) in its center, and supporting sustentacular cells at its base (SCs)<sup>24</sup> (Figure 1.2). Across the lumen is highly innervated and vascularized cavernous tissue that is key to stimulus uptake - vascular constriction causes lumen "pumping", leading to movement of contacted nonvolatile stimuli through the vomeronasal duct and into the lumen<sup>25-27</sup>. From here, mVSN dendrites that are projected into the lumen can interact with incoming pheromones and

kairomones<sup>23</sup>. Activity will travel up the axons of the mVSNs, which project out the top of the VNO “crescent” into nerve bundles that cross the cribriform plate and synapse onto the AOB.

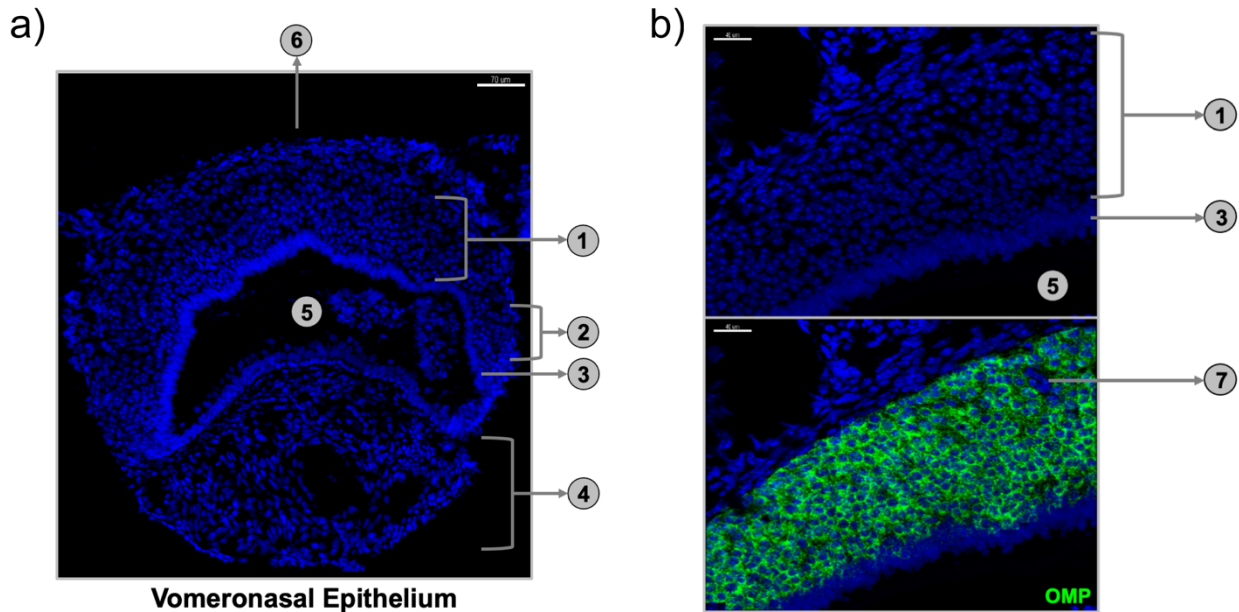


**Figure 1.2. Anatomy of the vomeronasal organ.**

The VNO contains a pair of cylindrical organs running parallel to the soft palette. **a**, 20x image of a coronal slice of the VNO, stained with DAPI and rotated 90 degrees for clarity. The vomeronasal epithelium is comprised of three cell types: mature VSNs (1), immature VSNs (2), and supporting sustentacular cells (3). Sensory stimuli enter the vomeronasal organ via pumping action of the cavernous tissue (4), which sucks stimuli into the mucus-filled lumen (5). Stimuli then interact with mature VSN dendrites that project into the lumen (not shown), causing the VSNs to fire. Sensory signals travel along VSN axon bundles that exit out the lateral edge of the VNO (6, axons not shown). **b**, 40x images of the sensory epithelium stained for DAPI (top), or DAPI and *OMP* (bottom). Images are rotated 90 degrees for clarity. Olfactory marker protein (*OMP*) labels mature VSNs and not the lamina propria (7).

Far less is known about pheromone detection itself. Each cell is able to detect multiple stimuli through G-protein-coupled vomeronasal receptors (VRs) on its dendritic surface<sup>28-30</sup>. As with its MOE counterpart<sup>31</sup>, sensory neurons in the VNO are thought to express only one of ~350 possible receptors<sup>28-29,32</sup>, with a few notable exceptions<sup>33</sup>. VRs allow cells to detect pheromones in mouse excretions such as urine and tears, and kairomones from predator droppings such as cat fur and snake skin<sup>18,23</sup>. Though several receptors have been successfully deorphanized<sup>18,33-36,134</sup>, efforts to pair ligands with receptors have been stymied by difficulties in expressing VRs in heterologous cell culture<sup>37</sup> and lack of high-throughput tools. This roadblock has resulted in a severe limit in the knowledge of VNO stimulus space. Indeed, less than 40% of VSNs can be

activated even when combining dozens of stimuli<sup>18</sup>. Currently, labs use in vitro tools such as calcium imaging<sup>34</sup> and ex-vivo tools such as immediate-early gene (IEG) staining with the VSN-specific *EGR1* to assess activity<sup>18</sup> (Figure 1.3); while the latter has unveiled several ligand-receptor pairs, efforts remain slow. Several labs have recently begun to develop technologies to assay VSN activity in vivo and on large scales<sup>38,39</sup>, which will greatly augment deorphanization efforts. A small population of VSNs express formyl-peptide receptors (FPRs) instead of VRs<sup>40-41</sup>, which have also not been deorphanized, though many hypothesize that they function to sense bacterial metabolites in animal excretions<sup>40-45</sup>.

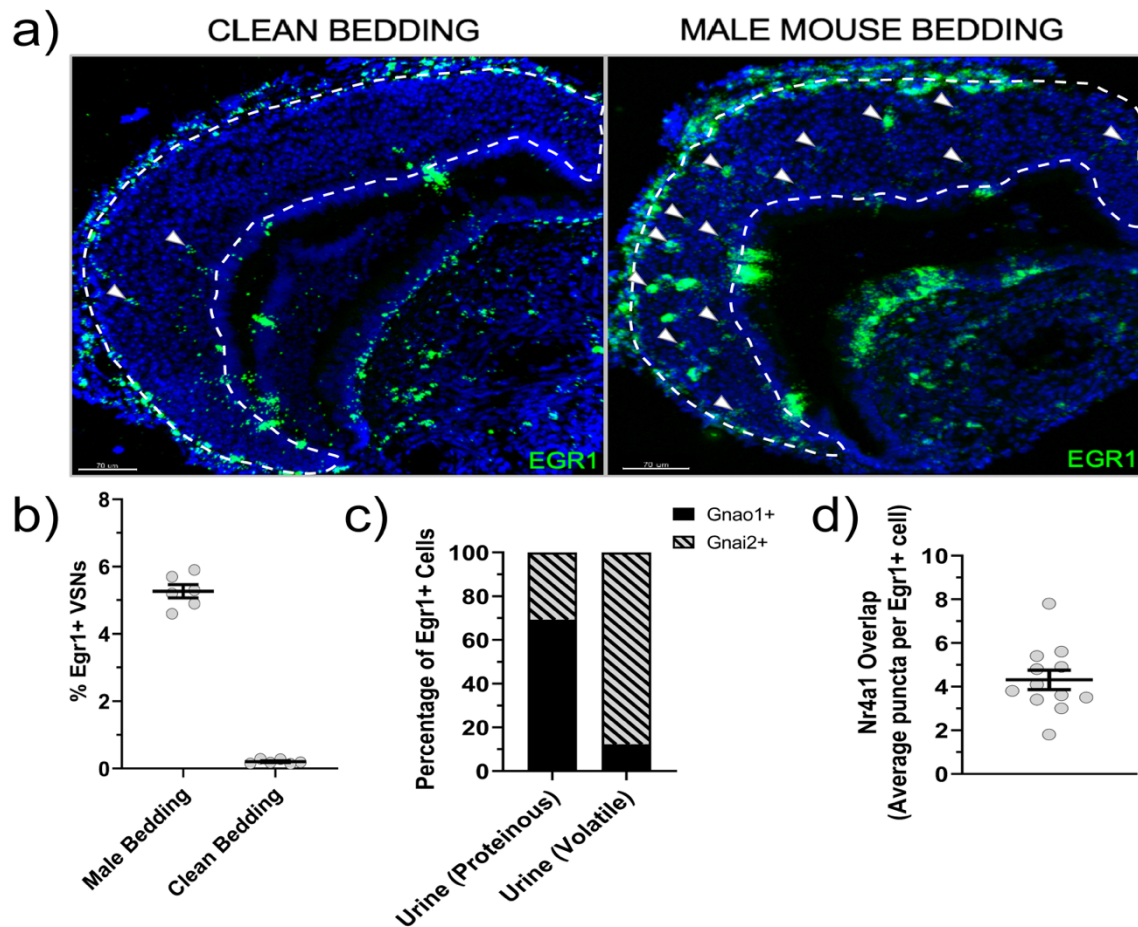


**Figure 1.3. The *EGR1* immediate early gene functions as a clean and reliable measure of activity in the VNO and can be assayed using small-molecule FISH.**

**a**, The VNOs of mice exposed to clean bedding (left) or male urine-soaked bedding (right). Staining for *EGR1* yields few *EGR1*+ cells in mice exposed to pheromone-devoid clean bedding and many *EGR1*+ cells in mice exposed to pheromone-rich male bedding. Arrows indicate *EGR1*+ cells. **b**, Quantification of **A**, n=6 ROIs across 2 animals per group. **c**, Overlap of *EGR1*+ cells with basal and apical markers across representative basal stimuli (HMW) and apical stimuli (LMW)<sup>137</sup>, n=8 ROIs per group. **d**, Overlap of the IEG *NR4A1* staining with *EGR1*+ cells, n=12 ROIs.



One compelling aspect of the vomeronasal organ is that it exhibits inherent spatial organization in its cell types<sup>46</sup>. The VNO is split into two rough halves (though this split is not linear, see Figure 1.4), an upper “basal” VNO and a lower “apical” VNO, which hold genetically different cell types. The basal versus apical cell classes use different signaling machinery, with each type of cell expressing unique receptors (V2R<sup>29</sup> versus V1R<sup>28</sup>, respectively) and G-protein subunits (Gn $\alpha$ o1 and G $\gamma$ 8 versus Gn $\alpha$ i2 and G $\gamma$ 2/3/8/13, respectively<sup>47,48</sup>), suggesting that these two cell classes form distinct classes. VSNs are regenerated throughout life<sup>49</sup>, and complex molecular programs have been found to maintain the basal-apical split in each new “round” of cells<sup>50</sup>. These cell populations remain distinct in the AOB<sup>51</sup>, further suggesting that this split is functionally relevant. Indeed, KO of Gn $\alpha$ o1<sup>43</sup> or G $\gamma$ 8<sup>52</sup> interrupts only a subset of social behaviors. However, the utility of this split largely remains a mystery. Researchers have attempted to find clues by looking at similarities within V2R-activating versus V1R-activating cells. One possible separation is that V2Rs bind to large involatile stimuli (e.g., proteins) while V1Rs bind to small volatile stimuli<sup>28-29</sup>. Predator stimuli preferentially, though not exclusively, activate V2R+ cells, while conspecific stimuli activates both cell types<sup>18</sup> – stimuli sources appear to correlate with but not match the divide, so an unknown uniting principle may still remain.

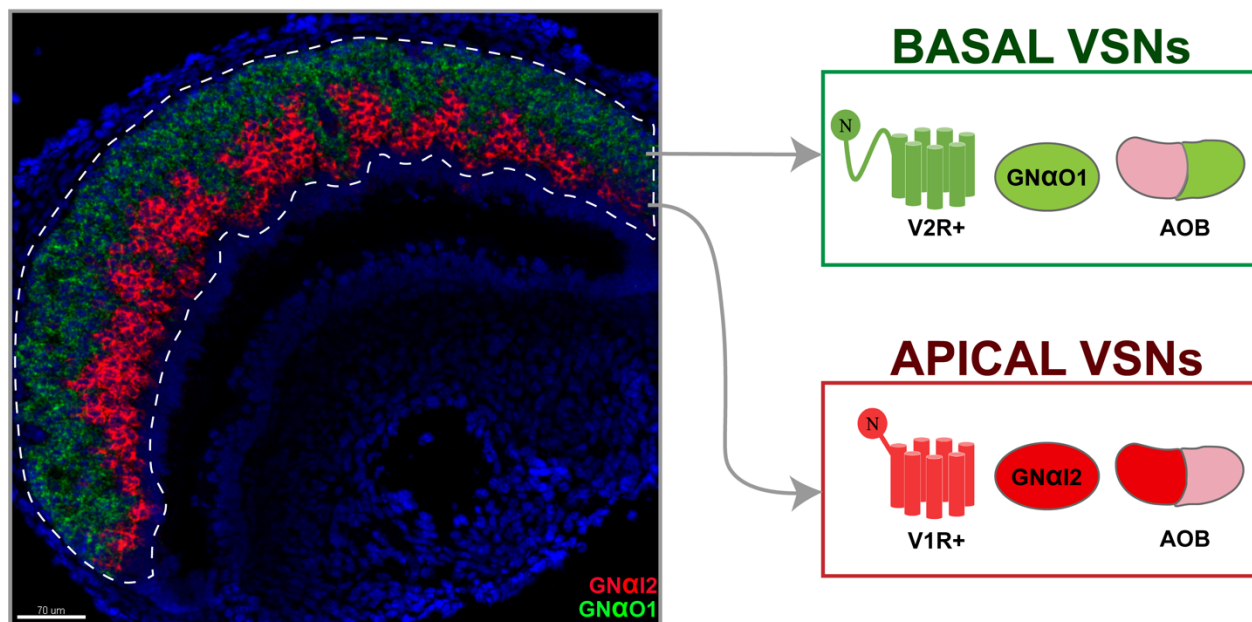


**Figure 1.4. The inherent spatial organization of the vomeronasal organ.**

The vomeronasal organ holds two major cell classes which segregate into distinct regions and are thought to perform distinct functions. The upper or “basal” region of the VNO holds cells expressing receptors from the vomeronasal type-2 family. Type-two receptors (“V2Rs”) have a longer N-terminus and are thought to respond to heavier, proteinous stimuli. Basal neurons also express distinct G-protein subunits, most notably  $Gn\alpha 1$ , and project to the posterior accessory olfactory bulb. The lower or “apical” region of the VNO holds cells expressing receptors from the vomeronasal type-1 family. Type-one receptors (“V1Rs”) respond to volatile stimuli. Apical neurons also express distinct G-protein subunits, most notably  $Gn\alpha 2$ , and project to the anterior accessory olfactory bulb.

Signal transduction of VSNs remains understudied, though certain components of the mechanism have been verified (Figure 1.5). After ligand-receptor binding, the G-protein subunits will become active and in turn activate the signal transducer, phospholipaseC beta 2 ( $PLC\beta 2$ )<sup>11-13</sup>. While G-protein alpha ( $G\alpha$ ) subunits have been shown to be important for VSN function<sup>43</sup>, G-beta gamma ( $G\beta\gamma$ ) subunits are as well<sup>53</sup>, so the relative contribution of each is not clear.  $PLC\beta 2$  activation leads to generation of DAG and  $IP_3$  small messenger molecules<sup>54,55</sup> which each open extracellular<sup>56</sup> and intracellular channels respectively<sup>57</sup>, though the latter may be dispensable for action potential generation<sup>58</sup>. The transient receptor potential cation member 2 ( $TrpC2$ ) channel opens upon DAG interaction<sup>59-61</sup>, letting in cations indiscriminately<sup>13</sup> – calcium binds to the anoctamin1 chloride channel and leads to cell firing<sup>62,63</sup>. As with other sensory modalities, all signal transduction components downstream of VRs are thought to be largely uniform between

VSNs. It is worth noting that, while knockout studies have confirmed the importance of channel components<sup>59,60,64</sup>, there is no experimental verification that VSN signaling is PLC $\beta$ 2-specific. Recent data has revealed that a small subset of mouse vomeronasal signaling is PLC $\beta$ 2-independent<sup>65</sup>, disproving this widely-accepted hypothesis. Multiple *PLC* subtypes are expressed in the vomeronasal organ, suggesting that other PLC subtypes likely make up this unexplained activity. However, whether this finding represents a break from may the PLC $\beta$ 2-centric vomeronasal signaling model or simply defines a new specialized sensory neuron type is unclear.

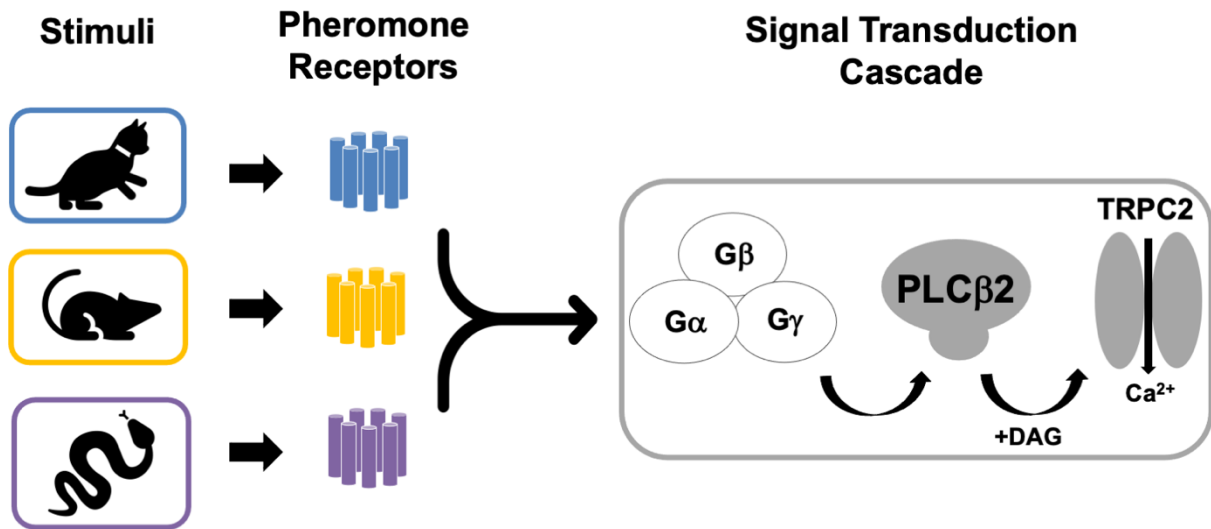


**Figure 1.5. The hypothesized signal transduction cascade of the mouse peripheral vomeronasal system.** The current model for vomeronasal signal transduction. The vomeronasal sensory neurons of mice respond to predator and conspecific stimuli (left). These stimuli each activate a unique combination of pheromone receptors out of the ~350 expressed within the vomeronasal organ (middle). After receptor activation, all activity is processed by a universal signal transduction cascade (right).

Phospholipase Cs (PLCs) are a group of signaling enzymes that are expressed throughout the body and critical for nearly every essential biological function<sup>66</sup>. Following cell stimulation, PLCs are bound and activated by an upstream partner, and PLCs will in turn bind to the membrane-bound phospholipid PIP<sub>2</sub> for conversion into membrane-bound diacylglycerol (DAG) and cytosolic IP<sub>3</sub><sup>54,55</sup>. DAG and IP<sub>3</sub> act as second messengers that amplify the original signal, typically through opening channel and initiating influx of external (DAG)<sup>56</sup> or internal (IP<sub>3</sub>)<sup>57</sup> cation stores. Through DAG and IP<sub>3</sub> creation, PLCs contribute to many bodily functions, such as

hematopoiesis<sup>67</sup>, fertility<sup>68</sup>, and sensory response<sup>7</sup>. The PLC's core structure, which has remained consistent across many species and centuries of evolution<sup>69-71</sup>, belies the enzyme's importance – PLCs share a pleckstrin homology (PH) domain that allows it to bind to PIP<sub>2</sub>, a catalytic domain (XY box) that allows it to convert PIP<sub>2</sub> into DAG/IP<sub>3</sub>, and several other regulatory domains<sup>72</sup>. PLCs are commonly phosphorylated for activity regulation, with the direction and amount of modulation differing by PLC subtype<sup>69,72</sup>. Phosphorylation often occurs through hormone-mediated pathways; a recent study reported such a case in vomeronasal tissue, with progesterone signaling directly silencing PLCβ2 in VSNs<sup>65</sup>.

Despite this highly conserved core structure, the mammalian PLC family is quite structurally and functionally diverse<sup>69,72</sup> (Figure 1.6). The family has 13 functionally-confirmed<sup>66,69</sup> and 18 PIP<sub>2</sub>-binding PLC subtypes<sup>73-75</sup>, each with unique expression profiles, upstream binding partners, and catalytic efficiencies<sup>66,69</sup>. While PLC subfamilies have higher functional and genetic similarity<sup>72</sup>, even subfamily members have relatively low structural and functional homology<sup>76-78</sup>. PLC's wide variability have made study difficult. Indeed, few subtype-specific tools exist with most using cell culture or global knockout models to draw conclusions regarding function. However, this technically troublesome PLC subtype variation makes the possibility that multiple function in the VNO interesting, as it could introduce previously unseen variation into the vomeronasal signal transduction cascade.

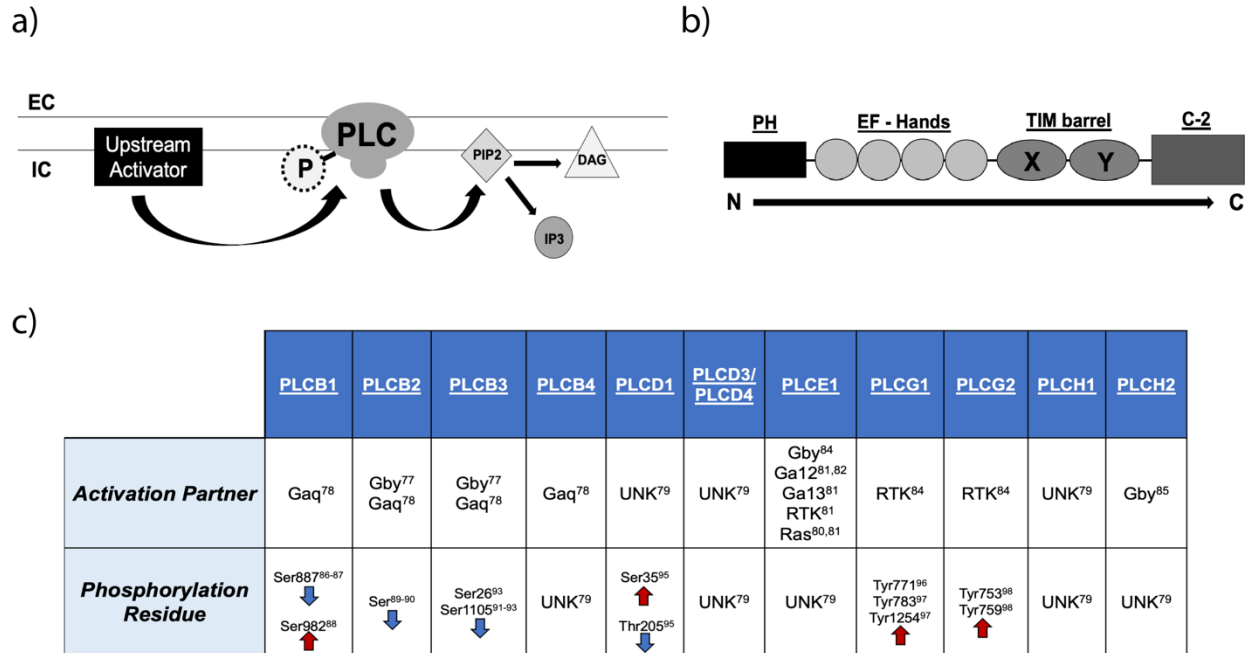


**Figure 1.6. Phospholipase C is a diverse family of signal transducers.**

**a**, Representation of PLC function. PLCs are activated by an upstream partner, allowing it to interact with membrane-bound PIP<sub>2</sub>. This interaction splits PIP<sub>2</sub> into two small messengers, membrane-bound DAG and cytosolic IP<sub>3</sub>, which interact with other effectors to amplify signals. PLCs can be phosphorylated, which changes activity in a subtype-specific manner. EC = extracellular, IC = intracellular. **b**, A PLC's core structure. PLCs have four main structural components, shown from N terminus (left) to C terminus (right). The pleckstrin domain (PH) binds to PIP<sub>2</sub>. The EF hands are of unknown function but may be involved in structural integrity. The TIM barrel domain binds to calcium ions, allowing for activation in certain PLC subtypes. The C-2 domain binds to calcium ions, allowing the enzyme to be trafficked to the cell surface. **c**, Comparison of different PLC subtypes. Each subtype has specific activation partners, phosphorylation sites, and responses to phosphorylation. RTKs = receptor tyrosine kinases, Ser = Serine, Thr = Threonine, Tyr = Tyrosine. Arrow direction indicates the direction of phosphorylation's effects.

The present work investigates PLC subtype patterning and function in the vomeronasal system using FISH, sequencing, and *EGR1* IEG analysis, so addressing this possibility. It investigates the previously identified PLCβ2-independent VSN activity and reveals that PLCβ2 comprises less than 10% of all vomeronasal activity. Further, it finds that ten PLC subtypes are consistently, reproducibly, and discretely expressed in VSNs themselves. These PLC subtypes have unique co-expression patterns with receptors and stimuli-activated cells, suggesting that disparate subtypes may play distinct roles in the VNO. Most surprisingly, multiple distinct signal transduction cascades are validated in the VNO, with at least half of VSN's activities still unaccounted for. While the utility of this variation in VSN signal transduction cascade is not yet verified, we hypothesize that it will provide a means for internal, hormonal state-specific sensory

activity variation – in support of this hypothesis, VSNs express various hormone receptors and show substantial inter-state and inter-individual variation in activity.

## RESULTS

### 1.1 PLC $\beta$ 2 is not the sole signal transducer in the VNO

Knockout studies have verified that most sensory cells within one modality signal through a primary signal transducer<sup>2-7</sup>. Likewise, the mouse vomeronasal system has long been thought to signal through an entirely PLC $\beta$ 2-dependent mechanism despite the absence of experimental verification<sup>11-13</sup>. Recent data suggests that a small subset of mouse vomeronasal signaling is PLC $\beta$ 2-independent<sup>65</sup>, but whether this finding represents a break from the PLC $\beta$ 2-centric vomeronasal signaling model or simply defines a rare, specialized sensory neuron class is unclear. To determine the extent of PLC $\beta$ 2-independent vomeronasal sensory signaling, we first measured *PLC $\beta$ 2* expression in mouse VSNs using *in situ* hybridization (FISH, Figure 1.7) and single-cell RNA sequencing (scRNAseq). Across both techniques *PLC $\beta$ 2* is expressed in fewer than 10% of mature VSNs (Figure 1.8). This suggests that, unlike current models of vomeronasal signal transduction, PLC $\beta$ 2 has a minimal role in pheromone signaling. Indeed, while male mouse urine generates activity that is >50% PLC $\beta$ 2-dependent<sup>65</sup> (Figure 1.9a-b), the extent to which PLC $\beta$ 2 is involved in sensing all other pheromone stimuli is unknown. To determine PLC $\beta$ 2's contribution to vomeronasal sensation, we exposed wildtype and PLC $\beta$ 2 mutant mice<sup>99</sup> to a broad pheromone cue mixture and the VSN-specific IEG *EGR1*<sup>18</sup> was used to assess the impact of PLC $\beta$ 2's removal on widespread VSN activity. Most stimulus-induced activity remained in animals with nonfunctional PLC $\beta$ 2, verifying that PLC $\beta$ 2's contribution to vomeronasal sensation is small (Figure 1.9c-d). This finding indicates that non-PLC $\beta$ 2 dependent activity is not an anomaly but a central feature of vomeronasal function. It further suggests that the vomeronasal system uses multiple signal transduction cascades, which would represent a fundamental departure from the current understanding of sensory systems.

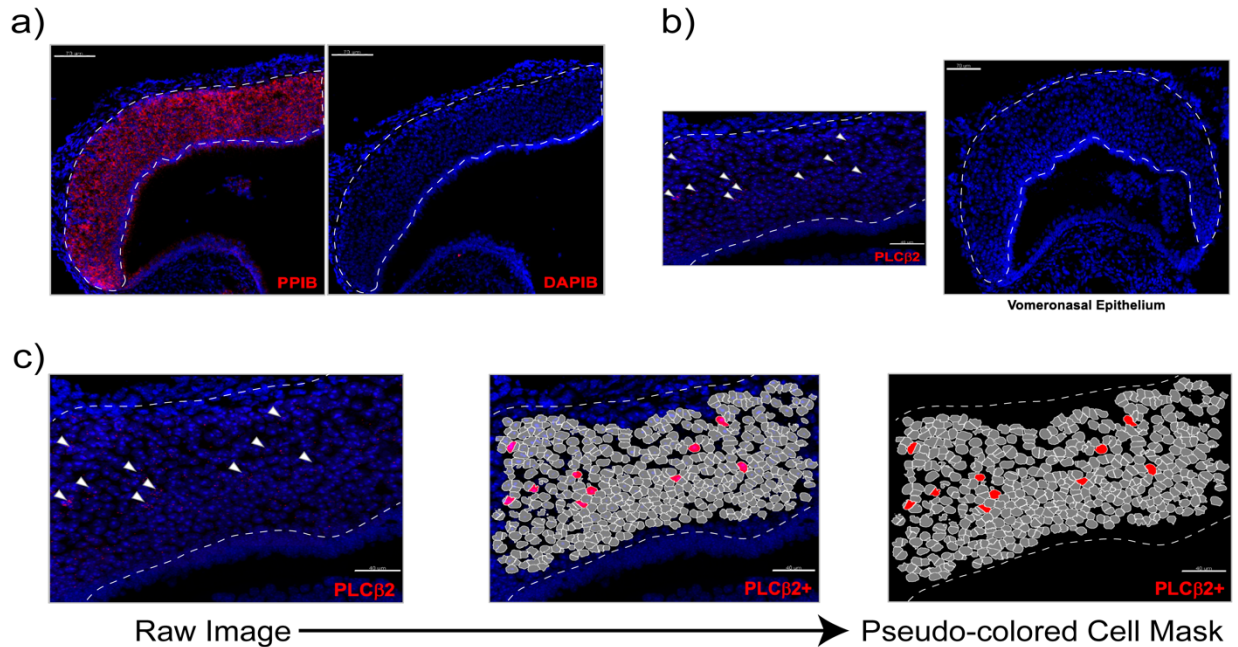


**Figure 1.7. Generating cell masks for depicting smFISH data.**

**a**, Positive (left) and negative (right) control FISH staining in the VNO. **b**, For most targets, zooming to 40x is necessary to detect the FISH signal. **c**, For most targets, a visual representation of target-positive cells is necessary given the punctate nature of the signal. To do this, a cell mask is created using quantification software such that one grey object represents one DAPI+ nucleus (one cell). Cells that are positive for the target gene of interest are then pseudocolored (see methods for details).

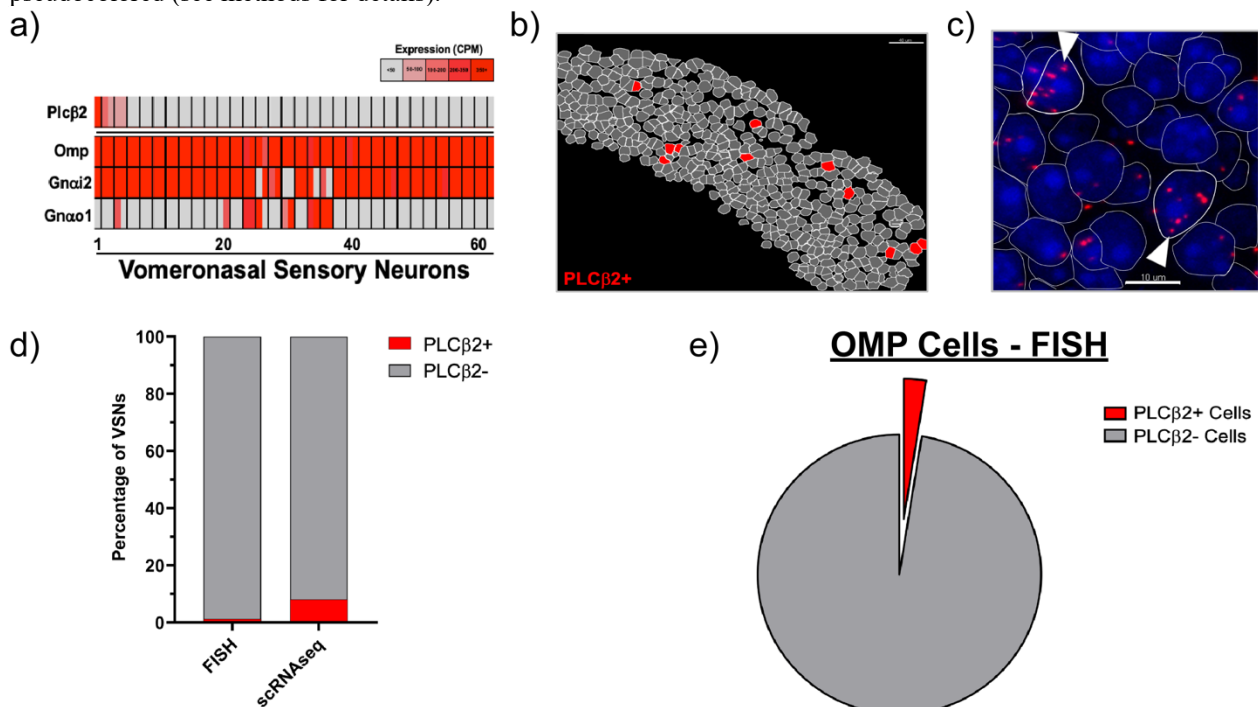


**Figure 1.8. Most VSNs do not express *PLCβ2*.**

**a**, Heatmap depicting gene expression within a 62-cell VSN RNA sequencing dataset. The VSNs shown express canonical sensory cell markers (*OMP* and G-proteins), yet few express *PLCβ2*. Data is shown in counts per million (CPM). **b**, A representative cell mask of *PLCβ2* FISH staining. **c**, Raw *PLCβ2* FISH data. **d**, Quantification of A and the dataset underlying B, FISH sample size is shown in Figure 1.12. **e**, Overlap between *PLCβ2*- cells and the mature VSN marker *OMP*. Cells that do not express *PLCβ2* are still *OMP*+.



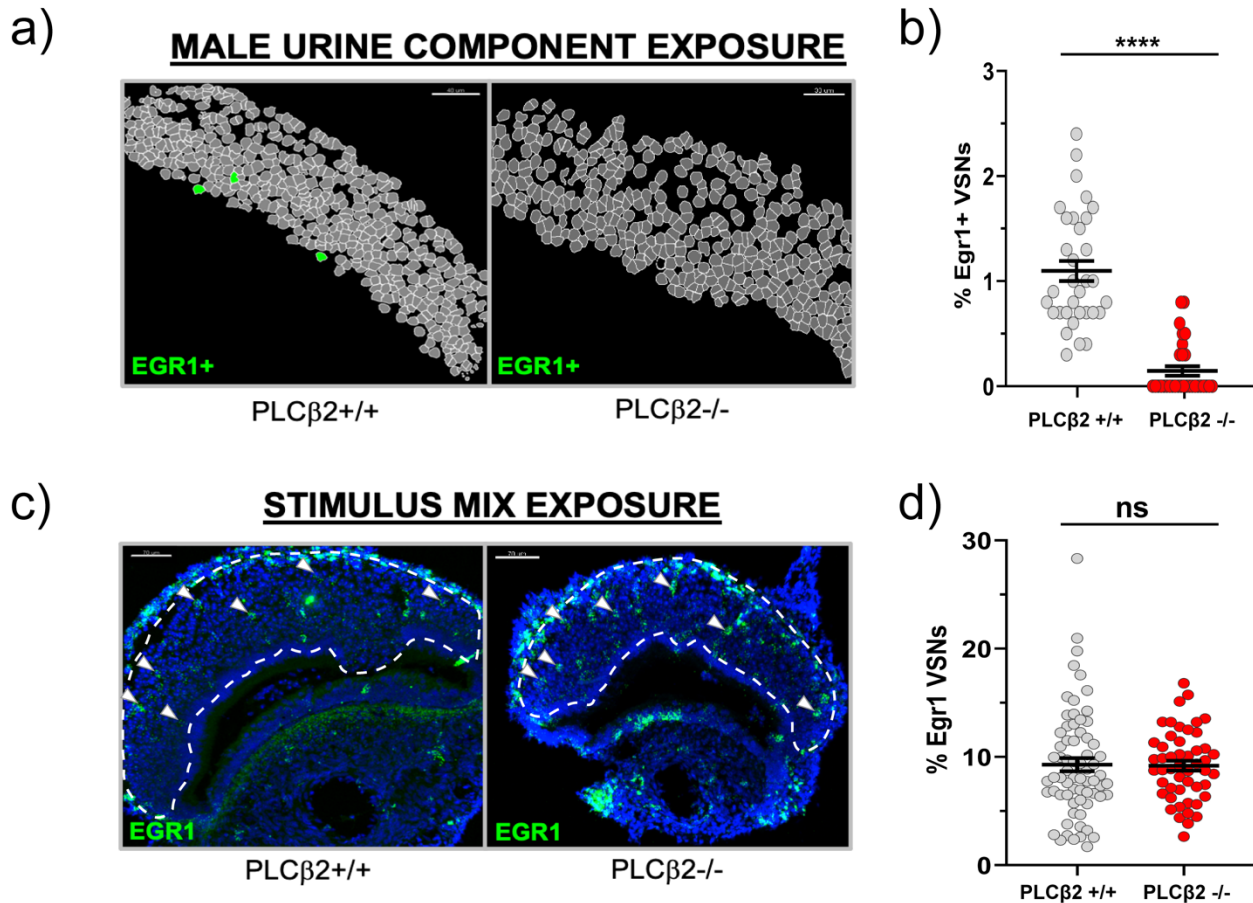


**Figure 1.9. Most VSNs do not use a PLC $\beta$ 2-dependent signal transduction cascade.**

**a**, Representative *EGR1*+ cell masks of male urine-exposed female mice with PLC $\beta$ 2 intact (left) or mutated (right). **b**, Quantification of **A**, n=25-30 ROIs across three animals per group. Mann-Whitney U test, p<.0001. **c**, Representative *EGR1*+ FISH images of stimulus mix-exposed mice with PLC $\beta$ 2 intact (left) or mutated (right). **d**, Quantification of **C**, n=50-60 ROIs across 5-6 animals per group. Mann-Whitney U test, p=.6243.

## 1.2 VSNs express many PLC subtypes

How do most VSNs fire, if not through PLC $\beta$ 2? As pheromone sensation relies on the DAG-responsive TrpC2 channel<sup>59,60</sup>, data suggests other DAG-releasing PLC subtypes generate the unexplained activity<sup>11-13</sup>. However, whether one or several PLCs make up the remaining ~95% of VSN activity is unknown – the former would indicate that the PLC $\beta$ 2-mediated mechanism represents a rare and specialized cell type, while the latter would signify a departure from the entire sensory signaling schema. Previous data shows that all *PLC* subtypes are expressed in VNO<sup>65</sup> and so are potential signal transducers, yet this data lacks VSN specificity - total VNO contains other cell types apart from sensory neurons<sup>23</sup>, including epithelial cells, blood

cells, and stem cells, each of which may have their own PLC repertoire<sup>66,69</sup>. In order to screen for *PLC* subtypes expressed within only mature sensory neurons, VSNs were isolated from OMP-GFP mice<sup>100</sup> using FACs and the harvested genetic material was PCR'ed for all 18 PIP<sub>2</sub>-responsive *PLC* family members.

Unexpectedly, VSN-specific PCR reproducibly yielded clear signal from 12 *PLC* subtypes, revealing a large pool of potential signal transducers (Figure 1.10a, Figure 1.34). To replicate this finding with single cell resolution, mouse VNO was stained for all *PLCs* verified by VSN-specific PCR. FISH affirmed that 10 *PLC* subtypes are reproducibly expressed in VSNs (Figure 1.10c) and scRNAseq data<sup>169</sup> shared expression of the same 10 subtypes in mature, *VR*-expressing VSNs (Figure 1.10b). If pheromone sensory signaling is mediated through many *PLC* subtypes, this would represent a previously-unrecognized, receptor-independent source of signaling flexibility in pheromone sensation. It is worth noting that many *PLC* subtypes expressed in VSNs don't traditionally function in sensory neurons or couple with G-proteins<sup>69,73-75,84</sup> while some that do are not found within the VNO<sup>69,101</sup>, suggesting an expression logic beyond current molecular intuition and knowledge (Figure 1.11).

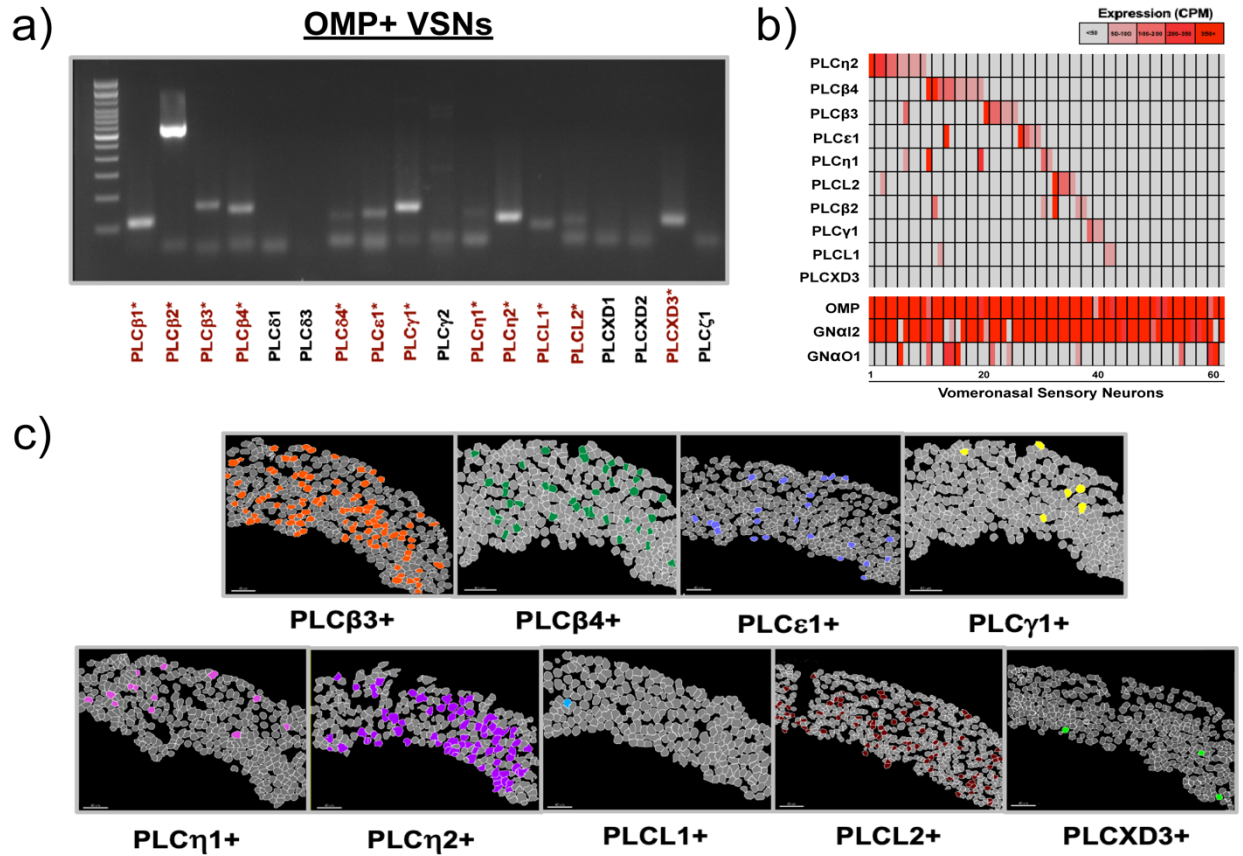


**Figure 1.10. VSNS express many *PLC* subtypes.**

**a**, PCR of OMP-GFP+ VNO cells for the 18 *PLC* subtypes. Red, starred names indicate genes verified across three animals (see Methods, Figure 1.12). Sample contains >10000 cells from nine animals. **b**, Heatmap depicting *PLC* expression within a 62-cell VSN single cell RNA sequencing dataset<sup>169</sup>. Ten of the twelve *PLC* subtypes found in A are also found in VSNS by scRNAseq. **c**, Representative cell masks for the nine new *PLC* subtypes found in a and b.

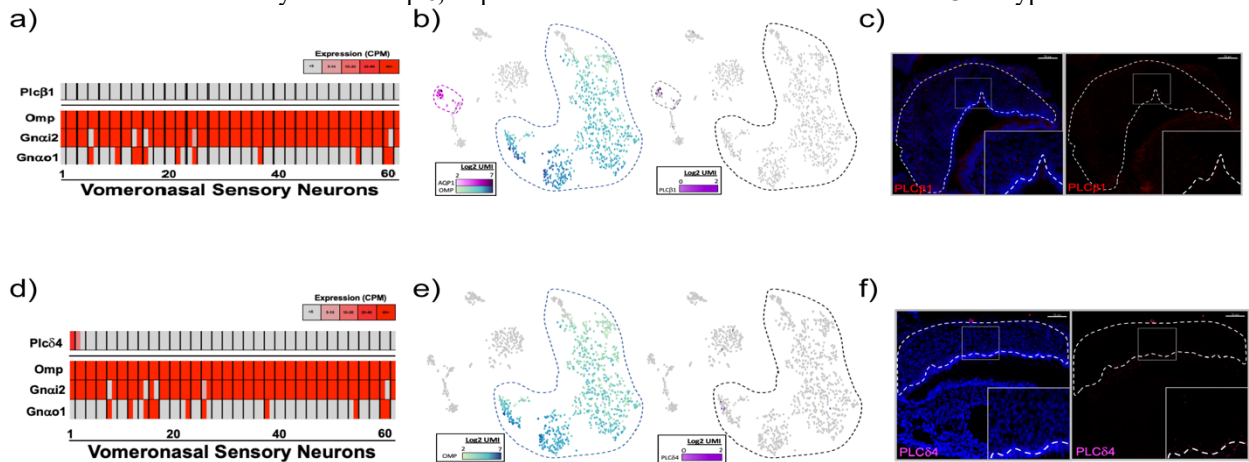


**Figure 1.11. VSNS don't express every *PLC* subtype.**

**a**, Heatmap depicting *PLCβ1* expression within a deep, 62-VSN RNA sequencing dataset. Note that the threshold has been taken down to 5CPM. **b**, A tSNE plot of 1,234 VNO cells in a shallowly-sequenced scRNAseq dataset. The dataset has been colored in for the genes of interest: *AQP1* and *OMP*, markers for the lamina propria and mature VSNS respectively (left), and *PLCβ1* (right). The tSNE-generated cell clusters that are positive for either cell type marker are circled. **c**, FISH for *PLCβ1* in VNO. **d**, Heatmap depicting *PLCδ4* expression using the same cells and cutoff as A. **e**, A tSNE plot of the same dataset used in B. The dataset has been colored in for the genes of interest: *OMP* (left), and *PLCδ4* (right). The *OMP*+ tSNE-generated cell cluster is circled. **f**, FISH of *PLCδ4* in VNO.

### 1.3 PLC subtypes are potential signal transducers

In other sensory modalities, the primary signal transducer is widely-expressed across the system's sensory cells<sup>1-7</sup>. Though there are many *PLC* subtypes expressed within VSNs, perhaps there is one dominant subtype that is the primary signaling element, making any other signaling cascade(s) sparse and specialized. In order to determine if there is a widely-expressed *PLC* amongst the subtypes found, abundance of all ten confirmed *PLC* subtypes was characterized in VSNs using FISH. Staining data shows that no one *PLC* subtype is expressed in more than ~30% of VSNs (Figure 1.12a-b); similarly, VSN scRNAseq data has no one *PLC* subtype in more than ~1/6<sup>th</sup> of all cells (Figure 1.12c). This trend appears to be consistent between mice of different sexes and states, at least when using bulk RNAseq as a proxy (Figure 1.13). This finding suggests that there are no dominant signal transducers in the VNO, and that the vomeronasal organ signals in a fundamentally different manner than other GPCR-based sensory modalities. Indeed, other chemical modalities' sensory cells do not display the signal transducer expression heterogeneity seen in VSNs (Figure 1.14). Overall, this data suggests that PLC $\beta$ 2-independent pheromone signaling is likely mediated by multiple PLC subtypes, none of which dominate sensory activity generation.

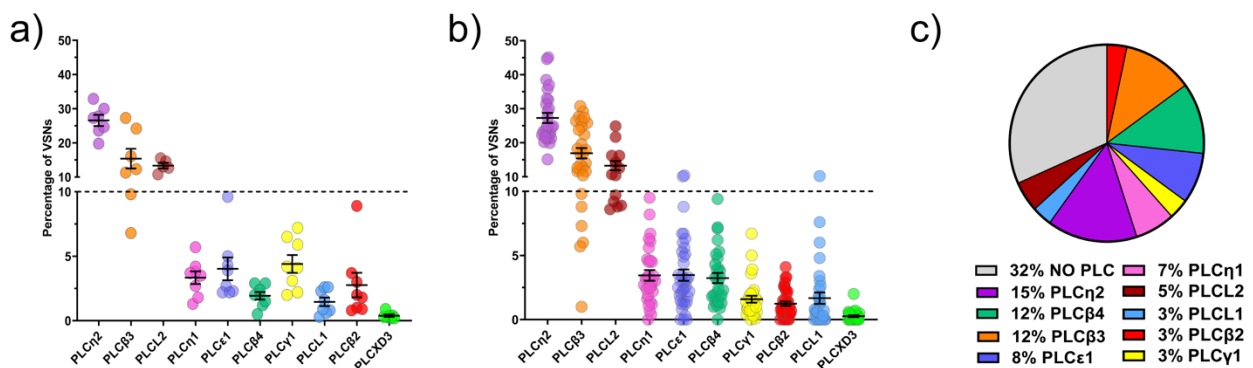


**Figure 1.12. VSNs express no dominant signal transducer.**

**a.** Percentage of VSNs that express each *PLC* subtype, as assayed by FISH. Each dot represents one animal, n=4-8 animals. **b.** 1.11a's data displayed per ROI, n=11-27 ROIs. **c.** Quantification of 1.10b, with the most highly-expressed *PLC* subtype recorded for each VSN.

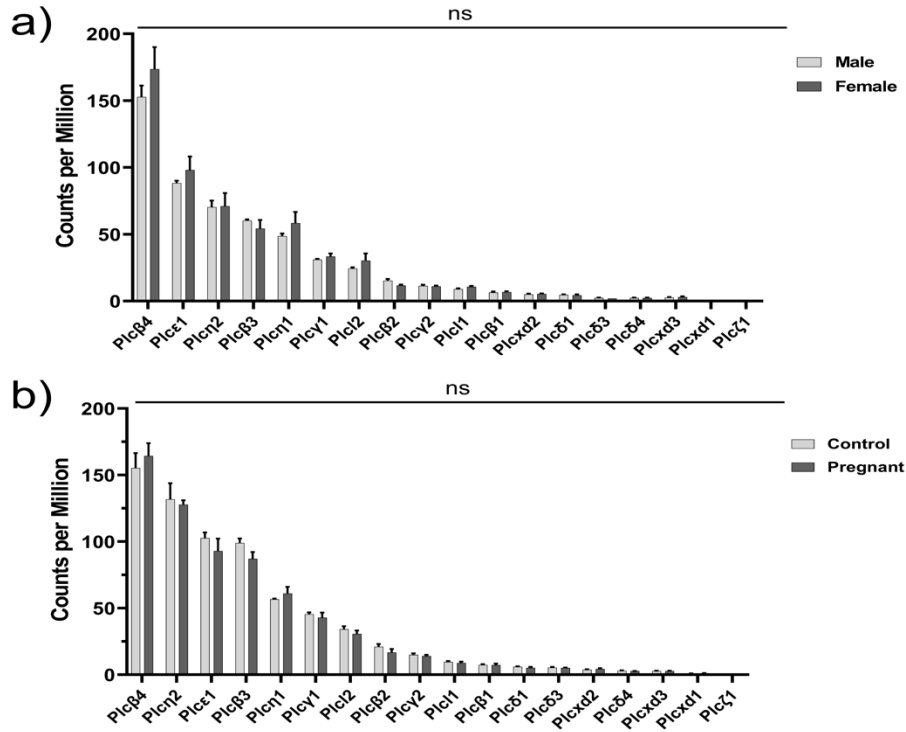


**Figure 1.13. The VNO's PLC expression is consistent across sex and state.**

**a**, Abundance of PLCs from a published VNO bulk RNAseq dataset<sup>102</sup> containing adult male and female data. PLCs are organized from most to least abundant, n=3 samples per group. Multiple Mann-Whitney U tests, adjusted  $p > .980$ .  
**b**, Abundance of PLCs from a published VNO bulk RNAseq dataset<sup>103</sup> containing adult male and female data. PLCs are organized from most to least abundant, n=3 samples per group. Multiple Mann-Whitney U tests with Holm-Sidak correction, adjusted  $p > .980$ .

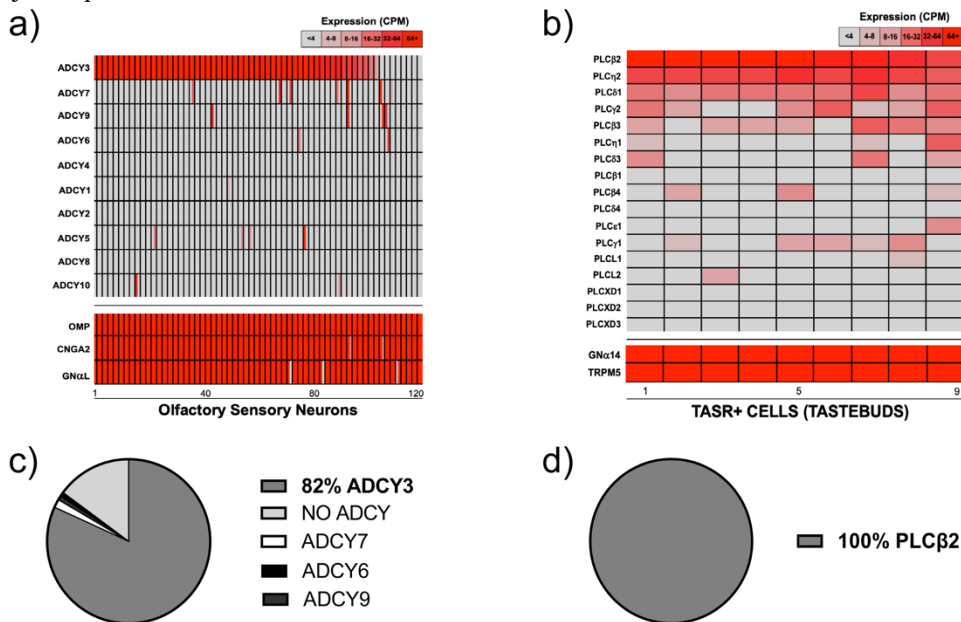


**Figure 1.14. Signal transducer heterogeneity is largely absent in non-pheromonal chemical senses.**

**a**, Heatmap depicting signal transducer (*ADCY*) expression in a deep, 121-cell OSN single cell RNA sequencing dataset. Dataset contains both published<sup>104-106</sup> and unpublished data. **b**, Heatmap depicting signal transducer (*PLC*) expression within a deep, published<sup>107</sup>, 9-cell taste cells single cell RNA sequencing dataset. **c**, Quantification from **a** with the most highly-expressed *ADCY* subtype recorded for each OSN. **d**, Quantification from **b**, with the most highly-expressed *PLC* subtype recorded for each taste cell.

Another possibility is that multiple PLC subtypes form one central signal transduction cascade. Indeed, PLC subtypes can work together by forming a hybrid signaling pathway<sup>108-110</sup>. As such, VSNs' ten *PLC* subtypes may work together, which would indicate massive functional redundancy among subtypes and so limit the novelty of our findings. To determine whether VSN's multiple signal transducers form a hybrid signaling pathway, *PLC* subtype overlap was analyzed. Sequenced vomeronasal neurons most commonly express one *PLC* with >95% of cells expressing two or fewer subtypes (Figure 1.15a), and FISH data also shows most cells expressing zero to two *PLC* subtypes (Figure 1.16). This data indicates that *PLCs* are discretely expressed with no instances of heavy overlap, making widespread hybrid signaling unlikely. The identified instances of scRNAseq *PLC* overlap were investigated further by comparing expression ratios of co-expressed *PLCs*. The most highly-expressed *PLC* has ~>50% more reads than the next most abundant subtype, such that each VSN has a dominant *PLC* in most cases of co-expression (Figure 1.15b-c). These findings indicate that even when *PLCs* are expressed together, there is one that likely performs most or all of the signal transduction. All together, *PLC* subtype patterning suggests that PLC $\beta$ 2-independent VSN signal transduction occurs through multiple discrete signaling pathways which each have substantial contribution to brain-bound vomeronasal messages.

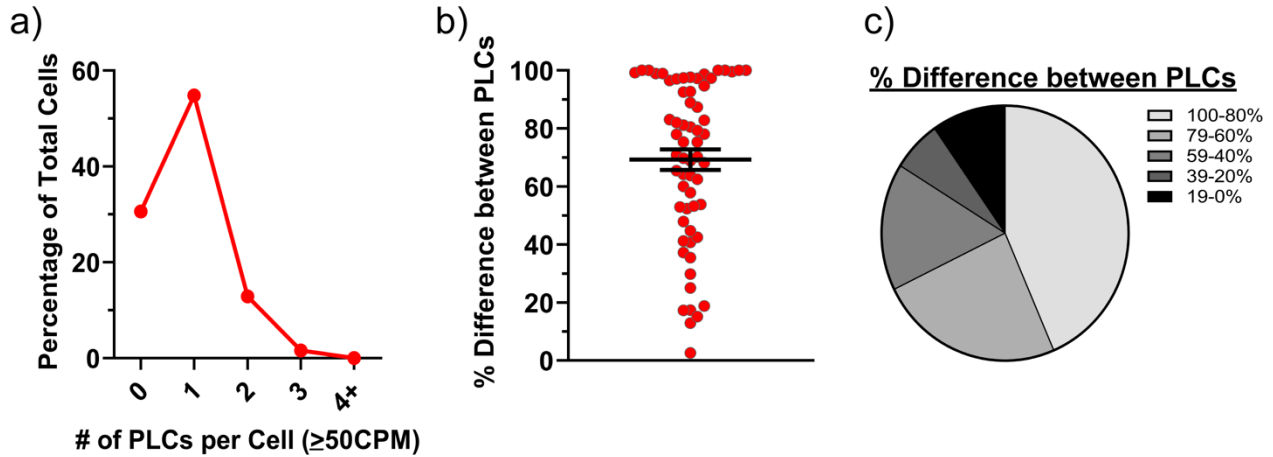


**Figure 1.15. PLCs show little overlap in scRNAseq VSN data.**

**a,** Quantification of 1.10b. The number of *PLC* subtypes expressed per cell was quantified for each VSN and totals were tallied throughout the entire dataset and represented as a percentage of total VSNS. **b,** Quantification of 1.10b. The difference between the two most-highly expressed *PLC* subtypes in each cell was calculated as follows: (the most highly expressed *PLC* CPM) – (2<sup>nd</sup> most highly expressed *PLC* subtype’s CPM) divided by (the expression of the most highly expressed *PLC* subtype’s CPM). Each dot represents the percentage difference for one cell. **c,** Binning and quantification of B.

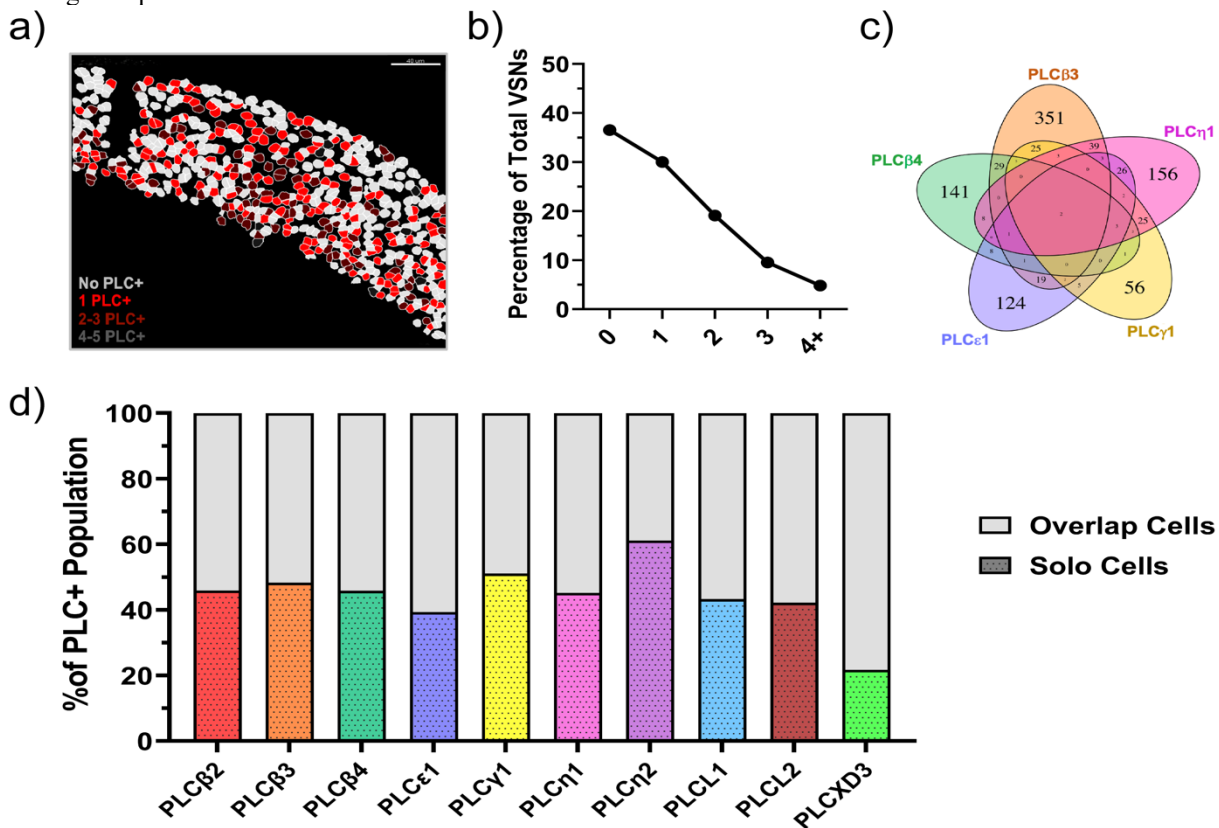


**Figure 1.16. PLCs show little overlap in multiplexed FISH VSN data.**

*PLC* overlap was assessed by staining for all ten verified *PLC* subtypes in a highly multiplexed FISH assay,  $n=12$  ROIs across 4 animals. **a,** A representative cell mask of VSNs stained for all ten verified *PLC* subtypes. Pseudocoloring denotes the number of *PLC* subtypes per cell. **b,** Quantification of A and underlying data. The number of *PLC* subtypes expressed per cell was quantified for each VSN (see Methods), and totals were tallied throughout the entire dataset and represented as a percentage of total VSNS. **c,** Venn diagram of five representative *PLC* subtypes’ expressions. **d,** Quantification of the total percentage of *PLC* subtype-expressing cells that are only expressing that subtype. Most subtypes are expressed alone in  $>40\%$  of VSNS.



#### 1.4 PLC subtypes are not functionally redundant

Past research asserts that different PLC subtypes function in fundamentally different ways<sup>69,72</sup>, which could introduce previously-unknown signaling heterogeneity into the vomeronasal system. However, it is not clear if PLC subtypes function differently in the VNO itself. One way to establish the existence of distinct PLC subtype functions in the VNO is to look at subtypes' comparative expression patterns – if PLCs are not functionally redundant, we would expect logical patterning overall and discrete patterning between subtypes. We began by investigating relative *PLC* subtype abundances. *PLC* abundance data suggests that subtype expression is not random overall, as all subtypes differ from a chance percentage of 10% (Figure 1.12a-b). To investigate abundance patterning between subtypes, individual data points' z-scores from *PLC* subtype means were used as a metric of similarity (Figure 1.17). VSN *PLCs* fall into at least three distinct abundance classes: highly-expressed *PLCs* (*PLCβ3*, *PLCL2*), moderately-expressed *PLCs* (*PLCβ4*, *PLCε1*, *PLCη1*), and rarely-expressed *PLCs* (*PLCβ2*, *PLCγ1*, *PLCL1*). In all, our analyses show that individual PLC subtypes' abundances are both patterned and unique, suggesting non-overlapping signal transducer functions in the VNO.



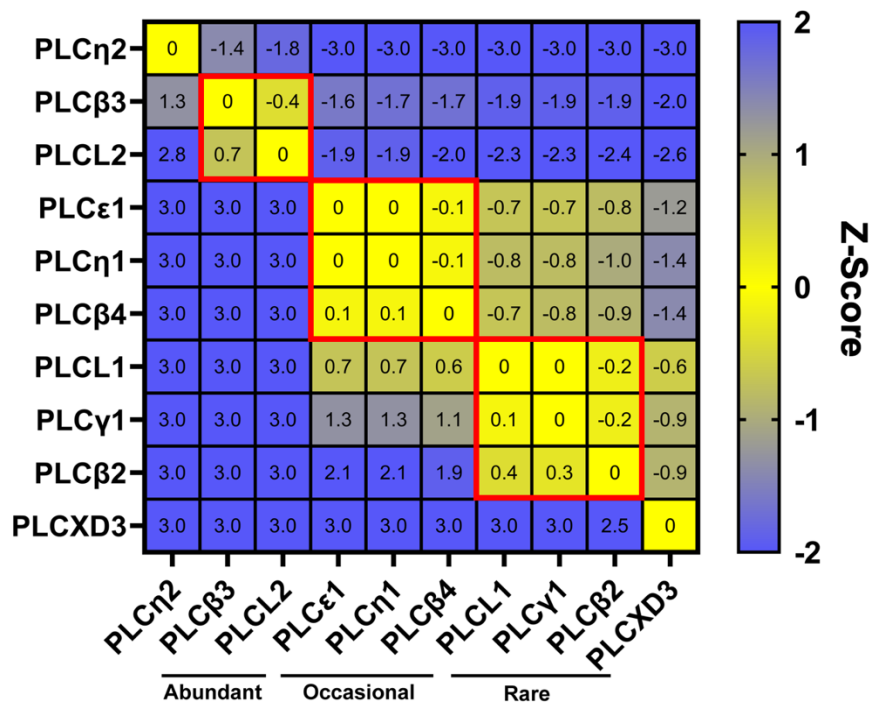


**Figure 1.17. PLCs fall into distinct abundance classes.**

PLC abundance data from Figure 1.12b was used to generate a metric of similarity. Briefly, z-scores between each abundance data point and PLC subtypes were generated using subtype abundance mean and standard deviation, and z-scores were averaged for each subtype-subtype comparison. Results averages were then plotted on a heatmap, with color warmth indicating similarity. Groups that were close together (within +/- .5) of each other were considered groups. Groups are circled in red and labeled.

Another way to test global and relative PLC subtype patterning in the VNO is by determining subtype co-expression with known cell types. The VNO has exquisite spatial and hypothesized functional separation between V1R+ and V2R+ cells<sup>46</sup> - if PLC subtypes serve distinct functions in the VNO, we expect that subtype expression would be organized in relation to these populations. To understand whether PLC subtypes preferably express in or avoid certain cell types, subtype co-expression with the spatial, V2R-specific marker *Gnao1* was assessed (Figure 1.18). Here, each cell expressing a PLC subtype (e.g., *PLCβ2*) was determined to be *Gnao1*+ or *Gnao1*-, and the proportion of *Gnao1*+ and *Gnao1*- cells across a total PLC subtype pool (e.g., all *PLCβ2* cells across an animal) was collated to generate an index of PLC subtype spatial and VR bias. Seven out of ten PLC subtypes exhibited a significant expression bias (Figure 1.18d), indicating that most PLC subtypes co-express in specific locations and with

specific receptor families. Further, PLC subtypes exhibited unique relative patterning, with V2R-biased, V1R-biased, and unbiased groups. These data show that PLC subtype expression is not random in the VNO, suggesting that different signal transduction pathways perform unique functions in the VNO. Further, VR co-expression biases may provide critical clues as to PLC subtype's individual functions.

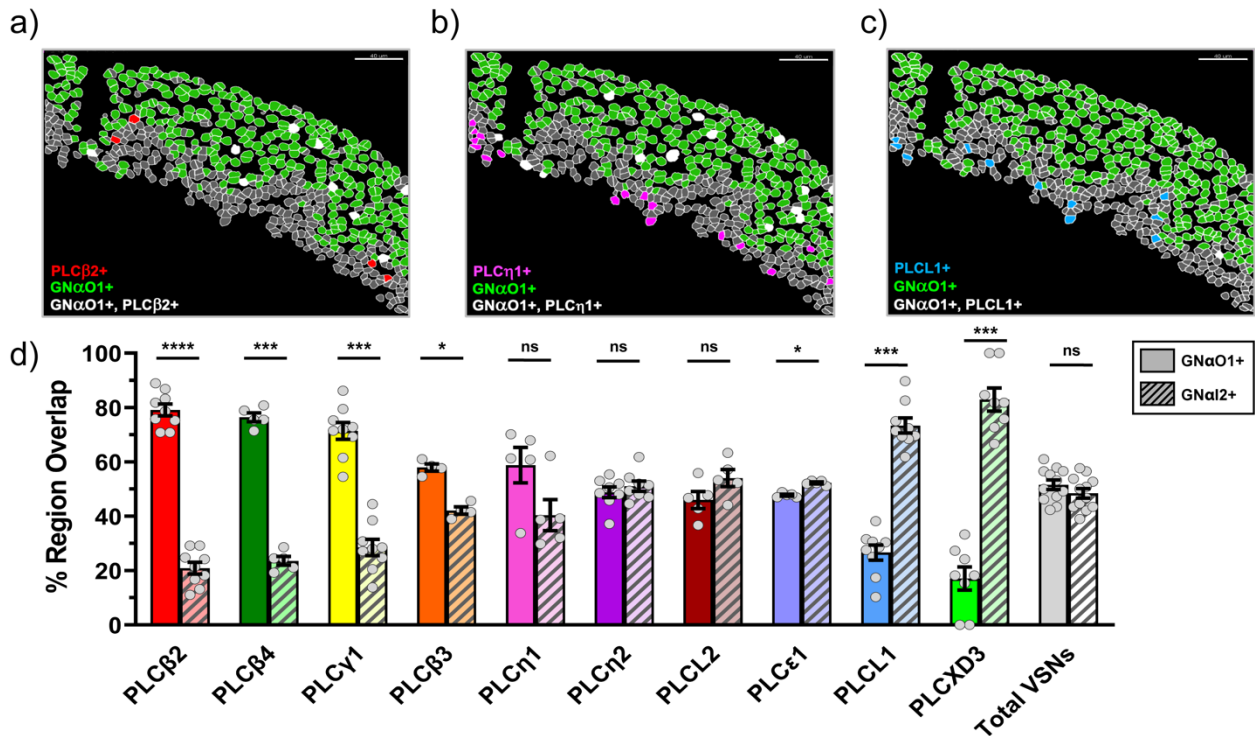


**Figure 1.18. PLCs exhibit spatial, cell-type-specific patterning.**

Spatial patterning of PLC subtypes within the VNO was assessed by quantifying co-expression with *Gnao1*, a marker for basal V2R+ cells. Cells lacking *Gnao1* are assumed to be positive for *Gnai2* and V1R. **a-c**, Representative cell masks showing *Gnao1* overlap with a basal-biased (a), neutral (b), or apical-biased (c) PLC. White indicates PLC+ cells that co-express *Gnao1*. **d**, Quantification of *Gnao1* or *Gnai2* (*Gnao1*-) overlap for each verified PLC subtype. Names represent PLC subtype or a mixed-identity group (“Total VSNs”). Circles represent animals, with at least four slices sampled per animal, n=4-12 animals per group. Paired t-tests with Holm-Sidak correction. Adjusted p-values are as follows: *PLCβ2*, p>.0001; *PLCβ4*, p=.0007; *PLCγ1*, p=.0008; *PLCβ3*, p=.047; *PLCη1*, p=.606; *PLCη2*, p=.620; *PLCL2*, p=.609; *PLCε1*, p=.020; *PLCL1*, p=.0003; *PLCXD3*, p=.0009; Total VSNs, p=.620.

## 1.5 Multiple signal transduction cascades exist in the VNO

While many discretely and uniquely-expressed PLC subtypes have been found in VSNs, mRNA expression does not equate to function and PLCs can play non-signaling roles<sup>66,69</sup>. In order to determine the extent of vomeronasal signal transducer heterogeneity and its practical

consequences, PLC subtype function must be directly evaluated. To test if certain PLC subtypes form signal transduction cascades in VSNs, we assessed the effect of subtype mutation on pheromone signaling. In brief, we exposed PLC subtype-intact and PLC subtype-mutant mice to the same stimuli and compared *EGR1* activity – we expect that, if a PLC subtype is involved in signal transduction, stimuli-evoked activity will drastically decrease upon its mutation. Further, we hypothesize that cells expressing the mutated PLC-subtype would preferentially stop functioning, which would lead to a sharp reduction in *Egr1-PLC* subtype overlap in mutant animals. We can assess the latter feature using a FISH probe that avoids the mutated *PLC* region, thus allowing us to see cells that were destined to express the PLC subtype in both wildtype (WT) and knockout (KO) animals. We note that these tests are done in global PLC knockout mice as few floxed PLC mice exist, so mutants are biologically different than wildtype mice. However, given that this assay is done in first-order neurons, we do not hypothesize that assay outcome will be impacted by effects external to the vomeronasal system.

Which of the ten *PLC* subtypes expressed in VSNs are signal transducers? The PLC Beta ( $PLC\beta$ ) subfamily has a well-established role in rapid, G-protein signaling in neurons<sup>7,9,69,101,111</sup>, making  $PLC\beta3$  and  $PLC\beta4$  prime candidates. However, in order to assay  $PLC\beta$  subtype function, we must be able to activate subtype-specific VSN populations. While the VNO responds to many known predator and mouse stimuli, less than 40% of stimulus space has been identified<sup>18</sup>, potentially making activation and so investigation of certain PLC subtypes impossible. Indeed, most *PLC* subtypes are expressed in less than 10% of VSNs (Figure 1.12) and thus may be hard to manipulate. To find stimuli that activate  $PLC\beta$  subtype-expressing VSNs, mice were exposed to one of a panel of ten known pheromone stimuli (Figure 1.19a), stimulated VSNs were stained for *EGR1* and *PLC $\beta$*  subtypes, and *EGR1-PLC* co-expression was quantified as a metric of a stimuli's "PLC $\beta$  repertoire" (Figure 1.19b). Results indicated that

*PLCβ3* and *PLCβ4* could be robustly activated with known stimuli (Figure 1.19c). Interestingly, *PLCβ* subtypes expressed within cells responding to specific classes of stimuli – *PLCβ2* expressed slightly more often in mouse stimuli-responsive cells, *PLCβ4* expressed slightly more often in predator stimuli-responsive cells, and *PLCβ3* expressed indiscriminately across stimuli. In addition, each stimulus had its own unique “PLC repertoire”. These findings suggest that vomeronasal signal transducers are stimuli-class specific, which could provide molecular handles and cellular characteristics to distinguish between both PLC subtypes and said stimuli classes.

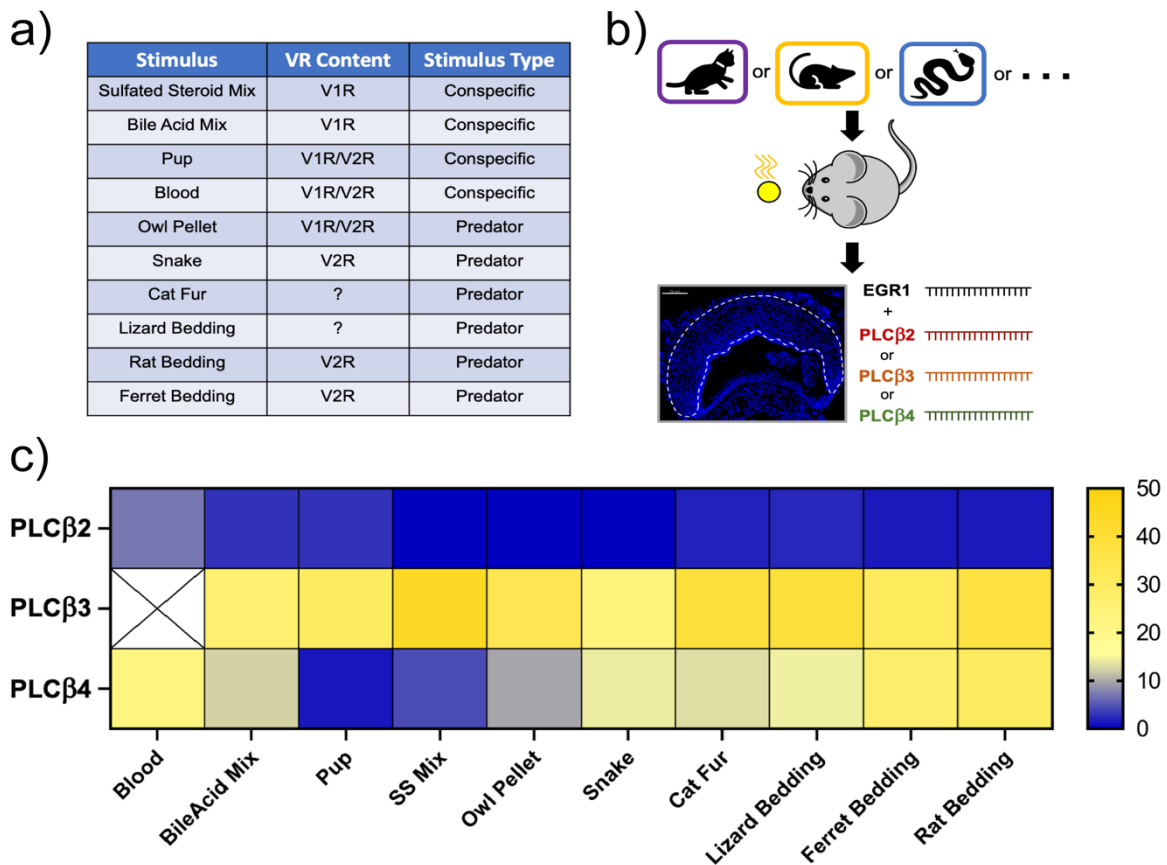


**Figure 1.19. Stimuli have unique PLC subtype co-expression patterns.**

Stimuli patterning of *PLC* subtypes within the VNO was assessed by quantifying co-expression with *EGRI*, a VNO-specific IEG, following stimulus exposure. **a**, Table of tested stimuli’s type and VR content, **b**, Experimental schematic. **c**, Heatmap of *PLC* overlap with cells responding to various stimuli. Rows denote *PLC* subtypes while columns denote stimuli types. Boxes with X’s have not been assayed.  $n=2-3$  mice,  $50+$  *EGRI*<sup>+</sup> cells each per square.

If a *PLC* subtype forms a distinct vomeronasal signal transduction cascade, we expect its removal to affect VSN activity in a specific and predicted manner. As such, we used *EGRI-PLC*

overlap data to select subtype-specific enriched stimuli for mutant exposure, with the hypothesis that this would result in a large activity reduction compared to wildtype mice. A mix of sulfated steroids (S.S. Mix), steroid hormones thought to be excreted and used as chemosignals<sup>112</sup>, robustly-activated PLC $\beta$ 3-expressing cells – over half of S.S. Mix-activated cells expressed PLC $\beta$ 3 (Figure 1.18c). To assess if PLC $\beta$ 3 is functional in VSNs, PLC $\beta$ 3 wildtype and mutant mice<sup>113</sup> were exposed to S.S. Mix and activity was compared using *EGR1* FISH. Mutant mice exposed to S.S. Mix had a >50% activity reduction compared to wildtypes (Figure 1.19a-b) and had few active PLC $\beta$ 3+ cells (Figure 1.19c), showing that PLC $\beta$ 3 mutation robustly impacts VSN function. Activity reduction was not explained by technical variables (Figure 1.20a), or a mutant-specific deficiency in development (Figure 1.20b) or specific PLC populations (Figure 1.20c-d). This finding indicates that PLC $\beta$ 3 forms a distinct and novel signal transduction cascade in the vomeronasal system, updating the current model for sensory signaling.

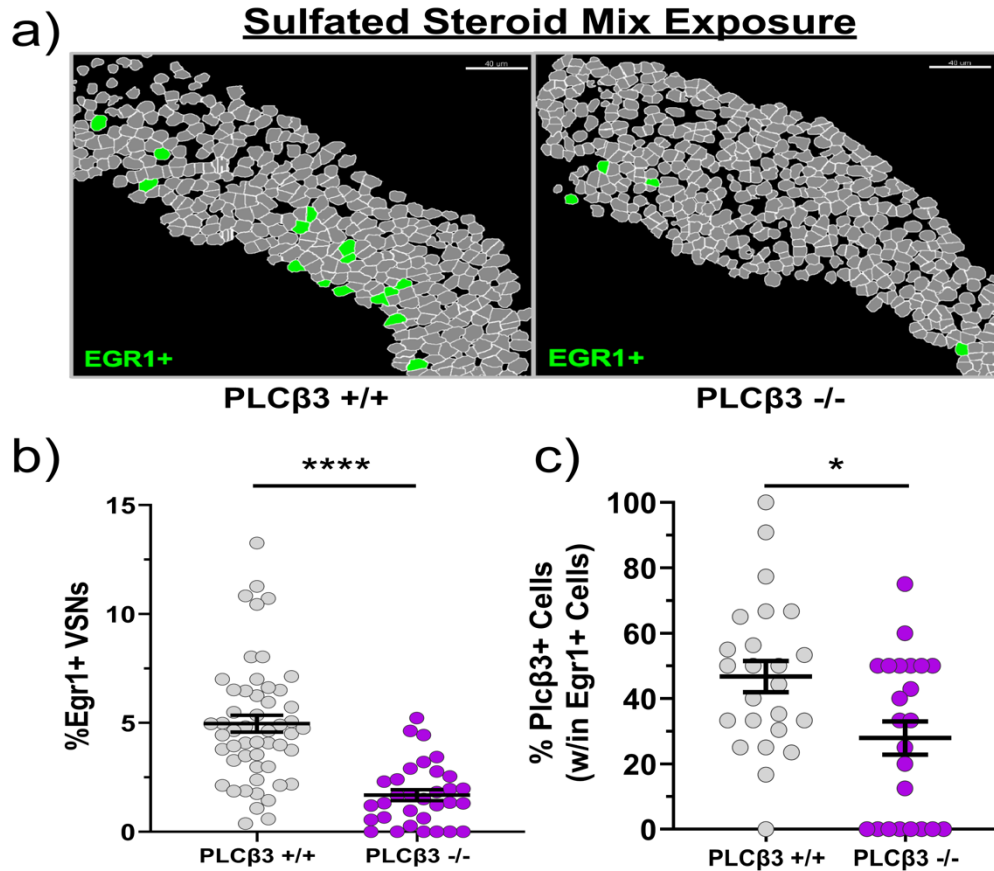


**Figure 1.20. PLC $\beta$ 3 mutation reduces VNO activity.**

Mice were exposed to the PLC $\beta$ 3-enriched stimuli sulfated steroid mix to assess effects of PLC $\beta$ 3 knockout. **a**, Representative cell masks of PLC $\beta$ 3 wildtype (left) and PLC $\beta$ 3 mutant (right) mice following exposure to sulfated steroid mix. **b**, Quantification of the dataset underlying A, n=27-30 ROI across 3 mice per group. Mann-Whitney U test, p<.0001. **c**, PLC $\beta$ 3 overlap with the EGR1 cells found in B. Mann-Whitney U test, p=.0193.

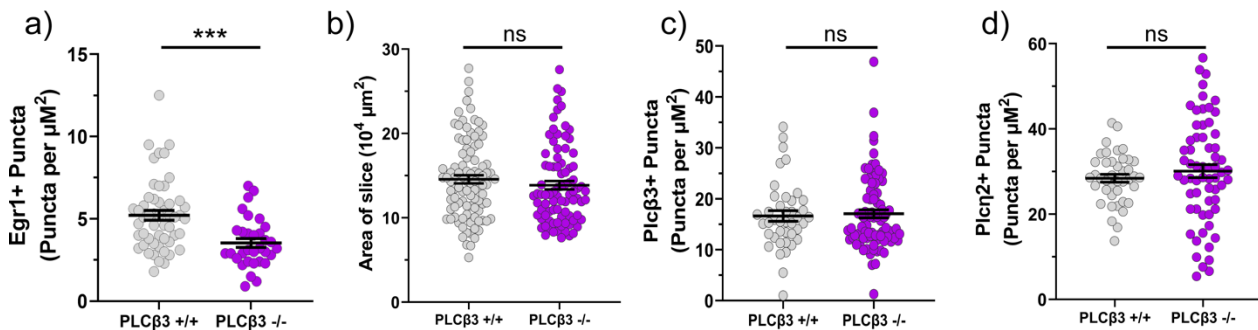


**Figure 1.21. PLC $\beta$ 3 phenotype is not due to technical, developmental, or population ratio concerns.**

Controls for Figure 1.20. **a**, Quantification of 1.20b using only overall EGR1 puncta number. Mann-Whitney U test, p<.0001. **b**, Area comparison between PLC $\beta$ 3 wildtype and mutant animals in Figure 1.20. Mann-Whitney U test, p=.1981. **c**, PLC $\beta$ 3 puncta comparison between PLC $\beta$ 3 wildtype and mutant animals in Figure 1.20. Mann-Whitney U test, p=.9473. **d**, PLC $\eta$ 2 puncta comparison between PLC $\beta$ 3 wildtype and mutant animals in Figure 1.20. Mann-Whitney U test, p=.4173.

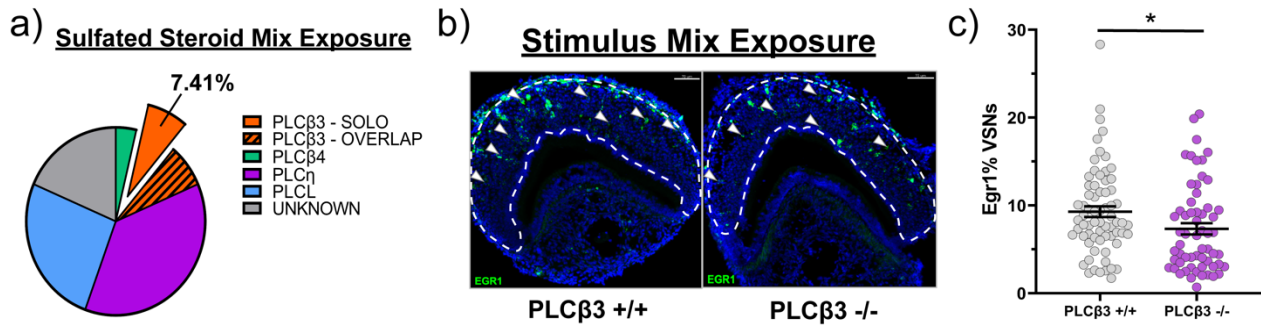


**Figure 1.22. PLCβ3 is not the main vomeronasal signal transducer.**

**a**, Quantification of *PLC* overlap with *EGR1*+ cells remaining in 1.20c, n=4 ROI within 1 animal. Note that *PLCβ3* is only a small proportion of the remaining cells. **b**, Representative 20x images of *PLCβ3* wildtype (left) and *PLCβ3* mutant (right) mice exposed to a stimulus mix. Arrows indicates *EGR1*+ cells. **c**, Quantification of dataset underlying C. n=5-6 per group. Mann-Whitney U test, p=.0193.

## 1.6 The VNO signals through multiple distinct transduction cascades

While *PLCβ3*'s function in the VNO is novel, this still fits cleanly into the sensory system framework outlined earlier (Figure 1.1). It may be that *PLCβ3* is the VNO's primary signal transducer and that *PLCβ2* represents a specialized cell type. Abundance data from FISH and scRNAseq suggests that there are more functional signal transducers to be found, as *PLCβ2* and *PLCβ3* express in <40% of VSNs (Figure 1.12). In addition, *PLCβ3* mutant mice retain VSN activity which was not explained by *PLCβ2* or residual *PLCβ3* expression (Figure 1.22a), yet it is unclear if this *PLCβ3*-independent activity is S.S. Mix-specific. To determine whether *PLCβ3* is VNO's primary signal transducer, wildtype and *PLCβ3*-mutant mice were exposed to the stimulus mix used in Figure 1.9. Most stimulus-induced activity remained in animals with nonfunctional *PLCβ3* (Figure 1.22b-c), though *PLCβ3* knockout did reduce activity significantly. This finding verifies that *PLCβ3* is not VNO's central signal transducer, and that the VNO follows a fundamentally different signaling model than other chemical senses.

More signaling elements account for the ~60% of unexplained VSN activity, and of the remaining *PLC* subtypes, neuron-specific *PLCβ4* is most likely. *PLCβ4* function in the VNO would be quite interesting given its enrichment in predator stimuli (Figure 1.19c). To test *PLCβ4*

function, wildtype and PLC $\beta$ 4 mutant mice<sup>114</sup> were exposed to PLC $\beta$ 4-enriched rat bedding. Mutant PLC $\beta$ 4 mice had far less rat bedding-evoked VSN activity compared to wildtype mice (Figure 1.23a-b) and PLC $\beta$ 4-specific activity compared to wildtype mice (Figure 1.23c), indicating the PLC $\beta$ 4 mutation substantially impacted VSN function. Activity differences were not attributable to technical variables (Figure 1.24a) or skewed PLC populations (Figure 1.24c-d). Slight significance was seen in developmental measures (Figure 1.24b), likely due to knockout-specific motor difficulties<sup>115</sup> interfering with nursing. Nonetheless, these data suggest that PLC $\beta$ 4 likely forms a distinct signal transduction pathway in VSNs. Interestingly, the PLC $\beta$  subtypes express in largely distinct VSN populations (Figure 1.24e), suggesting that the PLC $\beta$ s form distinct signal transduction cascades that explain <50% of remaining VSN activity. In all, we have found that the vomeronasal system uses multiple discrete and patterned signal transduction pathways to mediate signaling, updating our understanding of how sensory systems work.



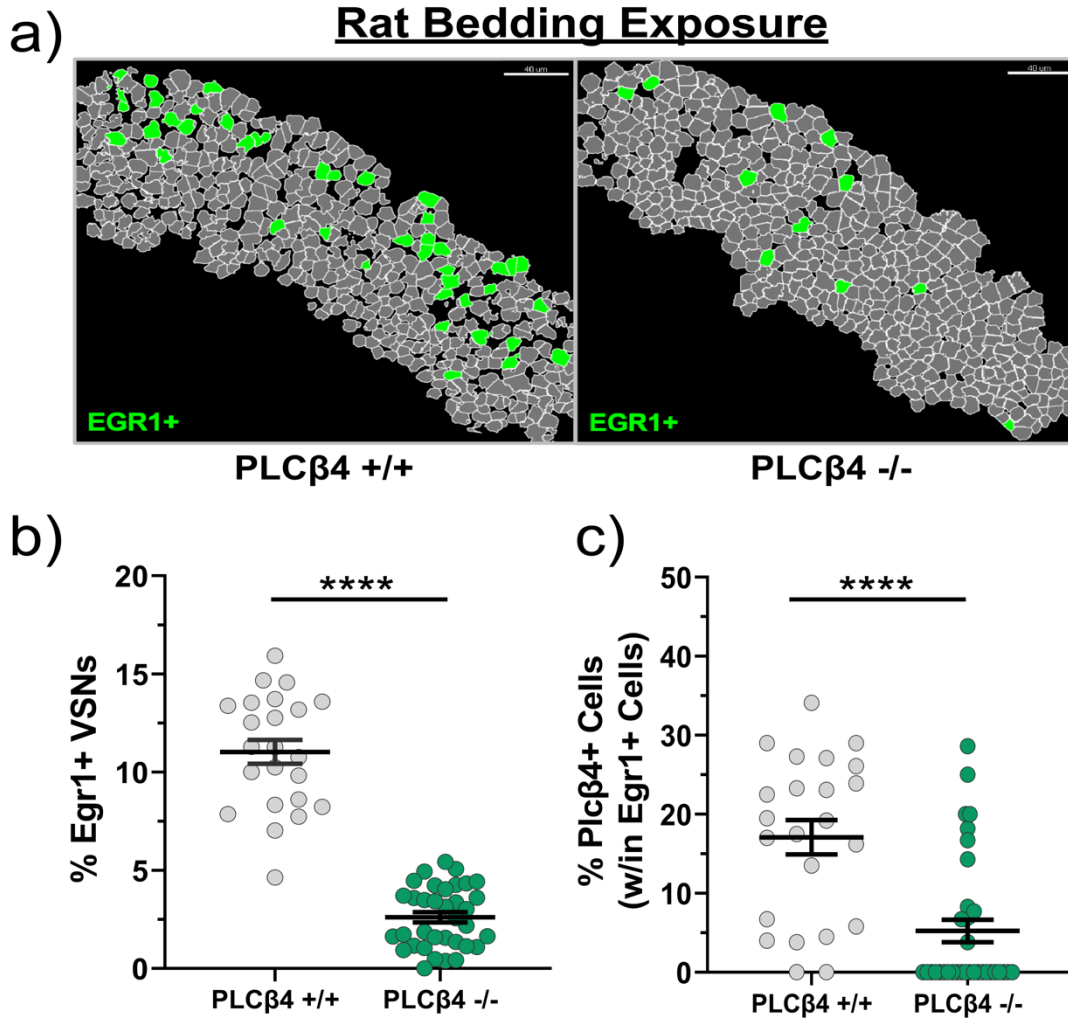


**Figure 1.23. PLCβ4 mutation reduces VNO activity.**

Mice were exposed to the *PLCβ4*-enriched stimuli rat bedding to assess effects of PLCβ4 knockout. **a**, Representative cell masks of PLCβ4 wildtype (left) and PLCβ4 mutant (right) mice following exposure to rat bedding. **b**, Quantification of the dataset underlying A, n=20-30 ROI across 3 mice per group. Mann-Whitney U test,  $p < .0001$ . **c**, *PLCβ4* overlap with the *EGR1* cells found in B. Mann-Whitney U test,  $p < .0001$ .

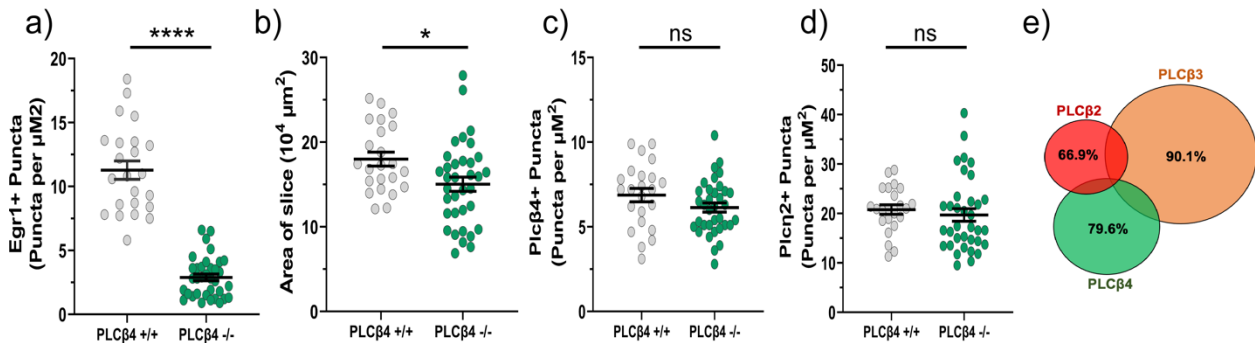


**Figure 1.24. PLCβ4 phenotype is not due to technical or population ratio concerns.**

Controls for Figure 1.23. **a**, Quantification of 1.23b using only overall *EGR1* puncta number. Mann-Whitney U test,  $p < .0001$ . **b**, Area comparison between PLCβ4 wildtype and mutant animals in Figure 1.23. Mann-Whitney U test,  $p = .0200$ . **c**, *PLCβ4* puncta comparison between PLCβ4 wildtype and mutant animals in Figure 1.23. Mann-Whitney U test,  $p = .1190$ . **d**, *PLCη2* puncta comparison between PLCβ4 wildtype and mutant animals in Figure 1.23. Mann-Whitney U test,  $p = .2432$ . **e**, Overlap of *PLCβ* subtype expression in VSN FISH.

## 1.7 PLC subtypes may not explain remaining VSN activity

The PLC $\beta$  subtypes' roles in VSN signal transduction do not entirely fill the gaps in the now-revised vomeronasal signaling model. Indeed, functional (Figure 1.9, 1.22) and abundance data (Figure 1.10) suggests that PLC $\beta$  subtypes account for less than half of pheromone-mediated activity. Our expression data suggests that some or all of the unexplained activity is mediated by the remaining PLC subtypes in VSNs. Determining if PLCs generate the remaining activity will allow us to define how far the VNO departs from traditional sensory signaling schema. A blend of logic and mouse line-availability was used to pick remaining PLC subtypes for further assessment. Our first choice was PLC $\epsilon$ 1, which can interact with G-proteins<sup>81,82,84</sup> despite its lack of neuronal expression<sup>119,120</sup> and so potentially fit in with known VSN molecular machinery<sup>28,29</sup>.

As PLC $\epsilon$ 1 has a middling abundance in VNO (Figure 1.10), finding a highly-enriched stimuli for testing proved difficult. To gain clues, we checked the receptors co-expressed in our deeply-sequenced *PLC $\epsilon$ 1*+ VSNs and matched them with the reported paired stimuli<sup>18</sup> (Figure 1.25a). Data shows that *PLC $\epsilon$ 1* co-expresses with *VMNIR89*, which is activated by E0893 and A7864<sup>18,23</sup> and was confirmed by *EGR1-PLC $\epsilon$ 1* staining (Figure 1.25b). A mix of these stimuli (S.A.E. Mix) was used for testing. Unlike tests with PLC $\beta$  subtypes, here wildtype and PLC $\epsilon$ 1 mutant mice<sup>121</sup> did not have significantly different activity levels (Figure 1.25c-d), indicating that PLC $\epsilon$ 1 mutation does not impact pheromone sensing. *PLC $\epsilon$ 1* overlap was also unexpectedly higher in mutant mice (Figure 1.25e), although this is likely due to a mutant-specific increase in overall *PLC $\epsilon$ 1* expression (Figure 1.26c). PLC $\beta$ 3 has been reported to co-express with PLC $\epsilon$ 1<sup>109</sup>, which may mask an effect of PLC $\epsilon$ 1 mutation; indeed, we have shown that PLC $\beta$ 3 acts in sulfated steroid signaling (Figure 1.20-1.21). Yet, *PLC $\epsilon$ 1* labeled active cells in PLC $\beta$ 3 knockout mice (Figure 1.26d), indicating that PLC $\beta$ 3 is not obscuring an impact. While it is possible that

the expected effect size for this assay was too small for our assay, *PLCε1* content did not decrease in mutants (Figure 1.25e), so non-functionality is more likely. All together this data suggests, though cannot confirm, that *PLCε1* does not function in a signaling role in VSNs or explain the remaining *PLCβ*-independent VNO activity.

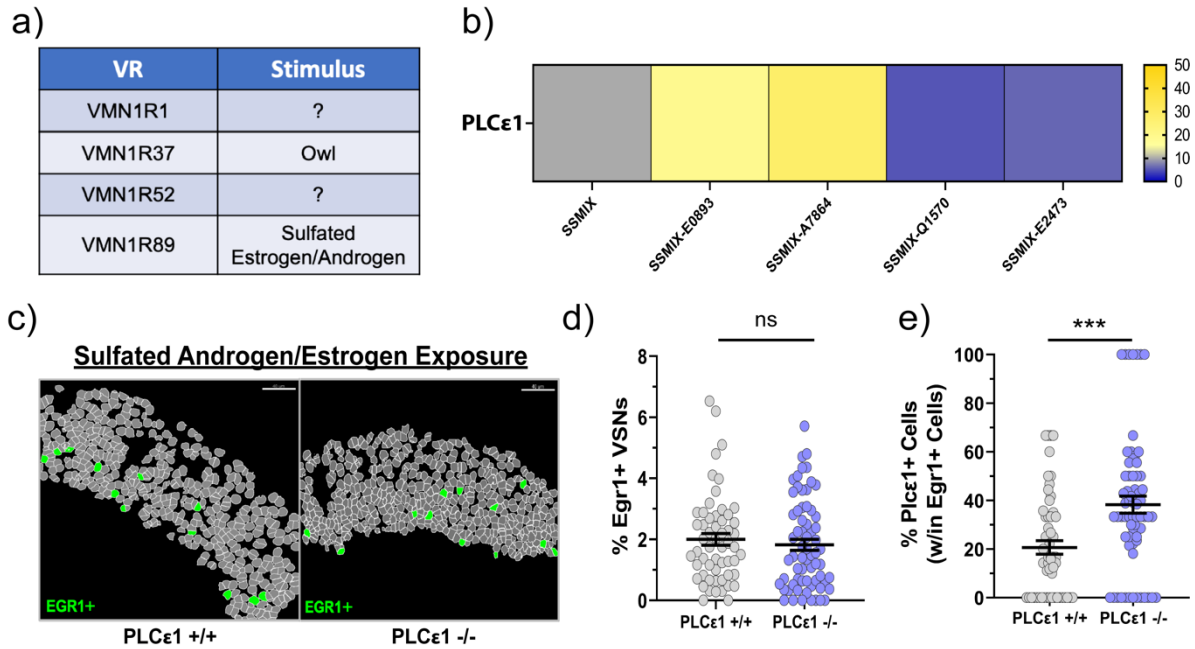


**Figure 1.25. *PLCε1* mutation does not affect S.A.E. Mix-mediated VNO activity.**

Mice were exposed to the *PLCε1*-enriched stimuli S.A.E. Mix to assess effects of *PLCε1* knockout. **a**, Single cells from a deep scRNAseq VSN dataset. Pheromone receptors expressed in cells co-expressing *PLCε1* (left) and predicted stimulus (right) are shown. **b**, Heatmap of *PLCε1* overlap with cells responding to components of S.S. Mix and total mix. Columns denote stimuli types, n=2-3 mice with 30+ *EGR1*+ cells each per square. **c**, Representative cell masks of *PLCε1* wildtype (left) and *PLCε1* mutant (right) mice following exposure to S.A.E. Mix. **d**, Quantification of the dataset underlying C, n=50-60 ROI across 5-6 mice per group. Mann-Whitney U test, p=.4174. **e**, *PLCε1* overlap with the *EGR1* cells found in D. Mann-Whitney U test, p=.0002.

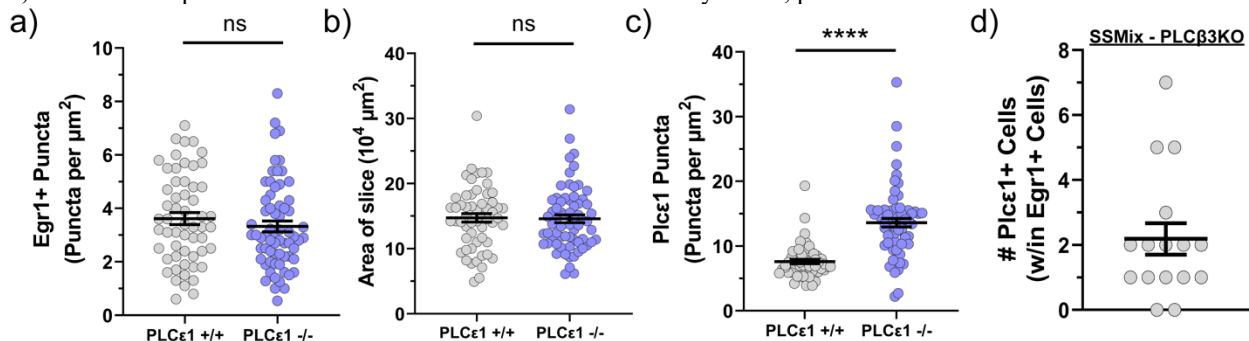


**Figure 1.26. *PLCε1* phenotype is not due to technical, developmental, population ratio, or overlap concerns.** Controls for Figure 1.25. **a**, Quantification of 1.25d using only overall *EGR1* puncta number. Mann-Whitney U test, p=2641. **b**, Area comparison between *PLCε1* wildtype and mutant animals in Figure 1.25. Mann-Whitney U test, p=.6294. **c**, *PLCε1* puncta comparison between *PLCε1* wildtype and mutant animals in Figure 1.25. Mann-Whitney U test, p < .0001. **d**, Number of *EGR1* and *PLCε1* co-expressing cells within *PLCβ3* knockout mice exposed to S.S. Mix. n=2 mice, 8 ROIs each.

Our next choice for functionality testing is PLC $\gamma$ 1, which despite typically interacting with RTKs<sup>84</sup> instead of GPCRs has recently been suggested to may play a role in neural firing<sup>122</sup>. Finding a stimulus for PLC $\gamma$ 1 was quite difficult, possibly as a function of its sparse expression in VSN tissue. Upon looking at the receptors expressed in our deeply-sequenced *PLC $\gamma$ 1*<sup>+</sup> VSNs, we found few useful stimuli<sup>18</sup> (Figure 1.27a); further, we only found *VIRs* despite *PLC $\gamma$ 1* being primarily *V2R*<sup>+</sup> (Figure 1.18), likely due to a technically-caused *VIR* enrichment in scRNAseq (personal observation). After screening *V2R*-mediated stimuli, we found that ferret bedding stimulated the most *PLC $\gamma$ 1*<sup>+</sup> cells out of our stimuli panel, so it was used for subsequent testing (Figure 1.27b). We found no significant activity difference between PLC $\gamma$ 1 mutants<sup>123</sup> and wildtype controls in response to ferret bedding (Figure 1.27c-e), indicating that PLC $\gamma$ 1 likely does not function in VNO sensory signaling. Oddly, we found a sharp activity decrease between PLC $\gamma$ 1-WT and PLC $\gamma$ 1-floxed animals, even when no Cre was present (Figure 1.27c-d). This suggests a general role for PLC $\gamma$ 1 in VSNs that does not require its PIP<sub>2</sub>-binding domain. However, qPCR analysis shows that PLC $\gamma$ 1 Flox sites do not impact VSN development or cell type population ratios (Figure 1.28b-e), two potential explanations for the seen effect. As such, even though we cannot definitely exclude a role for PLC $\gamma$ 1 in signal transduction, we hypothesize that the effect is more likely caused by a global effect of PLC $\gamma$ 1 Flox sites - a Cre-inducible system may be required to clarify these results. Nonetheless, this data altogether shows that PLC $\epsilon$ 1 and PLC $\gamma$ 1 are unlikely to contribute to the unexplained VSN activity. Of the untested PLC subtypes, only two have displayed catalytic activity (PLC $\eta$ ), and abundance data indicates that PLC $\eta$  cannot account for all remaining activity. This suggests that PLC-independent signaling may occur in the VNO providing an even deeper layer of signaling heterogeneity. However, direct testing is needed to confirm this hypothesis.

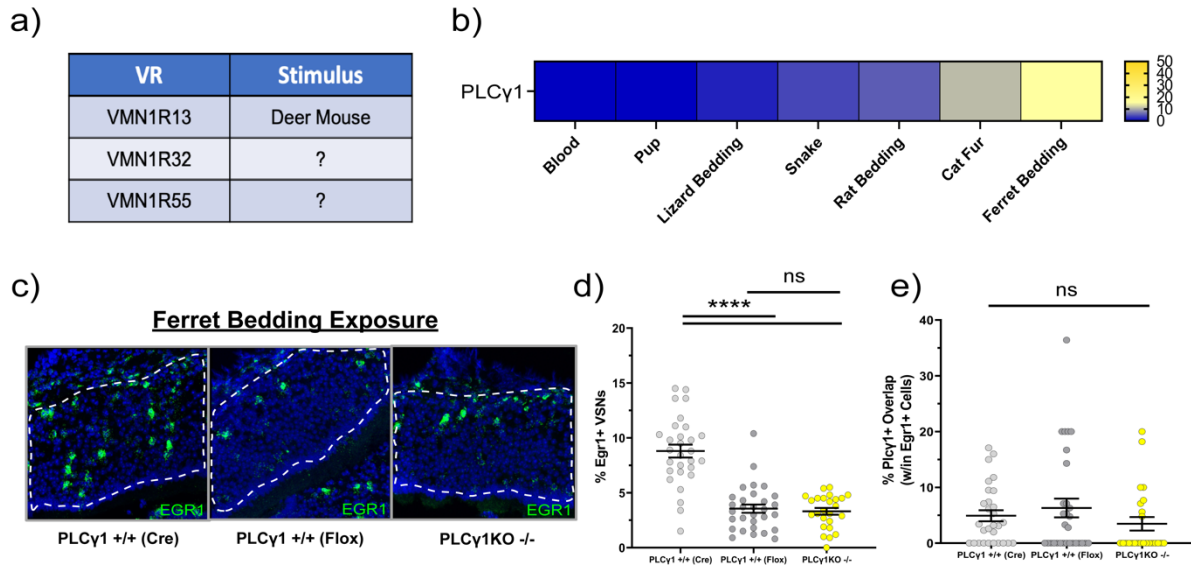


**Figure 1.27. Removal of the PLC $\gamma$ 1 PIP<sub>2</sub>-binding domain does not affect ferret bedding-mediated VNO activity.**

Mice were exposed to the *PLC $\gamma$ 1*-enriched stimuli ferret bedding to assess effects of PLC $\gamma$ 1 knockout. **a**, Single cells from a deep scRNAseq VSN dataset. Pheromone receptors expressed in cells co-expressing *PLC $\gamma$ 1* (left) and predicted stimulus (right) are shown. **b**, Heatmap of *PLC $\gamma$ 1* overlap with cells responding to various stimuli. Columns denote stimuli types, n=2-3 mice with 30+ *EGR1*+ cells per square. **c**, Representative cell masks of PLC $\gamma$ 1, OMPcre (left), PLC $\gamma$ 1Floxed (middle), and PLC $\gamma$ 1 mutant (right) mice following exposure to ferret bedding. **d**, Quantification of the dataset underlying C, n=30-35 ROI across 3 mice per group. Kruskal-Wallis test, p<.0001. **e**, *PLC $\gamma$ 1* overlap with the *EGR1* cells found in D. Kruskal-Wallis test, p=.2809.

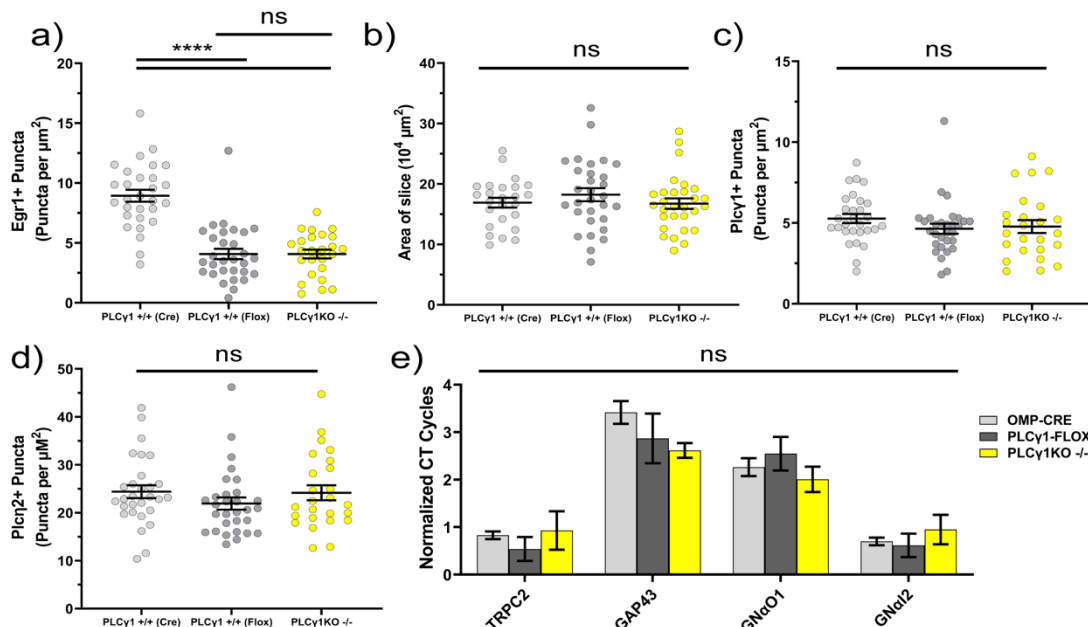


**Figure 1.28. PLC $\gamma$ 1 phenotype is not due to technical, developmental, or population ratio concerns.**

Controls for Figure 1.27. **a**, Quantification of 1.27d using only overall *EGR1* puncta number. Kruskal-Wallis test, p<.0001. **b**, Area comparison between PLC $\gamma$ 1 wildtype control and mutant animals in Figure 1.27. One-way ANOVA, p=.4612. **c**, *PLC $\gamma$ 1* puncta comparison between PLC $\gamma$ 1 wildtype control and mutant animals in Figure 1.27. Kruskal-Wallis test, p=.1709. **d**, *PLC $\eta$ 2* puncta comparison between PLC $\gamma$ 1 wildtype control and mutant animals in Figure 1.27. Kruskal-Wallis test, p=.1688. **e**, qPCR quantification of VSN population markers. n=3 mice per group. Multiple Mann-Whitney U tests with Holm-Sidak correction used. Adjusted p-values are as follows: TRPC2, p=.870; GAP43, p=.870; GNaO1, p>.999; GNaI2, p>.999.

## 1.8 The VNO expresses hormone recognition machinery

The above findings highlight a surprising source of variation in VSN signal transduction, yet the utility of such variation is unclear. Individual PLC subtypes differ functionally<sup>69</sup>, thus may form vomeronasal signal transduction cascades with divergent functions. Our data shows that each subtype has a unique expression pattern, further suggesting that they play disparate functional roles. One key difference between subtypes is that they can be differentially phosphorylated with unique impacts on activity<sup>66,69</sup> (Figure 1.6), which provides signal transduction pathways with unique capacities for modulation – indeed, previous studies have shown that VSN activity can vary across different hormonal states<sup>65,124</sup>, and that such variation can be mediated by direct, hormone-driven phosphorylation and subsequent silencing of PLC $\beta$ <sup>2</sup><sup>65</sup>. State-specific PLC phosphorylation would allow social and predator cue sensation to be context-specific, and would functionally differentiate the vomeronasal system from other senses. However, in order for modulation to be possible, the VNO must be able to respond to a range of hormones. To determine the VNO's capacity to sense hormones, we first assessed how many hormone receptors (HRs) were expressed on each cell. We found that most VSNs express at least two hormone receptors (Figure 1.29a), indicating a widespread and diverse capacity for hormone responsiveness. Next, we sought to determine a list of “best hormone receptor candidates”. Starting with a list of ~200 potential receptors, each HR was tested statistically and by manual inspection for bimodal expression, which was able to separate genes expressed in a cell subset (e.g., *Gnao1*) from globally-expressed genes (e.g., *OMP*) and rarely-expressed genes (e.g., specific *VRs*) (Figure 1.29b). Any candidate found to be bimodally distributed by several measures (see Methods) was chosen as a “candidate” for HR expression. Fifteen hormone receptors across several hormone classes passed our stringent criteria (Figure 1.29c), suggesting that the VNO can sense hormone changes across many different states. Several candidates have

been validated through the literature<sup>65,124</sup>, and some more-sparsely expressed HRs may remain currently undetected. Our candidate hormone receptors are found reproducibly in bulk RNAseq of both male and female mice (Figure 1.29d), suggesting that hormone responsiveness or at least its machinery is integral to mouse VNO structure.

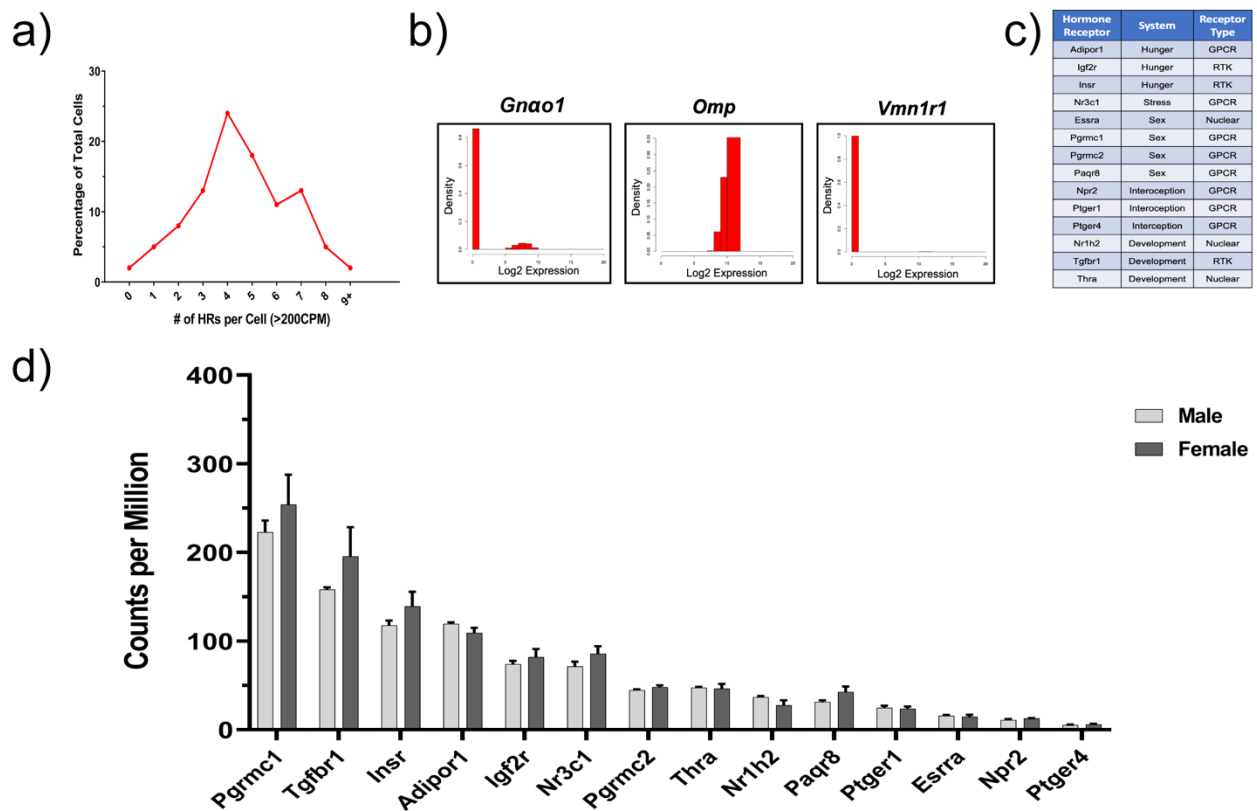


**Figure 1.29. The VNO expresses multiple types of hormone receptors.**

**a**, Quantification of deep scRNAseq mVSN dataset. The number of HR subtypes expressed per cell was quantified for each VSN and totals were tallied throughout the entire dataset and represented as a percentage of total VSNs **b**, Cumulative frequency charts showcasing ability to detect distinctly-expressed cell types, including one positive control (*Gnao1*, left) and two negative controls (*Omp*, middle and *Vmn1r1*, right). **c**, The 14 hormone receptors detected as bimodally-expressing in a deep scRNAseq mVSN dataset. **d**, Abundance of HRs from a published VNO bulk RNAseq dataset<sup>102</sup> containing adult male and female data. HRs are organized from most to least abundant, n=3 animals per group.

## 1.9 Intra-stimuli VSN activity varies between animals

If widespread hormonal modulation is possible in VSNs, we expect activity to vary between different states. This has been shown previously – activity can vary based on parental status<sup>124</sup> or estrus stage<sup>65</sup>. Interestingly, even mice in our *EGRI-PLC* panel, which are exposed with parallel methods, at the same time, and with the same stimulus, have highly variable activity

(Figure 1.30). Whether this variation stems from internal state differences or direct effects on VSNs is not yet clear, but it does suggest that VSN activity is particularly variable. Determining the extent of this effect, and if activity correlates with PLC content, will help clarify the purpose of signal transduction variation in the VNO.

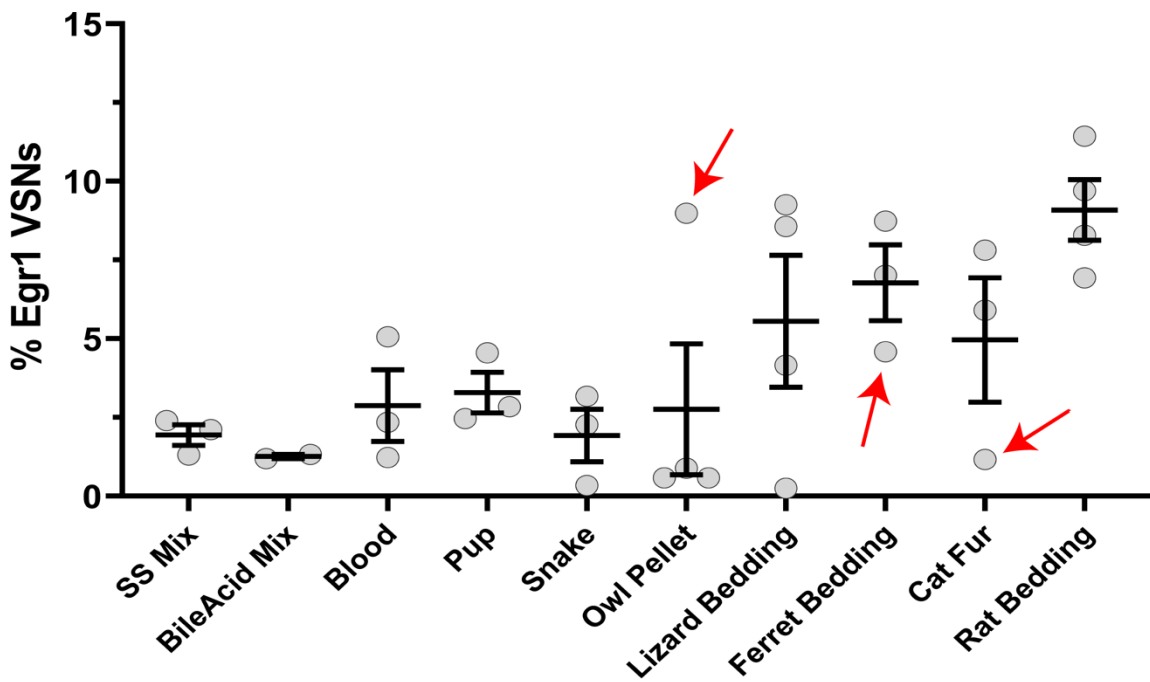


**Figure 1.30. VSN activity varies between individuals.**

*EGR1* quantification of dataset underlying 1.19c. Each circle represents one mouse. Note that activity varies widely within one stimulus type. Arrows denote mice with very different activity to a given stimulus compared to others in the group.



## DISCUSSION

Sensory systems typically use one primary signal transduction cascade<sup>1</sup>, and the vomeronasal organ is thought to follow this model as well<sup>11-13</sup>. Here, we show that the VNO follows a unique mechanistic model where signal transduction, as well as ligand detection, is varied, such that the VNO signals through multiple signal transducers. In addition, the three tested PLC $\beta$ s have largely discrete expression with different expression levels (abundance) and patterns (spatial distribution and stimulus-overlap), indicating that they are not interchangeable and likely exhibit distinct functions in VNO. The effect of PLC $\beta$ 4 knockout on VSN activity is unexpected, as PLC $\beta$ 4 is not known to pair with the G-alpha proteins found in the VNO<sup>47,77,78</sup>; single cell RNAseq analysis suggests that *PLC $\beta$ 4*<sup>+</sup> cells do not express a PLC $\beta$ 4-specific subunit (personal observation), so this finding may represent a previously unreported mechanism of activation for PLC $\beta$ 4. Interestingly, while PLC $\beta$  subtypes form signal transduction cascades in the VNO, *PLC $\beta$ 1* is not expressed in VSNs despite functioning in neurons<sup>101</sup>. This, in addition to the three remaining PLC $\beta$ s residing in disparate genomic locations<sup>72</sup>, suggests that their use is not a PLC $\beta$ -centric accident of expression but instead is or was of evolutionary advantage to the system and the animal at large. In total, our data updates the vomeronasal system signal transduction model, as well as our global understanding of sensory systems.

### ***The extent of signal transducer variation***

While PLC $\beta$  signaling controls some vomeronasal signaling, much activity remains unexplained. PLC $\beta$  mutation rarely eliminated all stimuli-evoked activity (Figure 1.10, 1.20, 1.22, 1.23), and no stimuli's activity was fully accounted for by PLC $\beta$  subtype overlap (Figure 1.19), indicating that more signal transduction cascades can be uncovered. As ten PLC subtypes are expressed in the VNO but few could be rigorously tested, one or more of the remaining

subtypes likely underlie the unexplained VSN activity. Of the seven subtypes remaining, only two could feasibly interact with GPCRs: PLC $\epsilon$ 1<sup>81,82,84</sup> and PLC $\eta$ 2<sup>85</sup>. PLC $\epsilon$ 1 mutation provides no clear effect on VSN activity (Figure 1.25). PLC $\eta$ 2 is abundant in the VNO<sup>65</sup> yet knockout mice have no clear phenotypic abnormalities<sup>125</sup>, making a signaling function unlikely. Despite these data and observations, we cannot yet definitively exclude PLC $\epsilon$ 1 and PLC $\eta$ 2. There may be compensation by a yet unknown signal transducer, or PLC subtypes may function in cells that cannot be activated. Indeed, we cannot currently prove that a subtype is not involved in primary signaling given the difficulty of activating VSNs<sup>18,23</sup>. However, even if both PLC $\epsilon$ 1 and PLC $\eta$ 2 were functional in VNO, abundance data suggests that at least 20% of VSN activity would remain unaccounted for. Thus, either an unexpected PLC subtype or a previously-undetermined signal transducer function in the vomeronasal system.

Most of the remaining PLC subtypes can be invalidated through literature review. PLCL1 and PLCL2 do not express the domain that allows for PIP<sub>2</sub> interaction and are not known to generate small messengers in vitro<sup>74,75</sup>. PLCXD3 likewise expresses only half of the catalytic domain and has not exhibited functional activity in vitro<sup>73</sup>. PLC $\gamma$ 1 is activated by RTKs<sup>84</sup> making interaction with sensory GPCRs unlikely, and removal of PLC $\gamma$ 1 PIP<sub>2</sub>-binding capacity activity did not have an effect on VSN activity. While PLC $\eta$ 1 is not known to interact with G-proteins<sup>85</sup>, research on PLC $\eta$ 1 has been scarce so *EGR1* experimentation in VSNs is warranted.

Not all VSNs express a *PLC* subtype. Both scRNAseq and FISH analyses reveal a substantial proportion of “*PLC*-less” VSNs (30% and 15% respectively, Figure 1.12). While this may be due to technical variables, the literature supports the existence of a non-PLC signal transducer in the vomeronasal system. Initial experiments confirming PLC’s role in the VNO used urine<sup>11-13</sup> which activates only a fraction of VSNs<sup>23,65</sup>, and the continued inability to

activate all VSNs makes validation of a entirely PLC-dependent mechanism impossible. Logic rather than data asserts PLC's exclusive importance in VSN signaling. VNO's critical cation channel TrpC2<sup>59,60</sup> interacts with DAG and calcium<sup>61</sup>, with the former only generated by PLCs<sup>56</sup> and the latter invalidated as a primary activation source of VSN activity<sup>58</sup>, though activation difficulties may likewise mask a calcium effect. Studies suggest TrpC2-independent activation of VSNs is possible<sup>126,127</sup>, which allows signal transducers that do not release DAG to play a role in vomeronasal signaling. Despite the implications of this data, the existence of PLC-independent signaling must be confirmed experimentally before signal transducer search can continue.

Also noteworthy is the portion of cells that express multiple PLCs. While not as common as discretely-expressed PLCs or "PLC-less" VSNs, these cells may represent further signaling variation. PLC subtypes express together in other organ systems and can act synergistically to transduce signals<sup>108</sup>, allowing for modulation of signal length<sup>109</sup> or strength<sup>128</sup>. As such, each specific PLC subtype combination may represent a unique signal transduction cascade. PLC $\beta$  subtypes overlap in certain VSNs (Figure 1.24d), potentially increasing the number of verified VSN signal transduction cascades.

PLC $\epsilon$ 1 Sensory systems typically use various GPCRs to capture information from the external sensory environment and a primary signal transduction pathway to convert activity into a common language<sup>1</sup>. Here, we show that the vomeronasal system uses a different strategy, employing several signal transducers to transmit information to the brain. Why VSNs would adopt a method that could make brain-bound information difficult to interpret is unclear. Individual PLC $\beta$  subtypes differ drastically<sup>69,72</sup>, interacting with different binding partners and with various speeds and strengths<sup>77,78</sup>. Given this, it is likely that PLCs do not just function in different VSNs, but form vomeronasal signal transduction cascades with divergent functions.

What is the utility of having several distinct signal transduction cascades in the vomeronasal system? Given the importance of the vomeronasal system in mice, it is extremely unlikely that signal transduction variation would only harm the system – any deterrent to pheromone detection would impair crucial social behaviors and so be under strong evolutionary pressure. There is likely a benefit to counter the possible downsides of expressing multiple signal transducers, which include noisier signals and more complex developmental programs. This benefit could be due to PLC variation itself or genetic hitchhiking with a related beneficial trait. The latter, though not disproven, is unlikely. There is no chromosomal proximity between the three expressed PLC $\beta$ s<sup>72</sup> and common vomeronasal machinery (G-proteins<sup>77,78</sup>, pheromone receptors<sup>28,29</sup>, or TrpC2<sup>59,60</sup>), and no recorded interaction between their expressions<sup>129,130</sup>. Further, PLC $\beta$ 1 and PLC $\beta$ 4 are proximal on chromosome 2<sup>72</sup> yet only the latter is expressed in VSNs, suggesting that there is no link between PLC chromosomal location and function. However, we cannot exclude the possibility that signal transducer variation is a byproduct of genetic hitchhiking with a known or unknown important VNO function.

On the other hand, the inherent functional differences between the PLC $\beta$ s<sup>69</sup> may confer a direct benefit. These functional differences likely introduce variability to VSN activity; indeed, vomeronasal sensory responses are variable between and within studies, with resting potentials and response strengths differing between neurons<sup>131-133</sup>. Given that PLC subtype expression is logically patterned in the VNO, a possible benefit of signal variation may be the introduction of new information to pheromone sensory signals. Here, variation would allow for one sensory message to contain both receptor-generated stimuli-specific information and PLC $\beta$ -mediated stimuli class-specific information.

How the brain makes sense of vomeronasal signaling is a mystery<sup>23</sup>. Receptor information

has not been sufficient to understand brain signals or ensuing behavior. While several direct receptor-to-behavior links exist<sup>34-36</sup>, stimuli typically activate multiple receptors<sup>18,23</sup>; in addition, the VNO's ~350 receptors would be redundant if a handful carried all relevant information. The V1R-V2R split, while well-studied, has not provided many clues. These two receptor families do not effectively split stimuli by class or behavioral relevance<sup>18,35,43,65,134</sup>; for example, snake and male mouse urine both activate V2Rs<sup>18</sup> yet have different ethological meanings and elicit different behavioral responses<sup>135,136</sup>. This suggests that there is an unknown classification factor, in between the granular receptor and global receptor family classifications, that differentiates stimuli in brain-bound sensory messages. The PLC $\beta$ s could provide such a classification factor. These PLC subtypes do appear to segregate stimuli more accurately than receptor families, with V2R+ predator stimuli co-expressing higher with PLC $\beta$ 4 and lower with PLC $\beta$ 2, while V2R+ conspecific stimuli shows the reverse expression pattern (Figure 1.19). This may provide both a molecular handle on certain VSN types and an important hint about how the brain makes sense of incoming pheromone signals – however, further investigation into the sensory and behavioral effects of PLC $\beta$ 2 versus PLC $\beta$ 4 knockout is needed to confirm this hypothesis. We note that, while PLC subtypes do appear to segregate stimuli more finely than receptor families, this split is not completely clean. What these anomalies represent is not yet clear, and profiling more stimuli may help reveal the extent of PLC-stimulus patterning.

PLCs differ in their capacity for and response to phosphorylation. PLCs can be phosphorylated and said phosphorylation can impact its activity depending on phosphate location and subtype identity<sup>66,86-98</sup> (Figure 1.6). In PLC $\beta$  subtypes, phosphorylation is typically used for negative feedback, with DAG activating PKA/PKC and so leading to the inhibition of PLC activity<sup>89</sup>. However, phosphorylation can also allow molecular pathways to crosstalk<sup>66,89,138</sup>. The

PLC $\beta$  subtypes have unique responses to phosphorylation – only PLC $\beta$ 2 and PLC $\beta$ 3 respond to phosphorylation<sup>79,89-93</sup>, and PLC $\beta$ 2 and PLC $\beta$ 3 have different inhibition types (e.g., inhibiting G $\beta$  $\gamma$  versus G $\alpha$ q interaction), phosphorylation sites, and phosphorylation partners<sup>89-93</sup>. As such, expressing different PLC $\beta$ s could give VSNs different “phosphorylation-capacities”, and so various capacities for crosstalk between the sensory signaling cascade and other molecular pathways occurring within the cell.

PLC phosphorylation has been reported in the vomeronasal system, with crosstalk occurring between pheromone signaling and hormone signaling. PLC $\beta$ 2 is phosphorylated and silenced by the membrane-bound hormone receptor *Pgrmc1*<sup>140</sup> during progesterone-rich mouse diestrus<sup>139</sup>, inhibiting male urine-evoked VSN activity and typical mating behaviors<sup>65</sup>. A hypothetical utility for various signal transduction cascades in VSNs, then, may be unique capacities for hormone-driven modulation. In this model, PLCs would act as the node of interaction between sensing external state (through pheromone receptors) and internal state (through hormone receptors), allowing for activity and behavior to be shaped in a context-appropriate way. Indeed, VSNs express more hormone receptors than *Pgrmc1* (Figure 1.29c-d), and another instance of hormone-mediated VSN activity modulation has since been reported<sup>124</sup>. Here, each PLC subtype would provide stimuli with specific modulation capacities; for example, predator-biased PLC $\beta$ 4+ VSNs may be modulation-resistant and so allow predator activity to remain constant despite internal states. This hypothesis assumes that pheromone activity is highly individualized, which we see in our *EGR1*+ VSN data (Figure 1.30). Despite the circumstantial evidence pointing towards this hypothesis, we note that several tests are still needed to validate it. We do not know how many states VSNs respond to, if PLCs are phosphorylated in different states, and if such PLC phosphorylation causes VSN activity change. To answer these questions,

development of high-throughput tools for assaying VSN activity, identifying PLC phosphorylation status, and manipulating PLC phospho-sites will be needed.

### ***The utility of non-primary signaling PLCs***

While ten PLC subtypes are expressed in the VNO, many subtypes have no currently understood use. While some subtypes may not be used at all – protein expression is not yet confirmed and mRNA does not always equal utilized protein<sup>141</sup> – the patterning exhibited suggests uses for many. Catalytic PLCs are thought to belong to two functional groups: primary and secondary<sup>108</sup>. The former, which includes PLC $\beta$  and PLC $\gamma$ , mediates extracellular signals directly; the latter, which includes PLC $\epsilon$ , PLC $\delta$ , and PLC $\eta$ , help amplify signals generated by other signal transducers. While we do not yet know if the seven remaining PLCs have direct signalling function in VSNs, these subtypes may serve different purposes. Here, we will postulate roles for the two PLCs we believe to have a non-primary signaling role, PLC $\gamma$ 1 and PLC $\epsilon$ 1. The remaining PLC subtypes (PLC $\eta$ , PLCL, and PLCXD) must be tested before we can hypothesize about potential VNO utilities.

PLC $\gamma$ 1 is a primary PLC<sup>108</sup> and may function in neurons<sup>122</sup>, so we ran a functional assay on a PLC $\gamma$ 1-mutant mouse line<sup>123</sup>. Removal of the PLC $\gamma$ 1 PIP<sub>2</sub>-binding does not affect VSN activity, yet insertion of Flox sites does (Figure 1.27c-e), suggesting an important PLC $\gamma$ 1 function unrelated to sensory signaling. The reduction shown is much more than the expected PLC $\gamma$ 1 overlap would suggest (Figure 1.27b) and affects many more cells than PLC $\gamma$ 1 is expressed in (Figure 1.12), hinting at a non-specific effect. PLC $\gamma$ 1 has a well-known role in neural growth and development. The subtype is widespread throughout the brain<sup>122</sup> and has been implicated in neurite outgrowth, axon targeting, and synaptic formation<sup>142-144</sup>. It also can interact with BDNF and growth hormones through RTKs such as EGFR. Perhaps the seen *EGR1*

depletion is due to a global effect on VNO's structure, cell groups, or overall patterning. However, we did not see differences in VNO size, mature neuron number, or the ratio of V1R versus V2R groups in floxed-PLC $\gamma$ 1 or PLC $\gamma$ 1-KO mice (Figure 1.28b-e). Relatedly, PLC $\gamma$ 1 interruption may affect *EGR1* expression itself. PLC $\gamma$ 1 manipulation has been shown to affect IEG expression in vitro, although individual studies draw opposite conclusions on the effect's direction<sup>145,146</sup>. Testing with a non IEG-mediated assay is necessary to disprove the possibility that PLC $\gamma$ 1 is disrupting *EGR1* directly. PLC $\gamma$ 1 interacts with hormone receptors, including RTKs and select GPCRs<sup>79,147</sup>, to generate DAG and IP<sub>3</sub>. VSNs express many hormone receptors, including several RTKs<sup>65,124</sup> (Figure 1.29c-d) - PLC $\gamma$ 1 signaling may occur with non-VR receptors or RTKs, which would be missed in our *EGR1* assay. One intriguing candidate is insulin receptor, which is expressed in >30% of VSNs and signals through the PLC $\gamma$ s<sup>148</sup>. While our results suggest that PLC $\gamma$ 1's role is more fundamental, further tests are needed to exclude this possibility.

PLC $\epsilon$ 1 is unique in its ability to act as both a primary and a secondary PLC<sup>108</sup> and can be activated by G-proteins<sup>81,82,84</sup>. However, our data suggests that PLC $\epsilon$ 1 does not play a signaling role in the VNO, though this may be due to technical factors. As a secondary PLC, PLC $\epsilon$ 1 can operate downstream of many signaling cascades and so allow crosstalk between various signaling paths<sup>80-84</sup>. In one study, PLC $\beta$  knockdown in fibroblasts deterred initial IP<sub>3</sub> creation after receptor activation (<30 seconds), while PLC $\epsilon$ 1 knockdown in the same cells affected prolonged IP<sub>3</sub> creation (up to 60 minutes)<sup>109</sup>. PLC $\epsilon$ 1 could play a similar role in VSNs, operating downstream of another signal transducer to change the intensity or duration of signals, although we note that PLC $\epsilon$ 1 is expressed alone in some cells (Figure 1.15d). PLC $\epsilon$ 1 can also function as a guanine-exchange factor (GEF), activating small GTPase pathways downstream of receptor activation<sup>80,81</sup>.



Small GTPase cascades are typically associated with neural growth and differentiation<sup>149</sup>, which is unlikely given that PLC $\epsilon$ 1 is specific to mature VSNs (personal observation). Still, PLC $\epsilon$ 1 may signal through a small GTPase cascade not associated with growth. Finally, PLC $\epsilon$ 1 functions downstream of several hormone receptors including the beta-adrenergic receptor<sup>119</sup>, which is expressed in total VNO<sup>102</sup>. As with PLC $\gamma$ 1, experimentation is needed to evaluate the possible roles for PLC $\epsilon$ 1 hypothesized above.

### ***PLC patterning mechanisms***

PLC subtypes form a striking spatial bias in VNO across VR families and stimuli types. While the potential use of this patterning has been previously discussed (see “The utility of primary signaling PLCs”), how this patterning occurs is unknown. As mentioned above, expression patterns do not correlate with genetic location or PLC subtype<sup>72</sup>, suggesting a more complex mechanism. A logical hypothesis is that PLCs are patterned by a similar mechanism as Gna $\alpha$ 2/ Gna $\alpha$ 1 VSN groups. How the V1R/V2R split occurs largely remains a mystery, though several key transcription factors have been identified<sup>50</sup>. Analysis of PLC patterning in relevant transcription factor knockout mice would provide critical clues. However, as PLC patterning goes beyond the V1R/V2R split, more than these known TFs would likely be involved. MicroRNAs are another potential culprit - these small noncoding RNAs have been shown to affect main olfactory development<sup>150-151</sup>, though effects in mature OSNs or immature/mature VSNs have not been reported<sup>150</sup>.

### ***Revising the sensory signaling model***

The data presented represents a substantial revision of traditional “receptor-centric” sensory signaling model<sup>1</sup>. Is this a VNO-specific departure? Knockout analyses suggest this, given that removal of one signal transducer can quiet large swathes of each modality<sup>2-7</sup>. Yet, it remains possible that unknown alternate signal transduction pathways exist in other senses -

whatever utility multiple signal transduction pathways confer to VSNs would likely apply to all senses. Interestingly, though variation in the primary signaling ADCY is largely absent in OSNs (Figure 15a,c), PLC signaling has been shown to modulate ADCY-dependent odorant responses in OSNs<sup>152-154</sup>. Indeed, many of the same PLC subtypes shown here are expressed in OSNs, and with similarly discrete expression (data not shown). However, studies do not address the scope of PLC modulation in OSNs, so further testing is required.

Conversely, one could argue that the VNO has always been unique. Unlike other sensory systems, the purpose of the VNO has never been clear<sup>155</sup>. The MOE has a similar role and a variety of social and olfactory-reliant species use only an MOE, calling into question the VNO's utility. Multiple signal transduction cascades and the functions this heterogeneity confers could be a key distinction between the VNO and the MOE. Determining the utility of signal transduction variation, then, may be of critical importance to understand the evolutionary origins of the vomeronasal system.

## MATERIALS AND METHODS

### Mice

All mice were c57BL/6J, 8-16 weeks, and males unless otherwise specified. For stimuli exposure, mice were group-housed until the time of exposure. For artificial sulfated steroid exposure, animals were single-housed for five days before exposure. Age-matched mice were used when possible, and mice within one experiment were always born within two weeks of each other. When possible, littermate controls were used. All genetic mouse lines used were of c57BL/6J background. The genetic lines for PLC $\beta$ 2KO<sup>99</sup> (#018016), PLC $\beta$ 3KO<sup>113</sup> (#109023), PLC $\beta$ 4KO<sup>114</sup> (#019024) and OMP-GFP<sup>100</sup> (#006667) mice were obtained from Jax laboratories. PLC $\epsilon$ 1KO<sup>121</sup> mice were kindly donated by Dr. Alan Smrcka and were tested in his laboratory. PLC $\gamma$ 1-Flox<sup>123</sup> mice were kindly donated by Dr. Florian Heidel and were crossed to OMP-Cre mice<sup>156</sup> from Jax (#006668) for olfactory-specific knockout.

### Estrus staging

All adult female mice used (Figure 1.10d, 1.24c, 1.25, 1.26; half of each of these datasets were generated from female mice) were staged prior to stimulus exposure to assure equal internal state. In order to stage mice, females were lightly scruffed and subjected to vaginal lavage as previously described<sup>65,139</sup>. Estrus stage was determined as previously described. Females were assayed over four days to ensure proper cycling before use. Staging was done at least four hours before odor exposure to avoid staging-generated stress. Mice were always taken in estrus to avoid the reported diestrus-specific deficits in pheromone sensation<sup>65</sup>.

### Stimulus Exposure

All exposures occurred in one of two clean, quiet locations, one for conspecific stimuli and one for predator stimuli. Counters were washed with 70% ethanol and a deodorizer before stimulus exposure. Only three animals were exposed at a time, and all exposure groups were

exposed to the same stimulus. Gloves are changed between each mouse exposure. Exposures were staggered by ten minutes each to allow for dissection time. Mice are exposed for 40 total minutes before euthanasia and VNO dissection (see “Tissue Collection”). All mice were assayed between 6pm-12am on a regular light cycle.

Prior to exposure, mice were transferred into a fresh cage and habituated for 120 minutes. For mouse bedding and stimulus mix exposures, mice were transferred to a stimulus-lined cage. For all other stimuli, exposure occurred in the habituation cage. For blood, mouse urine, S.S. Mix, S.A.E mix, and B.A. Mix, mice were exposed by pipetting liquid stimuli onto a clean 1' by 1' blotting paper that was placed into the cage for exposure. Animals were observed from across the room until the mouse nose had contacted the stimulus or bedding for at least three seconds, at which point the exposure period began. For stimuli mix exposure, stimuli were presented in a pseudorandomized order (conspecific before predator) to ensure proper sampling.

In order to control for potential differences in baseline exploration, PLC $\beta$ 3KO and PLC $\epsilon$ 1KO functional experiments were performed by nasally-injecting experimental animals. Mice were habituated to handling and nasal injection for five days prior to experiments. Nasal injection was performed by scruffing and dotting 5 $\mu$ L of liquid on each nostril (PBS for habituation, stimulus for experiments). On the day of experimentation, mice were scruffed and 5 $\mu$ L of stimulus was dotted onto each nostril. Nasal injection was always completed within 90 seconds of scruffing. Exposure time started as soon as stimuli were applied to both nostrils. Individual stimulus aliquots were used to avoid contamination between animals. PLC $\beta$ 4 mutant mouse exposure was done in pups (P10-P20), as PLC $\beta$ 4 mice occasionally fail to thrive<sup>114</sup>.

## Stimuli

For all solutions other than mouse urine, 50 $\mu$ L was used for blotting paper exposure and 10 $\mu$ L was used for nasal-injection exposure. For mouse urine, 100 $\mu$ L was used per exposure. For solid stimuli, mice were exposed to 50mL of predator stimuli (rat bedding, cat fur, and lizard bedding) or 200mL (mouse bedding). For snakeskin, one 3' by 3' square was used. For ferret bedding, one corner of a ferret's soiled blanket was used. For owl pellet, one pellet was used. For pup, one mouse P3-P8 was used, and was removed once pups signaled distress. All predator stimuli were used within one week of collection. Blood, mouse bedding, and urine were collected within one hour of exposure. Sulfated steroid and bile acid mixes were created fresh from powder on the day of assaying. Stimulus mix consisted of rat bedding, lizard bedding, cat fur, snakeskin, male mouse bedding, female mouse bedding, B.A. Mix, S.S. Mix, and blood. All non-pup stimuli were stored at 4°C until 30 minutes before exposure to ensure volatile movement.

Mouse urine was collected and combined from three 2–4-month-old Balb/C animals from multiple cages. HMW and LMW urine fractions were generated from total male urine as previously published<sup>65</sup>; LMW flowthrough was used undiluted, while HMW was diluted to a 20mg/mL concentration. Mouse bedding including fecal and urine samples was collected from two strains (c57BL/6J and Balb/C) of the desired sex after at least three days of soiling. Blood stimuli was collected from at least three freshly-euthanized P3-P8 pups. Corn snakeskin was collected from a local pet store and sliced into 3' by 3' squares. Owl pellets were purchased from Amazon.com (<https://tinyurl.com/BarnOwlPellet>). Cat fur was collected from the neck and body of cats owned by either Stowers lab members (Jingyi Chen, initial experiments) or neighboring lab members (Ardem Patapoutian, final experiments). Rat bedding including fecal and urine samples was collected from soiled male Sprague Daley rat cages after at least three days of soiling. Lizard bedding including fecal and urine samples was collected from a blue tegu in a

local pet store, and any mouse remains were tossed before use. Ferret bedding stimuli was donated by a local ferret owner (CLIFFnotes@legalizeferrets.com) and consisted of blankets slept on by ferrets for at least three days. For sulfated steroid mix exposure, five sulfated steroids (Steraloids) representing different hormone groups were combined (E0893, E2473, Q1570, Q5545, A7864). For sulfated androgen estrogen mix, E0893 and A7864 were combined. Sulfated steroids were mixed together in PBS and used at 40 $\mu$ M. For bile acid mix (Sigma Aldrich), four bile acids (CDCA, DCA, CA, LA) were mixed in a 100 $\mu$ M 1:1000 MeOH-PBS solution, as previously described<sup>38</sup>.

### **Tissue Collection and Preparation Cutting**

Mouse were euthanized 40 minutes after stimulus exposure using isoflurane. VNOs were dissected and placed in cold 1x RNase-free PBS. VNOs were quickly removed from cartilage and frozen in OCT by placing into an ethanol and dry ice slurry, then put into -80°C for storage. VNO tissue was sliced on a cryostat at 16 $\mu$ M, with 1-3 VNOs on each slide. Slices were taken from the medial VNO across 5-7 slides, were taken in series, and were taken with 10-15 slices per VNO per slide. For functional experiments, each slide contained at least one wildtype and one mutant VNO. Tissue was stained within one year of slicing.

### **FISH Staining (RNAscope)**

*In situ* hybridization was done using the RNAscope<sup>157</sup> Multiplex v2 kit. The standard ACD protocol was followed with certain VNO-specific modifications. Briefly, VNO slides were placed directly into fresh, chilled 4% PFA (EMS) in 1x PBS (Gibco) for 15 minutes, followed by 3x PBS wash. VNO slides were then dehydrated in 50% EtOH, 70% EtOH, and 100% EtOH for only two minutes each to avoid background. Slides were treated with H<sub>2</sub>O<sub>2</sub> at room temperature for ten minutes followed by washing. Slides were then treated with Protease IV for five minutes followed by washing – VNO ISH does not typically require protease digestion<sup>18</sup> - and probe

mixes were placed on slides. Each slide was covered with 300 $\mu$ L of probe mix. PLC probes were diluted to 1:3 of suggested amount while non-PLC probes were diluted to suggested amount (this decreases background while not affecting signal, Figure 1.31). All tissues were washed 3x in wash buffer after each step. Tissues were treated with separately purchased DAPI (Sigma Aldrich) for five minutes, after which slides were rinsed with H<sub>2</sub>O and mounted with Prolong Diamond Antifade Mountant (ThermoFisher). Slides were stored in 4°C and imaged within three weeks. For assays using more than three channels, a modified version of the ACD RNAscope Hiplex kit was used. All pretreatment modifications were retained for VNO slides, and the standard protocol was followed after pretreatment. After fluorophore mix was applied, autofluorescence quencher (Vector Labs) was used as directed to reduce background. Slides were imaged within 24 hours of each round's completion.

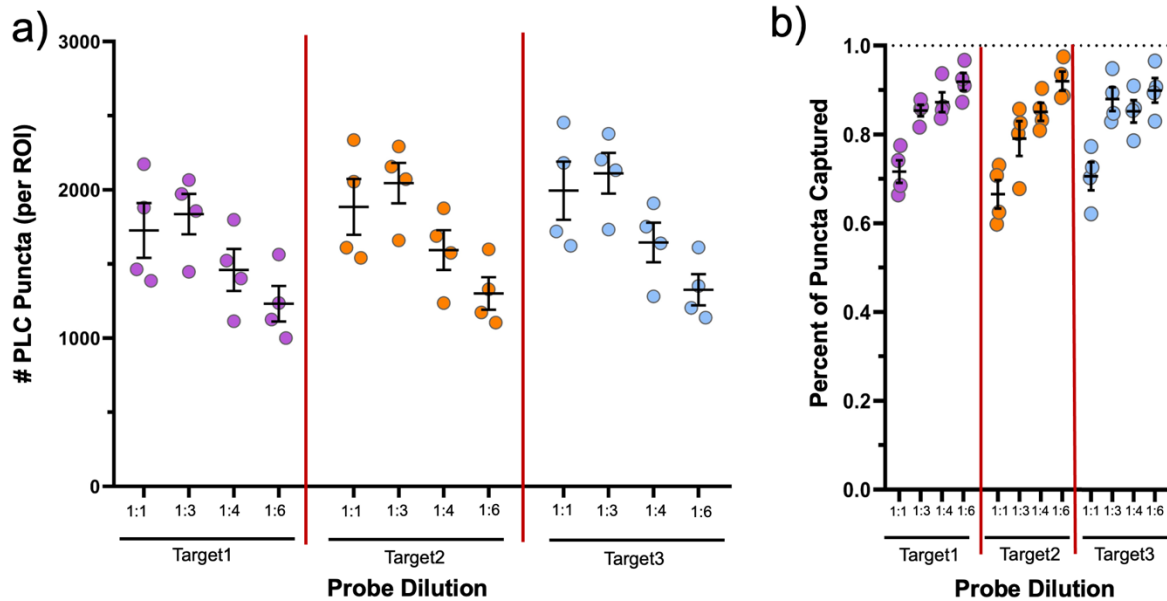


**Figure 1.31. Probe dilution can be done to remove noise yet retain signal.**

**a**, Quantification of the amount of target+ puncta are captured with different puncta dilutions. **b**, Quantification of the amount of probe information within 1 $\mu$ M of the nucleus with different probe dilutions. Each circle represents one ROI.

### RNAscope probes

Probes were tested in positive control tissues before use (Figure 1.32), with the exception

of already-validated VNO targets (*OMP*, *Gnao1*, *Gnai2*, *VRs*, *EGR1*, *PLCβ2*) and those not in brain (*PLCε1* and *PLCL2*); positive control tissues were assessed by eye and compared to Allen Brain Atlas ISH images<sup>120</sup>. For *EGR1*, the probe used was designed to target VSN-specific *EGR1* transcripts, using data from RNAseq for design. For knockout experiments, PLC probes were redesigned to avoid the interrupted mRNA region and so allow PLC transcript assay in mutant mice. All PLC probes used hit all known functional splice variants of the PLC subtype in question.

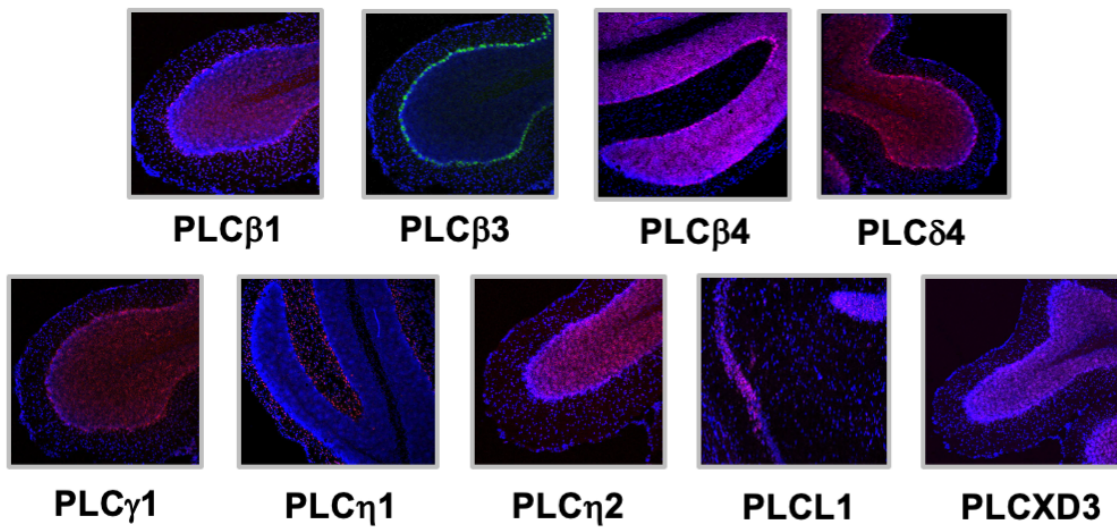


**Figure 1.32. PLC Probe controls.**

Positive controls for the PLC probes used in this study. All controls were tested in cerebellum, except for PLCL1 with was tested in hypothalamus.



## **Imaging**

All slides were imaged using a Nikon A1 Confocal Microscope. Quantified images were taken with a 40x oil objective, and certain visual representations and *EGR1* pilot studies were taken with a 20x air objective. Images with z-stacks were taken with a .5 $\mu$ M step size and with laser power below 5%. Laser power, gain and offset was adjusted as little as possible between images, with adjustments made to attain a similar LUT distribution (2-5 oversaturated pixels within the VSN layer). Lasers were stacked to speed up imaging, with the 405 and 568 channels stacked and the 488 and 647 channels stacked; at the laser power used, no bleed-through was detected. Hiplex images were manually adjusted along the XY axis to align with the region of previous imaging rounds.

## **Image Quantification**

Pilot *EGR1* experiments were quantified by eye and used a personally-generated approximation of 20x cell count to obtain percentage of *EGR1*+ cells (600 cells per slice). All other experiments were quantified using IMARIS Quantification (version 2.1.1). To quantify 40x images in IMARIS, the Cell or Surface tool was used to create cell masks, with cells always remaining between 200-500 in the IMARIS-generated "Quality" metric. The cell mask was either 1) edited entirely and manually (total *PLC* abundance, *OMP* overlap, *Gnao1* overlap) or 2) target+ cells were visually identified, edited manually, and all target- cells were deleted (*EGR1*+ data). For both types of masks, lamina propria and blood cells were identified by morphology and removed (Figure 1.33). Target-positive puncta were generated using the Spots tool and the computer's automatic Quality parameter, except when Quality was not between 100-400 (personal observations indicate that thresholds outside of this range represented inaccurate assessment). The Distance Transformation Matlab extension was used to filter out spots greater than 1 $\mu$ M from a cell nucleus, which captured >80% of data (Figure 1.34). The Vesicle Outside

Cell Matlab extension was used to assign the filtered puncta to their closest cells. Puncta within  $1\mu\text{M}$  of each cell were counted, and cells with puncta numbers past the pre-determined, target-specific “cutoff” were deemed as target-positive cells.

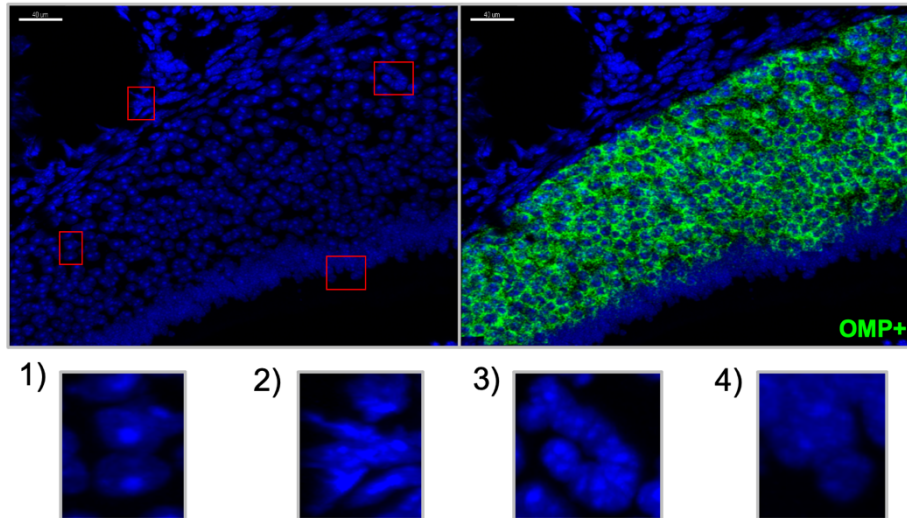


**Figure 1.33 – Morphology can be used to identify VSNs.**

A 40x image of the VNO sensory epithelium stained with DAPI (left) or DAPI and *OMP* (right) using FISH. Boxes circle different cell types, which include: 1) mature VSNs, 2) epithelial cells, 3) lamina propria cells, 4) sustentacular cells. Note that only #1 overlapped with *OMP*, confirming it as shows sensory neuron. Also note that cells can be easily distinguished based on morphology and nuclei number.

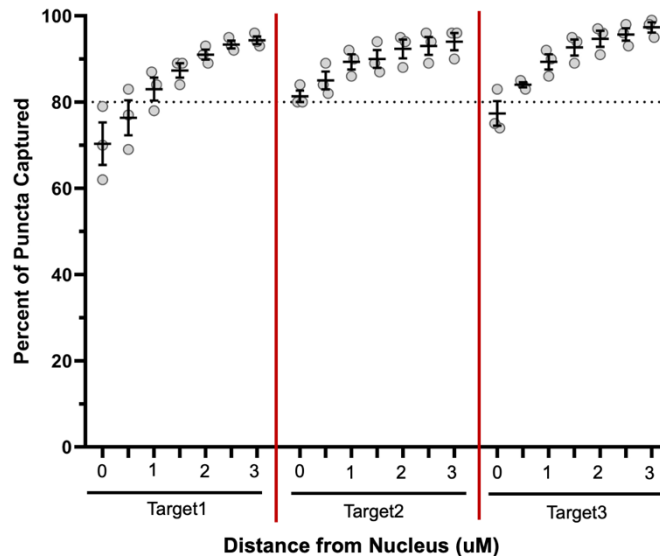


**Figure 1.34. Most data captured within  $1\mu\text{M}$  from cell nucleus.**

Quantification of the amount of target+ puncta are captured within certain distances from the cell. Note that over 80% of information is captured within  $1\mu\text{M}$  of the cell across three target types. Each circle represents one ROI.

Puncta cutoffs were generated to minimize false negatives where possible. The *PLC* puncta cutoff chosen was five, as it best matched existing RNAseq data (personal observation). Note that changing the cutoff does not change underlying conclusions of abundance groups or *Gn $\alpha$ 1* overlap (personal observation). The *Gn $\alpha$ 1* cutoff used was ten. This cutoff was chosen based on visual comparison of staining to puncta coverage. The *OMP* and *Gn $\alpha$ 2* cutoff was five. This is due to: 1) strong signals decreasing the quantifiable, punctate nature of the data, and 2) this staining partially fell outside of the nucleus (personal observation). The *EGR1* cutoff used was at eight. This cutoff was chosen based on matching stimuli to previously published *EGR1* staining<sup>18</sup>.

To determine percentages of target+ cells within VNO slices, the number of target+ cells was generated from ROI volume. Volume included only VSNs and was converted into an approximation of VSN number per ROI by dividing cell volume by 524, based on the observation that VSN diameters average 10 $\mu$ M in IMARIS (Figure 1.35). To assess puncta number per slice, puncta within 3 $\mu$ M of VSNs were counted, normalized to the area, and multiplied by 1000. To make representative cell masks, cell masks were created and cut, and cells positive for an individual target were pseudo-colored.

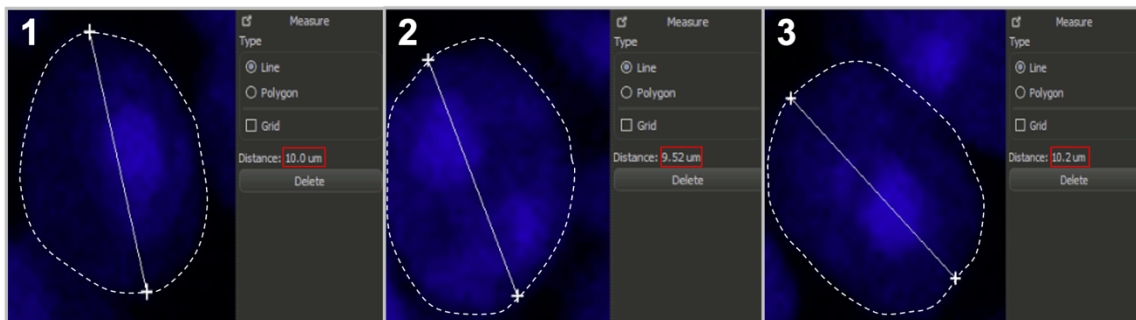


**Figure 1.35. Diameters of vomeronasal sensory neurons in IMARIS.**

## **Dataset Creation and Statistics**

For every dataset, at least three animals were used per group, with at least seven ROIs taken from five slices in each animal, as done in previous publications<sup>18,134</sup>. For *PLC* abundance data, at least 1000 total VSNs were assayed per subtype. For *Gnα1-PLC*, at least 100 PLC+ cells were used per subtype were used. For *EGR1-PLC* data, at least 50 *EGR1+* cells were used per mouse, stimulus, and *PLC* type. All data is represented as mean +/- standard error of mean (S.E.M.) unless otherwise stated. All statistics were completed using GraphPad Prism 6.0 software. Unless otherwise stated, the Shapiro-Wilkinson normality test was used to determine the nature of the data's distribution. For normally-distributed comparisons, a student's t-test (2 groups) or one-way ANOVA (3 groups) was used to evaluate significance. For non-normally distributed comparisons, the non-parametric Mann-Whitney U test (2 groups) or Kruskal-Wallis test (3 groups) was used to evaluate significance. For *Gnα1-PLC* data in Figure 1.18, Wilcoxon-Rank test were used to evaluate significance. For the z-score assessment of *PLC* groups, the z-score was between each datapoint (ROI) and group mean was generated using mean and standard deviation, then averaged for each *PLC* subtype combination.

## **FACs and PCR**

To isolate mature VSNs, three groups of three 10-week-old male and female mice OMP-GFP heterozygous mice had VNOs dissociated as previously described<sup>158</sup>. Briefly, VNOs were removed from cartilage in chilled RNase-free 1x PBS, then incubated in pre-heated papain (Worthington Biochemical) and minced for five minutes. VNOs were digested for ten minutes with trituration every five minutes. DNaseI (Roche) and 10% DMEM-FBS (Gibco) was added to stop digestion. The solution was added to a Optiprep density column (Sigma-Aldrich) and spun for 15 minutes. The cell suspension was washed in 10% DMEM-FBS and filtered through a cell

strainer tube (Fisher Scientific). Cell suspensions were stained in DAPI (Sigma Aldrich) and DRAQ5 (ThermoFisher) prior to sorting.

Cell suspensions were sorted in an MoFlo Astrios EQ (Beckman Coulter). Gates were set to eliminate doublets (forward- and side-scatter), dead cells (DAPI+ events), and debris (DRAQ5- events). The GFP gate was set as previously described<sup>105</sup>. Over 10000 GFP+ cells were sorted into Trizol (ThermoFisher). RNA was extracted using an RNA Microprep Kit (Zymo Research) and cDNA was created using SuperscriptIII (ThermoFisher). The OMP+ samples were PCR'ed for *PLC* subtypes and controls using Dreamtaq (ThermoFisher) and designed primers (IDT) created using primerBLAST<sup>159</sup>. Products were run on a 2% TAE gel for two hours at 100 volts. Controls were run to assess cleanness of sample and probe robustness (Figure 1.36).

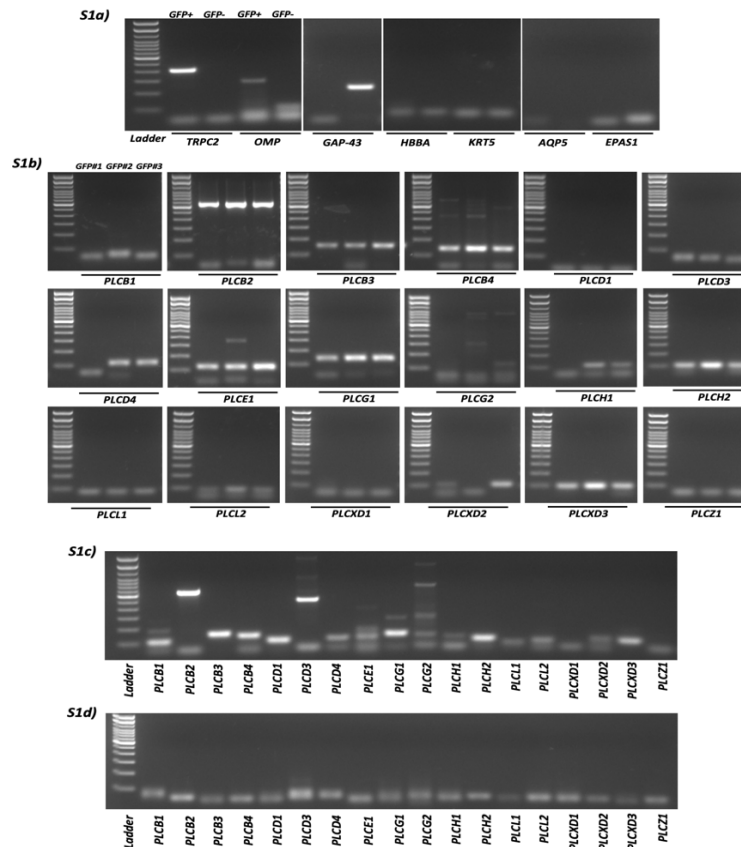


**Figure 1.36. Controls for VSN-specific PLC PCR.**

**a**, Assessment of GFP+ and GFP- samples with known VNO cell-type markers. Note that GFP+ cells are only positive for mVSN markers. **b**, Replicates for all PLCs run through Figure 1.12a. Each replicate is a composite of three animals, with Figure 1.12a is a composite of all nine animals. **c**, Positive controls for all PLC primers, run with total VNO cDNA. **d**, Negative controls for all PLC primers, run with no cDNA.

## RNA Sequencing

All datasets were converted into CPM for use. For bulk datasets, raw bulk RNAseq datasets were downloaded from publications<sup>102,103</sup>. For deep single cell RNAseq datasets, published<sup>104-106,160</sup> and unpublished datasets were combined for OSNs and VSNs. For scVSNs, the HPC cluster at Scripps Research Institute – La Jolla was used to quality check fastq files (FastQC<sup>161</sup>), align sequences to the GRCm38 genome (STAR 2.3<sup>162</sup>), and count sequences (HTseq<sup>163</sup>). OSNs and VSNs were combined into individual datasets using the Rstudio<sup>164</sup> package ComBat<sup>165</sup>. VSNs were filtered through a quality control process as was previously described<sup>160</sup>, and cells expressing blood markers, lamina propria markers, sustentacular cell markers or immature cell markers were removed. All cells used had at least a one million read depth and >75% reads uniquely-mapped. For shallow single cell RNAseq datasets, a single-cell VNO dataset was generated by dissociating VSNs as previously described (“FACs and PCR”) and using 10x Chromium Single Cell v2 kit<sup>166</sup>. Cells were run on a NextSeq2000 (Illumina) and analyzed using the Cell Ranger v2 Pipeline<sup>167</sup>.

Shallow scVSN datasets were mapped using Loupe Cell Browser v5<sup>168</sup>. Deep scVSN data was analyzed for PLC and HR expression using cutoffs of 50CPM and 200CPM, respectively – these cutoffs were generated by constructing a cumulative frequency chart of gene expression across cells using R Studio’s diptest package<sup>178</sup> to establish the cutoff between the two bimodal peaks (an “on” peak and an “off” peak). The list of candidate hormone receptors was analyzed using three criteria: 1) high mean and high variance, 2) visual inspection of bimodality, 3) diptest package assessment of bimodality. Hormone receptors had to be positive for at least two of these three criteria to be considered a candidate.

## qPCR

VNOs from wildtype and mutant mice were dissected, homogenized (Qiashredder, Qiagen), and placed into Trizol (ThermoFisher). RNA was extracted using an RNA Microprep Kit (Zymo Research) and cDNA was created using SuperscriptIII (ThermoFisher). Samples were qPCR'ed using SYBR Green/ROX mix (ThermoFisher) and designed primers (IDT) created using primerBLAST<sup>169</sup>. Results were normalized to ActB and quantified using the delta-delta CT method.

Chapter 1, in part, is a reprint of material that is currently being prepared for publication. Koblesky, Norah; Patel, Kushagra; Fodoulian, Léon; Rodriguez, Ivan, Stowers, Lisa. “The Vomeronasal System Signals through Multiple Stimuli-Specific Signal Transduction Cascades”. The dissertation author was the primary investigator and author of this paper.

Chapter 1, in part, contains unpublished material. Koblesky, Norah; Smrcka, Alan; Heidel, Florian; Matsunami, Hiroaki; Chien, Mingshan; Stowers, Lisa. Chapter 1. “The Vomeronasal System Signals through Multiple Stimuli-Specific Signal Transduction Cascades”. The dissertation author was the primary investigator and author of this paper.

## REFERENCES

1. Squire, L., Berg, D., Bloom, F. E., du Lac, S., Ghosh, A., & Spitzer, N. C. (2013). *Fundamental Neuroscience*, Fourth Edition. Academic Press.
2. Wong, S. T., Trinh, K., Hacker, B., Chan, G. C., Lowe, G., Gaggar, A., Xia, Z., Gold, G. H., & Storm, D. R. (2000). Disruption of the type III adenylyl cyclase gene leads to peripheral and behavioral anosmia in transgenic mice. *Neuron*, 27(3), 487–497.
3. Yang, J., Qiu, L., Strobel, M., Kabel, A., Zha, X. M., & Chen, X. (2020). Acid-Sensing Ion Channels Contribute to Type III Adenylyl Cyclase-Independent Acid Sensing of Mouse Olfactory Sensory Neurons. *Molecular neurobiology*, 57(7), 3042–3056.
4. Tsang, S. H., Gouras, P., Yamashita, C. K., Kjeldbye, H., Fisher, J., Farber, D. B., & Goff, S. P. (1996). Retinal degeneration in mice lacking the gamma subunit of the rod cGMP phosphodiesterase. *Science (New York, N.Y.)*, 272(5264), 1026–1029.
5. Bowes, C., Li, T., Danciger, M., Baxter, L. C., Applebury, M. L., & Farber, D. B. (1990). Retinal degeneration in the rd mouse is caused by a defect in the beta subunit of rod cGMP-phosphodiesterase. *Nature*, 347(6294), 677–680.
6. Stearns, G., Evangelista, M., Fadool, J. M., & Brockerhoff, S. E. (2007). A mutation in the cone-specific pde6 gene causes rapid cone photoreceptor degeneration in zebrafish. *The Journal of neuroscience : the official journal of the Society for Neuroscience*, 27(50), 13866–13874.
7. Zhang, Y., Hoon, M. A., Chandrashekar, J., Mueller, K. L., Cook, B., Wu, D., Zuker, C. S., & Ryba, N. J. (2003). Coding of sweet, bitter, and umami tastes: different receptor cells sharing similar signaling pathways. *Cell*, 112(3), 293–301.
8. Greer, P. L., Bear, D. M., Lassance, J. M., Bloom, M. L., Tsukahara, T., Pashkovski, S. L., Masuda, F. K., Nowlan, A. C., Kirchner, R., Hoekstra, H. E., & Datta, S. R. (2016). A Family of non-GPCR Chemosensors Defines an Alternative Logic for Mammalian Olfaction. *Cell*, 165(7), 1734–1748.
9. Graham, D. M., Wong, K. Y., Shapiro, P., Frederick, C., Pattabiraman, K., & Berson, D. M. (2008). Melanopsin ganglion cells use a membrane-associated rhabdomeric phototransduction cascade. *Journal of neurophysiology*, 99(5), 2522–2532.
10. von Molitor, E., Riedel, K., Krohn, M., Rudolf, R., Hafner, M., & Cesetti, T. (2020). An alternative pathway for sweet sensation: possible mechanisms and physiological relevance. *Pflugers Archiv : European journal of physiology*, 472(12), 1667–1691.
11. Holy, T. E., Dulac, C., & Meister, M. (2000). Responses of vomeronasal neurons to natural stimuli. *Science (New York, N.Y.)*, 289(5484), 1569–1572.



12. Spehr, M., Hatt, H., & Wetzel, C. H. (2002). Arachidonic acid plays a role in rat vomeronasal signal transduction. *The Journal of neuroscience : the official journal of the Society for Neuroscience*, 22(19), 8429–8437.
13. Lucas, P., Ukhanov, K., Leinders-Zufall, T., & Zufall, F. (2003). A diacylglycerol-gated cation channel in vomeronasal neuron dendrites is impaired in TRPC2 mutant mice: mechanism of pheromone transduction. *Neuron*, 40(3), 551–561.
14. Chamero, P., Leinders-Zufall, T., & Zufall, F. (2012). From genes to social communication: molecular sensing by the vomeronasal organ. *Trends in neurosciences*, 35(10), 597–606.
15. Gire, D. H., Kapoor, V., Arrighi-Allisan, A., Seminara, A., and Murthy, V. N. (2016). Mice develop efficient strategies for foraging and navigation using complex natural stimuli. *Curr. Biol.* 26, 1261–1273.
16. Howard, W. E., Marsh, R. E., & Cole, R. E. (1968). Food detection by deer mice using olfactory rather than visual cues. *Animal behaviour*, 16(1), 13–17.
17. Keverne, E. B. (1999). The vomeronasal organ. *Science* 286, 716–720.
18. Isogai, Y., Si, S., Pont-Lezica, L., Tan, T., Kapoor, V., Murthy, V. N., et al. (2011). Molecular organization of vomeronasal chemoreception. *Nature* 478, 241–245.
19. Restrepo, D., Arellano, J., Oliva, A. M., Schaefer, M. L., and Lin, W. H. (2004). Emerging views on the distinct but related roles of the main and accessory olfactory systems in responsiveness to chemosensory signals in mice. *Horm. Behav.* 46, 247–256.
20. Holy T. E. (2018). The Accessory Olfactory System: Innately Specialized or Microcosm of Mammalian Circuitry?. *Annual review of neuroscience*, 41, 501–525.
21. Mucignat-Caretta, C., Redaelli, M., & Caretta, A. (2012). One nose, one brain: contribution of the main and accessory olfactory system to chemosensation. *Frontiers in neuroanatomy*, 6, 46.
22. Jacobson, L., Trotier, D., & Døving, K. B. (1998). Anatomical description of a new organ in the nose of domesticated animals by Ludvig Jacobson (1813). *Chemical senses*, 23(6), 743–754.
23. Mohrhardt, J., Nagel, M., Fleck, D., Ben-Shaul, Y., & Spehr, M. (2018). Signal Detection and Coding in the Accessory Olfactory System. *Chemical senses*, 43(9), 667–695.
24. Tarozzo, G., Cappello, P., De Andrea, M., Walters, E., Margolis, F. L., Oestreicher, B., & Fasolo, A. (1998). Prenatal differentiation of mouse vomeronasal neurones. *The European journal of neuroscience*, 10(1), 392–396.
25. Meredith, M., Marques, D. M., O'Connell, R. O., & Stern, F. L. (1980). Vomeronasal pump: significance for male hamster sexual behavior. *Science (New York, N.Y.)*, 207(4436), 1224–1226.

26. Meredith, M. (1994). Chronic recording of vomeronasal pump activation in awake behaving hamsters. *Physiology & Behavior*, *56*, 345-354.
27. Wysocki, C. J., Wellington, J. L., & Beauchamp, G. K. (1980). Access of urinary nonvolatiles to the mammalian vomeronasal organ. *Science (New York, N.Y.)*, *207*(4432), 781-783.
28. Dulac, C., & Axel, R. (1995). A novel family of genes encoding putative pheromone receptors in mammals. *Cell*, *83*(2), 195-206.
29. Ryba, N. J., & Tirindelli, R. (1997). A new multigene family of putative pheromone receptors. *Neuron*, *19*(2), 371-379.
30. Del Punta, K., Leinders-Zufall, T., Rodriguez, I., Jukam, D., Wysocki, C. J., Ogawa, S., Zufall, F., & Mombaerts, P. (2002). Deficient pheromone responses in mice lacking a cluster of vomeronasal receptor genes. *Nature*, *419*(6902), 70-74.
31. Serizawa, S., Miyamichi, K., Nakatani, H., Suzuki, M., Saito, M., Yoshihara, Y., & Sakano, H. (2003). Negative feedback regulation ensures the one receptor-one olfactory neuron rule in mouse. *Science (New York, N.Y.)*, *302*(5653), 2088-2094.
32. Martini, S., Silvotti, L., Shirazi, A., Ryba, N. J., & Tirindelli, R. (2001). Co-expression of putative pheromone receptors in the sensory neurons of the vomeronasal organ. *The Journal of neuroscience : the official journal of the Society for Neuroscience*, *21*(3), 843-848.
33. Boschhat, C., Pélofi, C., Randin, O., Roppolo, D., Lüscher, C., Broillet, M. C., & Rodriguez, I. (2002). Pheromone detection mediated by a V1r vomeronasal receptor. *Nature neuroscience*, *5*(12), 1261-1262.
34. Haga-Yamanaka, S., Ma, L., He, J., Qiu, Q., Lavis, L. D., Looger, L. L., & Yu, C. R. (2014). Integrated action of pheromone signals in promoting courtship behavior in male mice. *eLife*, *3*, e03025.
35. Leinders-Zufall, T., Ishii, T., Mombaerts, P., Zufall, F., & Boehm, T. (2009). Structural requirements for the activation of vomeronasal sensory neurons by MHC peptides. *Nature neuroscience*, *12*(12), 1551-1558.
36. Haga, S., Hattori, T., Sato, T., Sato, K., Matsuda, S., Kobayakawa, R., Sakano, H., Yoshihara, Y., Kikusui, T., & Touhara, K. (2010). The male mouse pheromone ESP1 enhances female sexual receptive behaviour through a specific vomeronasal receptor. *Nature*, *466*(7302), 118-122.
37. Dey, S., & Matsunami, H. (2011). Calreticulin chaperones regulate functional expression of vomeronasal type 2 pheromone receptors. *Proceedings of the National Academy of Sciences of the United States of America*, *108*(40), 16651-16656.

38. Wong, W. M., Cao, J., Zhang, X., Doyle, W. I., Mercado, L. L., Gautron, L., & Meeks, J. P. (2020). Physiology-forward identification of bile acid-sensitive vomeronasal receptors. *Science advances*, 6(22), eaaz6868.
39. Lee, D., Kume, M., & Holy, T. E. (2019). Sensory coding mechanisms revealed by optical tagging of physiologically defined neuronal types. *Science (New York, N.Y.)*, 366(6471), 1384–1389.
40. Liberles, S. D., Horowitz, L. F., Kuang, D., Contos, J. J., Wilson, K. L., Siltberg-Liberles, J., Liberles, D. A., & Buck, L. B. (2009). Formyl peptide receptors are candidate chemosensory receptors in the vomeronasal organ. *Proceedings of the National Academy of Sciences of the United States of America*, 106(24), 9842–9847.
41. Rivière, S., Challet, L., Fluegge, D., Spehr, M., & Rodriguez, I. (2009). Formyl peptide receptor-like proteins are a novel family of vomeronasal chemosensors. *Nature*, 459(7246), 574–577.
42. Bufe, B., Schumann, T., & Zufall, F. (2012). Formyl peptide receptors from immune and vomeronasal system exhibit distinct agonist properties. *The Journal of biological chemistry*, 287(40), 33644–33655.
43. Chamero, P., Katsoulidou, V., Hendrix, P., Bufe, B., Roberts, R., Matsunami, H., Abramowitz, J., Birnbaumer, L., Zufall, F., & Leinders-Zufall, T. (2011). G protein G(alpha)o is essential for vomeronasal function and aggressive behavior in mice. *Proceedings of the National Academy of Sciences of the United States of America*, 108(31), 12898–12903.
44. Stempel, H., Jung, M., Pérez-Gómez, A., Leinders-Zufall, T., Zufall, F., & Bufe, B. (2016). Strain-specific Loss of Formyl Peptide Receptor 3 in the Murine Vomeronasal and Immune Systems. *The Journal of biological chemistry*, 291(18), 9762–9775.
45. Boillat, M., Challet, L., Rossier, D., Kan, C., Carleton, A., & Rodriguez, I. (2015). The vomeronasal system mediates sick conspecific avoidance. *Current biology : CB*, 25(2), 251–255.
46. Dulac, C., & Torello, A. T. (2003). Molecular detection of pheromone signals in mammals: from genes to behaviour. *Nature reviews. Neuroscience*, 4(7), 551–562.
47. Berghard, A., & Buck, L. B. (1996). Sensory transduction in vomeronasal neurons: evidence for G alpha o, G alpha i2, and adenylyl cyclase II as major components of a pheromone signaling cascade. *The Journal of neuroscience : the official journal of the Society for Neuroscience*, 16(3), 909–918.
48. Sathyanesan, A., Feijoo, A. A., Mehta, S. T., Nimarko, A. F., & Lin, W. (2013). Expression profile of G-protein  $\beta\gamma$  subunit gene transcripts in the mouse olfactory sensory epithelia. *Frontiers in cellular neuroscience*, 7, 84.

49. Brann, J. H., & Firestein, S. (2010). Regeneration of new neurons is preserved in aged vomeronasal epithelia. *The Journal of neuroscience : the official journal of the Society for Neuroscience*, 30(46), 15686–15694.
50. Katreddi, R. R., & Forni, P. E. (2021). Mechanisms underlying pre- and postnatal development of the vomeronasal organ. *Cellular and molecular life sciences : CMLS*, 78(12), 5069–5082.
51. Shinohara, H., Asano, T., & Kato, K. (1992). Differential localization of G-proteins Gi and Go in the accessory olfactory bulb of the rat. *The Journal of neuroscience : the official journal of the Society for Neuroscience*, 12(4), 1275–1279.
52. Montani, G., Tonelli, S., Sanghez, V., Ferrari, P. F., Palanza, P., Zimmer, A., & Tirindelli, R. (2013). Aggressive behaviour and physiological responses to pheromones are strongly impaired in mice deficient for the olfactory G-protein -subunit G8. *The Journal of physiology*, 591(16), 3949–3962.
53. Rünneburger, K., Breer, H., & Boekhoff, I. (2002). Selective G protein beta gamma-subunit compositions mediate phospholipase C activation in the vomeronasal organ. *European journal of cell biology*, 81(10), 539–547.
54. Michell, R. H., & Allan, D. (1975). Inositol cyclis phosphate as a product of phosphatidylinositol breakdown by phospholipase C (*Bacillus cereus*). *FEBS letters*, 53(3), 302–304.
55. Suh, P. G., Ryu, S. H., Moon, K. H., Suh, H. W., & Rhee, S. G. (1988). Inositol phospholipid-specific phospholipase C: complete cDNA and protein sequences and sequence homology to tyrosine kinase-related oncogene products. *Proceedings of the National Academy of Sciences of the United States of America*, 85(15), 5419–5423.
56. Eichmann, T. O., & Lass, A. (2015). DAG tales: the multiple faces of diacylglycerol-- stereochemistry, metabolism, and signaling. *Cellular and molecular life sciences : CMLS*, 72(20), 3931–3952.
57. Berridge M. J. (2016). The Inositol Trisphosphate/Calcium Signaling Pathway in Health and Disease. *Physiological reviews*, 96(4), 1261–1296.
58. Chamero, P., Weiss, J., Alonso, M. T., Rodríguez-Prados, M., Hisatsune, C., Mikoshiba, K., Leinders-Zufall, T., & Zufall, F. (2017). Type 3 inositol 1,4,5-trisphosphate receptor is dispensable for sensory activation of the mammalian vomeronasal organ. *Scientific reports*, 7(1), 10260.
59. Stowers, L., Holy, T. E., Meister, M., Dulac, C., & Koentges, G. (2002). Loss of sex discrimination and male-male aggression in mice deficient for TRP2. *Science (New York, N.Y.)*, 295(5559), 1493–1500.

60. Leypold, B. G., Yu, C. R., Leinders-Zufall, T., Kim, M. M., Zufall, F., & Axel, R. (2002). Altered sexual and social behaviors in *trp2* mutant mice. *Proceedings of the National Academy of Sciences of the United States of America*, *99*(9), 6376–6381.
61. Leinders-Zufall, T., Storch, U., Bleyemehl, K., Mederos Y Schnitzler, M., Frank, J. A., Konrad, D. B., Trauner, D., Gudermann, T., & Zufall, F. (2018). PhoDAGs Enable Optical Control of Diacylglycerol-Sensitive Transient Receptor Potential Channels. *Cell chemical biology*, *25*(2), 215–223.e3.
62. Caputo, A., Caci, E., Ferrera, L., Pedemonte, N., Barsanti, C., Sondo, E., Pfeffer, U., Ravazzolo, R., Zegarra-Moran, O., & Galletta, L. J. (2008). TMEM16A, a membrane protein associated with calcium-dependent chloride channel activity. *Science (New York, N.Y.)*, *322*(5901), 590–594.
63. Amjad, A., Hernandez-Clavijo, A., Pifferi, S., Maurya, D. K., Boccaccio, A., Franzot, J., Rock, J., & Menini, A. (2015). Conditional knockout of TMEM16A/anoctamin1 abolishes the calcium-activated chloride current in mouse vomeronasal sensory neurons. *The Journal of general physiology*, *145*(4), 285–301.
64. Münch, J., Billig, G., Hübner, C. A., Leinders-Zufall, T., Zufall, F., & Jentsch, T. J. (2018). Ca<sup>2+</sup>-activated Cl<sup>-</sup> currents in the murine vomeronasal organ enhance neuronal spiking but are dispensable for male-male aggression. *The Journal of biological chemistry*, *293*(26), 10392–10403.
65. Dey, S., Chamero, P., Pru, J. K., Chien, M. S., Ibarra-Soria, X., Spencer, K. R., Logan, D. W., Matsunami, H., Peluso, J. J., & Stowers, L. (2015). Cyclic Regulation of Sensory Perception by a Female Hormone Alters Behavior. *Cell*, *161*(6), 1334–1344.
66. Nakamura, Y., & Fukami, K. (2017). Regulation and physiological functions of mammalian phospholipase C. *Journal of biochemistry*, *161*(4), 315–321.
67. Liao, H. J., Kume, T., McKay, C., Xu, M. J., Ihle, J. N., & Carpenter, G. (2002). Absence of erythropoiesis and vasculogenesis in *Plcg1*-deficient mice. *The Journal of biological chemistry*, *277*(11), 9335–9341.
68. Knott, J. G., Kurokawa, M., Fissore, R. A., Schultz, R. M., & Williams, C. J. (2005). Transgenic RNA interference reveals role for mouse sperm phospholipase C $\zeta$  in triggering Ca<sup>2+</sup> oscillations during fertilization. *Biology of reproduction*, *72*(4), 992–996.
69. Kadamur, G., & Ross, E. M. (2013). Mammalian phospholipase C. *Annual review of physiology*, *75*, 127–154.
70. Rupwate, S. D., & Rajasekharan, R. (2012). Plant phosphoinositide-specific phospholipase C: an insight. *Plant signaling & behavior*, *7*(10), 1281–1283.

71. Roberts, M. F., Khan, H. M., Goldstein, R., Reuter, N., & Gershenson, A. (2018). Search and Subvert: Minimalist Bacterial Phosphatidylinositol-Specific Phospholipase C Enzymes. *Chemical reviews*, 118(18), 8435–8473.
72. Fukami K. (2002). Structure, regulation, and function of phospholipase C isozymes. *Journal of biochemistry*, 131(3), 293–299.
73. Gellatly, S. A., Kalujnaia, S., & Cramb, G. (2012). Cloning, tissue distribution and sub-cellular localisation of phospholipase C X-domain containing protein (PLCXD) isoforms. *Biochemical and biophysical research communications*, 424(4), 651–656.
74. Kanematsu, T., Takeya, H., Watanabe, Y., Ozaki, S., Yoshida, M., Koga, T., Iwanaga, S., & Hirata, M. (1992). Putative inositol 1,4,5-trisphosphate binding proteins in rat brain cytosol. *The Journal of biological chemistry*, 267(10), 6518–6525.
75. Asano, S., Ikura, Y., Nishimoto, M., Yamawaki, Y., Hamao, K., Kamijo, K., Hirata, M., & Kanematsu, T. (2019). Phospholipase C-related catalytically inactive protein regulates cytokinesis by protecting phosphatidylinositol 4,5-bisphosphate from metabolism in the cleavage furrow. *Scientific reports*, 9(1), 12729.
76. Fukami, K., Inanobe, S., Kanemaru, K., & Nakamura, Y. (2010). Phospholipase C is a key enzyme regulating intracellular calcium and modulating the phosphoinositide balance. *Progress in lipid research*, 49(4), 429–437.
77. Wang, T., Pentylala, S., Rebecchi, M. J., & Scarlata, S. (1999). Differential association of the pleckstrin homology domains of phospholipases C-beta 1, C-beta 2, and C-delta 1 with lipid bilayers and the beta gamma subunits of heterotrimeric G proteins. *Biochemistry*, 38(5), 1517–1524.
78. Wang, T., Pentylala, S., Elliott, J. T., Dowal, L., Gupta, E., Rebecchi, M. J., & Scarlata, S. (1999). Selective interaction of the C2 domains of phospholipase C-beta1 and -beta2 with activated Galphaq subunits: an alternative function for C2-signaling modules. *Proceedings of the National Academy of Sciences of the United States of America*, 96(14), 7843–7846.
79. Bill, C. A., & Vines, C. M. (2020). Phospholipase C. *Advances in experimental medicine and biology*, 1131, 215–242.
80. Jin, T. G., Satoh, T., Liao, Y., Song, C., Gao, X., Kariya, K., Hu, C. D., & Kataoka, T. (2001). Role of the CDC25 homology domain of phospholipase Cepsilon in amplification of Rap1-dependent signaling. *The Journal of biological chemistry*, 276(32), 30301–30307.
81. Kelley, G. G., Reks, S. E., & Smrcka, A. V. (2004). Hormonal regulation of phospholipase Cepsilon through distinct and overlapping pathways involving G12 and Ras family G-proteins. *The Biochemical journal*, 378(Pt 1), 129–139.

82. Seifert, J. P., Wing, M. R., Snyder, J. T., Gershburg, S., Sondek, J., & Harden, T. K. (2004). RhoA activates purified phospholipase C-epsilon by a guanine nucleotide-dependent mechanism. *The Journal of biological chemistry*, 279(46), 47992–47997.
83. Wing, M. R., Houston, D., Kelley, G. G., Der, C. J., Siderovski, D. P., & Harden, T. K. (2001). Activation of phospholipase C-epsilon by heterotrimeric G protein betagamma-subunits. *The Journal of biological chemistry*, 276(51), 48257–48261.
84. Carpenter, G., Hernández-Sotomayor, T., & Jones, G. (1993). Tyrosine phosphorylation of phospholipase C-gamma 1. *Advances in second messenger and phosphoprotein research*, 28, 179–185.
85. Zhou, Y., Wing, M. R., Sondek, J., & Harden, T. K. (2005). Molecular cloning and characterization of PLC-eta2. *The Biochemical journal*, 391(Pt 3), 667–676.
86. Ryu, S. H., Kim, U. H., Wahl, M. I., Brown, A. B., Carpenter, G., Huang, K. P., & Rhee, S. G. (1990). Feedback regulation of phospholipase C-beta by protein kinase C. *The Journal of biological chemistry*, 265(29), 17941–17945.
87. Xu, A., Wang, Y., Xu, L. Y., & Gilmour, R. S. (2001). Protein kinase C alpha -mediated negative feedback regulation is responsible for the termination of insulin-like growth factor I-induced activation of nuclear phospholipase C beta1 in Swiss 3T3 cells. *The Journal of biological chemistry*, 276(18), 14980–14986.
88. Xu, A., Suh, P. G., Marmy-Conus, N., Pearson, R. B., Seok, O. Y., Cocco, L., & Gilmour, R. S. (2001). Phosphorylation of nuclear phospholipase C beta1 by extracellular signal-regulated kinase mediates the mitogenic action of insulin-like growth factor I. *Molecular and cellular biology*, 21(9), 2981–2990.
89. Litosch I. (2002). Novel mechanisms for feedback regulation of phospholipase C-beta activity. *IUBMB life*, 54(5), 253–260.
90. Liu, M., & Simon, M. I. (1996). Regulation by cAMP-dependent protein kinase of a G-protein-mediated phospholipase C. *Nature*, 382(6586), 83–87.
91. Yue, C., Ku, C. Y., Liu, M., Simon, M. I., & Sanborn, B. M. (2000). Molecular mechanism of the inhibition of phospholipase C beta 3 by protein kinase C. *The Journal of biological chemistry*, 275(39), 30220–30225.
92. Yue, C., Dodge, K. L., Weber, G., & Sanborn, B. M. (1998). Phosphorylation of serine 1105 by protein kinase A inhibits phospholipase Cbeta3 stimulation by Galphaq. *The Journal of biological chemistry*, 273(29), 18023–18027.
93. Xia, C., Bao, Z., Yue, C., Sanborn, B. M., & Liu, M. (2001). Phosphorylation and regulation of G-protein-activated phospholipase C-beta 3 by cGMP-dependent protein kinases. *The Journal of biological chemistry*, 276(23), 19770–19777.

94. Fujii, M., Yi, K. S., Kim, M. J., Ha, S. H., Ryu, S. H., Suh, P. G., & Yagisawa, H. (2009). Phosphorylation of phospholipase C-delta 1 regulates its enzymatic activity. *Journal of cellular biochemistry*, *108*(3), 638–650.
95. Fujii, M., Yi, K. S., Kim, M. J., Ha, S. H., Ryu, S. H., Suh, P. G., & Yagisawa, H. (2009). Phosphorylation of phospholipase C-delta 1 regulates its enzymatic activity. *Journal of cellular biochemistry*, *108*(3), 638–650.
96. Serrano, C. J., Graham, L., DeBell, K., Rawat, R., Veri, M. C., Bonvini, E., Rellahan, B. L., & Reischl, I. G. (2005). A new tyrosine phosphorylation site in PLC gamma 1: the role of tyrosine 775 in immune receptor signaling. *Journal of immunology (Baltimore, Md. : 1950)*, *174*(10), 6233–6237.
97. Kim, H. K., Kim, J. W., Zilberstein, A., Margolis, B., Kim, J. G., Schlessinger, J., & Rhee, S. G. (1991). PDGF stimulation of inositol phospholipid hydrolysis requires PLC-gamma 1 phosphorylation on tyrosine residues 783 and 1254. *Cell*, *65*(3), 435–441.
98. Rodriguez, R., Matsuda, M., Perisic, O., Bravo, J., Paul, A., Jones, N. P., Light, Y., Swann, K., Williams, R. L., & Katan, M. (2001). Tyrosine residues in phospholipase Cgamma 2 essential for the enzyme function in B-cell signaling. *The Journal of biological chemistry*, *276*(51), 47982–47992.
99. Jiang, H., Kuang, Y., Wu, Y., Xie, W., Simon, M. I., & Wu, D. (1997). Roles of phospholipase C beta2 in chemoattractant-elicited responses. *Proceedings of the National Academy of Sciences of the United States of America*, *94*(15), 7971–7975.
100. Potter, S. M., Zheng, C., Koos, D. S., Feinstein, P., Fraser, S. E., & Mombaerts, P. (2001). Structure and emergence of specific olfactory glomeruli in the mouse. *The Journal of neuroscience : the official journal of the Society for Neuroscience*, *21*(24), 9713–9723.
101. Kim, D., Jun, K. S., Lee, S. B., Kang, N. G., Min, D. S., Kim, Y. H., Ryu, S. H., Suh, P. G., & Shin, H. S. (1997). Phospholipase C isozymes selectively couple to specific neurotransmitter receptors. *Nature*, *389*(6648), 290–293.
102. Ibarra-Soria, X., Levitin, M. O., Saraiva, L. R., & Logan, D. W. (2014). The olfactory transcriptomes of mice. *PLoS genetics*, *10*(9), e1004593.
103. Oboti, L., Ibarra-Soria, X., Pérez-Gómez, A., Schmid, A., Pyrski, M., Paschek, N., Kircher, S., Logan, D. W., Leinders-Zufall, T., Zufall, F., & Chamero, P. (2015). Pregnancy and estrogen enhance neural progenitor-cell proliferation in the vomeronasal sensory epithelium. *BMC biology*, *13*, 104.
104. Hanchate, N. K., Kondoh, K., Lu, Z., Kuang, D., Ye, X., Qiu, X., Pachter, L., Trapnell, C., & Buck, L. B. (2015). Single-cell transcriptomics reveals receptor transformations during olfactory neurogenesis. *Science (New York, N.Y.)*, *350*(6265), 1251–1255.



105. Saraiva, L. R., Ibarra-Soria, X., Khan, M., Omura, M., Scialdone, A., Mombaerts, P., Marioni, J. C., & Logan, D. W. (2015). Hierarchical deconstruction of mouse olfactory sensory neurons: from whole mucosa to single-cell RNA-seq. *Scientific reports*, 5, 18178.
106. Tan, L., Li, Q., & Xie, X. S. (2015). Olfactory sensory neurons transiently express multiple olfactory receptors during development. *Molecular systems biology*, 11(12), 844.
107. Sukumaran, S. K., Lewandowski, B. C., Qin, Y., Kotha, R., Bachmanov, A. A., & Margolskee, R. F. (2017). Whole transcriptome profiling of taste bud cells. *Scientific reports*, 7(1), 7595.
108. Yang, Y. R., Follo, M. Y., Cocco, L., & Suh, P. G. (2013). The physiological roles of primary phospholipase C. *Advances in biological regulation*, 53(3), 232–241.
109. Kelley, G. G., Kaproth-Joslin, K. A., Reks, S. E., Smrcka, A. V., & Wojcikiewicz, R. J. (2006). G-protein-coupled receptor agonists activate endogenous phospholipase Cepsilon and phospholipase Cbeta3 in a temporally distinct manner. *The Journal of biological chemistry*, 281(5), 2639–2648.
110. Kim, Y. H., Park, T. J., Lee, Y. H., Baek, K. J., Suh, P. G., Ryu, S. H., & Kim, K. T. (1999). Phospholipase C-delta1 is activated by capacitative calcium entry that follows phospholipase C-beta activation upon bradykinin stimulation. *The Journal of biological chemistry*, 274(37), 26127–26134.
111. Han, S. K., Mancino, V., & Simon, M. I. (2006). Phospholipase Cbeta 3 mediates the scratching response activated by the histamine H1 receptor on C-fiber nociceptive neurons. *Neuron*, 52(4), 691–703.
112. Nodari, F., Hsu, F. F., Fu, X., Holekamp, T. F., Kao, L. F., Turk, J., & Holy, T. E. (2008). Sulfated steroids as natural ligands of mouse pheromone-sensing neurons. *The Journal of neuroscience : the official journal of the Society for Neuroscience*, 28(25), 6407–6418.
113. Xie, W., Samoriski, G. M., McLaughlin, J. P., Romoser, V. A., Smrcka, A., Hinkle, P. M., Bidlack, J. M., Gross, R. A., Jiang, H., & Wu, D. (1999). Genetic alteration of phospholipase C beta3 expression modulates behavioral and cellular responses to mu opioids. *Proceedings of the National Academy of Sciences of the United States of America*, 96(18), 10385–10390.
114. Jiang, H., Lyubarsky, A., Dodd, R., Vardi, N., Pugh, E., Baylor, D., Simon, M. I., & Wu, D. (1996). Phospholipase C beta 4 is involved in modulating the visual response in mice. *Proceedings of the National Academy of Sciences of the United States of America*, 93(25), 14598–14601.
115. Hashimoto, K., Miyata, M., Watanabe, M., & Kano, M. (2001). Roles of phospholipase Cbeta4 in synapse elimination and plasticity in developing and mature cerebellum. *Molecular neurobiology*, 23(1), 69–82. <https://doi.org/10.1385/MN:23:1:69>

116. Jiang, Z., Yue, W., Chen, L., Sheng, Y., & Yau, K. W. (2018). Cyclic-Nucleotide- and HCN-Channel-Mediated Phototransduction in Intrinsically Photosensitive Retinal Ganglion Cells. *Cell*, *175*(3), 652–664.e12.
117. Lee, S., Ahmed, T., Lee, S., Kim, H., Choi, S., Kim, D. S., Kim, S. J., Cho, J., & Shin, H. S. (2011). Bidirectional modulation of fear extinction by mediodorsal thalamic firing in mice. *Nature neuroscience*, *15*(2), 308–314.
118. Ikeda, M., Hirono, M., Sugiyama, T., Moriya, T., Ikeda-Sagara, M., Eguchi, N., Urade, Y., & Yoshioka, T. (2009). Phospholipase C-beta4 is essential for the progression of the normal sleep sequence and ultradian body temperature rhythms in mice. *PloS one*, *4*(11), e7737.
119. Smrcka, A. V., Brown, J. H., & Holz, G. G. (2012). Role of phospholipase Cε in physiological phosphoinositide signaling networks. *Cellular signalling*, *24*(6), 1333–1343.
120. © 2004 Allen Institute for Brain Science. Allen Mouse Brain Atlas. Available from: <https://mouse.brainmap.org>. Lein, E.S. et al. (2007) Genome-wide atlas of gene expression in the adult mouse brain, *Nature* 445: 168-176.
121. Wang, H., Oestreich, E. A., Maekawa, N., Bullard, T. A., Vikstrom, K. L., Dirksen, R. T., Kelley, G. G., Blaxall, B. C., & Smrcka, A. V. (2005). Phospholipase C epsilon modulates beta-adrenergic receptor-dependent cardiac contraction and inhibits cardiac hypertrophy. *Circulation research*, *97*(12), 1305–1313.
122. Yang, Y. R., Kang, D. S., Lee, C., Seok, H., Follo, M. Y., Cocco, L., & Suh, P. G. (2016). Primary phospholipase C and brain disorders. *Advances in biological regulation*, *61*, 80–85.
123. Saliakoura, M., Rossi Sebastiano, M., Pozzato, C., Heidel, F. H., Schnöder, T. M., Savic Prince, S., Bubendorf, L., Pinton, P., A Schmid, R., Baumgartner, J., Freigang, S., Berezowska, S. A., Rimessi, A., & Konstantinidou, G. (2020). PLCγ1 suppression promotes the adaptation of KRAS-mutant lung adenocarcinomas to hypoxia. *Nature cell biology*, *22*(11), 1382–1395.
124. Nakahara, T. S., Camargo, A. P., Magalhães, P., Souza, M., Ribeiro, P. G., Martins-Netto, P. H., Carvalho, V., José, J., & Papes, F. (2020). Peripheral oxytocin injection modulates vomeronasal sensory activity and reduces pup-directed aggression in male mice. *Scientific reports*, *10*(1), 19943.
125. Kanemaru, K., Nakahara, M., Nakamura, Y., Hashiguchi, Y., Kouchi, Z., Yamaguchi, H., Oshima, N., Kiyonari, H., & Fukami, K. (2010). Phospholipase C-eta2 is highly expressed in the habenula and retina. *Gene expression patterns : GEP*, *10*(2-3), 119–126.
126. Zhang, P., Yang, C., & Delay, R. J. (2010). Odors activate dual pathways, a TRPC2 and a AA-dependent pathway, in mouse vomeronasal neurons. *American journal of physiology. Cell physiology*, *298*(5), C1253–C1264.
127. Yu C. R. (2015). TRICK or TRP? What *Trpc2*(*-/-*) mice tell us about vomeronasal organ mediated innate behaviors. *Frontiers in neuroscience*, *9*, 221

128. Kim, J. K., Choi, J. W., Lim, S., Kwon, O., Seo, J. K., Ryu, S. H., & Suh, P. G. (2011). Phospholipase C- $\eta$ 1 is activated by intracellular Ca<sup>2+</sup> mobilization and enhances GPCRs/PLC/Ca<sup>2+</sup> signaling. *Cellular signalling*, 23(6), 1022–1029.
129. Williams G. (2015). Database of Gene Co-Regulation (dGCR): A Web Tool for Analysing Patterns of Gene Co-regulation across Publicly Available Expression Data. *Journal of genomics*, 3, 29–35.
130. Williams, Gareth. (2013, July). Database of Gene Co-Regulation. [www.dGCR.org](http://www.dGCR.org)
131. Yang, C., & Delay, R. J. (2010). Calcium-activated chloride current amplifies the response to urine in mouse vomeronasal sensory neurons. *The Journal of general physiology*, 135(1), 3–13.
132. Ukhanov, K., Leinders-Zufall, T., & Zufall, F. (2007). Patch-clamp analysis of gene-targeted vomeronasal neurons expressing a defined V1r or V2r receptor: ionic mechanisms underlying persistent firing. *Journal of neurophysiology*, 98(4), 2357–2369.
133. Liman, E. R., & Corey, D. P. (1996). Electrophysiological characterization of chemosensory neurons from the mouse vomeronasal organ. *The Journal of neuroscience : the official journal of the Society for Neuroscience*, 16(15), 4625–4637.
134. Isogai, Y., Wu, Z., Love, M. I., Ahn, M. H., Bambah-Mukku, D., Hua, V., Farrell, K., & Dulac, C. (2018). Multisensory Logic of Infant-Directed Aggression by Males. *Cell*, 175(7), 1827–1841.e17.
135. Papes, F., Logan, D. W., & Stowers, L. (2010). The vomeronasal organ mediates interspecies defensive behaviors through detection of protein pheromone homologs. *Cell*, 141(4), 692–703.
136. Kaur, A. W., Ackels, T., Kuo, T. H., Cichy, A., Dey, S., Hays, C., Kateri, M., Logan, D. W., Marton, T. F., Spehr, M., & Stowers, L. (2014). Murine pheromone proteins constitute a context-dependent combinatorial code governing multiple social behaviors. *Cell*, 157(3), 676–688. <https://doi.org/10.1016/j.cell.2014.02.025>
137. Wyatt T. D. (2017). Pheromones. *Current biology : CB*, 27(15), R739–R743.
138. Xiao, W., Kawakami, Y., & Kawakami, T. (2013). Immune regulation by phospholipase C- $\beta$  isoforms. *Immunologic research*, 56(1), 9–19.
139. Wood, G. A., Fata, J. E., Watson, K. L., & Khokha, R. (2007). Circulating hormones and estrous stage predict cellular and stromal remodeling in murine uterus. *Reproduction (Cambridge, England)*, 133(5), 1035–1044.
140. Petersen, S. L., Intlekofer, K. A., Moura-Conlon, P. J., Brewer, D. N., Del Pino Sans, J., & Lopez, J. A. (2013). Novel progesterone receptors: neural localization and possible functions. *Frontiers in neuroscience*, 7, 164.

141. Liu, Y., Beyer, A., & Aebersold, R. (2016). On the Dependency of Cellular Protein Levels on mRNA Abundance. *Cell*, *165*(3), 535–550.
142. Kang, D. S., Kim, I. S., Baik, J. H., Kim, D., Cocco, L., & Suh, P. G. (2020). The function of PLC $\gamma$ 1 in developing mouse mDA system. *Advances in biological regulation*, *75*, 100654.
143. Kang, D. S., Yang, Y. R., Lee, C., Kim, S., Ryu, S. H., & Suh, P. G. (2016). Roles of phosphoinositide-specific phospholipase C $\gamma$ 1 in brain development. *Advances in biological regulation*, *60*, 167–173.
144. Jang, H. J., Yang, Y. R., Kim, J. K., Choi, J. H., Seo, Y. K., Lee, Y. H., Lee, J. E., Ryu, S. H., & Suh, P. G. (2013). Phospholipase C- $\gamma$ 1 involved in brain disorders. *Advances in biological regulation*, *53*(1), 51–62.
145. Liao, H. J., Ji, Q. S., & Carpenter, G. (2001). Phospholipase C-gamma1 is required for the induction of immediate early genes by platelet-derived growth factor. *The Journal of biological chemistry*, *276*(12), 8627–8630.
146. Shin, S. Y., Ko, J., Chang, J. S., Min, D. S., Choi, C., Bae, S. S., Kim, M. J., Hyun, D. S., Kim, J. H., Han, M. Y., Kim, Y. H., Kim, Y. S., Na, D. S., Suh, P. G., & Lee, Y. H. (2002). Negative regulatory role of overexpression of PLC gamma 1 in the expression of early growth response 1 gene in rat 3Y1 fibroblasts. *FASEB journal : official publication of the Federation of American Societies for Experimental Biology*, *16*(12), 1504–1514.
147. Shannon, L. A., Calloway, P. A., Welch, T. P., & Vines, C. M. (2010). CCR7/CCL21 migration on fibronectin is mediated by phospholipase Cgamma1 and ERK1/2 in primary T lymphocytes. *The Journal of biological chemistry*, *285*(50), 38781–38787.
148. Murillo-Maldonado, J. M., Zeineddine, F. B., Stock, R., Thackeray, J., & Riesgo-Escovar, J. R. (2011). Insulin receptor-mediated signaling via phospholipase C- $\gamma$  regulates growth and differentiation in *Drosophila*. *PloS one*, *6*(11), e28067.
149. Kalpachidou, T., Spiecker, L., Kress, M., & Quarta, S. (2019). Rho GTPases in the Physiology and Pathophysiology of Peripheral Sensory Neurons. *Cells*, *8*(6), 591.
150. Choi, P. S., Zakhary, L., Choi, W. Y., Caron, S., Alvarez-Saavedra, E., Miska, E. A., McManus, M., Harfe, B., Giraldez, A. J., Horvitz, H. R., Schier, A. F., & Dulac, C. (2008). Members of the miRNA-200 family regulate olfactory neurogenesis. *Neuron*, *57*(1), 41–55.
151. Garaffo, G., Conte, D., Provero, P., Tomaiuolo, D., Luo, Z., Pinciroli, P., Peano, C., D'Atri, I., Gitton, Y., Etzion, T., Gothilf, Y., Gays, D., Santoro, M. M., & Merlo, G. R. (2015). The Dlx5 and Foxg1 transcription factors, linked via miRNA-9 and -200, are required for the development of the olfactory and GnRH system. *Molecular and cellular neurosciences*, *68*, 103–119.

152. Szebenyi, S. A., Ogura, T., Sathyanesan, A., AlMatrouk, A. K., Chang, J., & Lin, W. (2014). Increases in intracellular calcium via activation of potentially multiple phospholipase C isozymes in mouse olfactory neurons. *Frontiers in cellular neuroscience*, *8*, 336.
153. Klasen, K., Corey, E. A., Kuck, F., Wetzel, C. H., Hatt, H., & Ache, B. W. (2010). Odorant-stimulated phosphoinositide signaling in mammalian olfactory receptor neurons. *Cellular signalling*, *22*(1), 150–157.
154. Ukhanov, K., Corey, E., & Ache, B. W. (2016). Phosphoinositide-3-Kinase Is the Primary Mediator of Phosphoinositide-Dependent Inhibition in Mammalian Olfactory Receptor Neurons. *Frontiers in cellular neuroscience*, *10*, 97.
155. D'Aniello, B., Semin, G. R., Scandurra, A., & Pinelli, C. (2017). The Vomeronasal Organ: A Neglected Organ. *Frontiers in neuroanatomy*, *11*, 70.
156. Li, J., Ishii, T., Feinstein, P., & Mombaerts, P. (2004). Odorant receptor gene choice is reset by nuclear transfer from mouse olfactory sensory neurons. *Nature*, *428*(6981), 393–399.
157. Wang, F., Flanagan, J., Su, N., Wang, L. C., Bui, S., Nielson, A., Wu, X., Vo, H. T., Ma, X. J., & Luo, Y. (2012). RNAscope: a novel in situ RNA analysis platform for formalin-fixed, paraffin-embedded tissues. *The Journal of molecular diagnostics : JMD*, *14*(1), 22–29.
158. Kaur, A., Dey, S., & Stowers, L. (2013). Live cell calcium imaging of dissociated vomeronasal neurons. *Methods in molecular biology (Clifton, N.J.)*, *1068*, 189–200.
159. Ye, J., Coulouris, G., Zaretskaya, I., Cutcutache, I., Rozen, S., & Madden, T. L. (2012). Primer-BLAST: a tool to design target-specific primers for polymerase chain reaction. *BMC bioinformatics*, *13*, 134.
160. Untiet, V., Moeller, L. M., Ibarra-Soria, X., Sánchez-Andrade, G., Stricker, M., Neuhaus, E. M., Logan, D. W., Gensch, T., & Spehr, M. (2016). Elevated Cytosolic Cl<sup>-</sup> Concentrations in Dendritic Knobs of Mouse Vomeronasal Sensory Neurons. *Chemical senses*, *41*(8), 669–676.
161. Andrews S, (2010) FastQC: a quality control tool for high throughput sequence data. Available online at:
162. Dobin, A., Davis, C. A., Schlesinger, F., Drenkow, J., Zaleski, C., Jha, S., Batut, P., Chaisson, M., & Gingeras, T. R. (2013). STAR: ultrafast universal RNA-seq aligner. *Bioinformatics (Oxford, England)*, *29*(1), 15–21.
163. Anders, S., Pyl, P. T., & Huber, W. (2015). HTSeq--a Python framework to work with high-throughput sequencing data. *Bioinformatics (Oxford, England)*, *31*(2), 166–169.
164. RStudio Team (2020). RStudio: Integrated Development for R. RStudio, PBC, Boston, MA Available online at: <http://www.rstudio.com/>.

165. Wang, M., Huang, J., Liu, Y., Ma, L., Potash, J. B., & Han, S. (2017). COMBAT: A Combined Association Test for Genes Using Summary Statistics. *Genetics*, 207(3), 883–891.
166. *Chromium Single Cell V(D)J Reagent Kits with Feature Barcoding technology for Cell Surface Protein*, Document Number CG000186 Rev A, 10x Genomics, (2019, July 25).
167. Zheng, Grace X.Y., Terry, Jessica M., [...] Bielas, Jason H. (2017). Massively parallel digital transcriptional profiling of single cells. *Nature Communications*. 8: 1-12,
168. 10X Genomics What is Loupe Cell Browser? - Software - Single Cell Gene Expression - Official 10x Genomics Support [Online]. Available at: <https://support.10xgenomics.com/single-cell-gene-expression/software/visualization/latest/what-is-loupe-cell-browser> [Accessed: 10 July 2019].
169. Maechler M, (2021). Hartigan’s Dip Test Statistic for Unimodality – Corrected. Available online at: <https://github.com/mmaechler/diptest>

## CHAPTER 2 – Sources of Variation in Innate Olfactory Valence Tests

### INTRODUCTION

Animals continuously process incoming olfactory stimuli to identify odorants, yet how the brain decodes this sensory information is a mystery. To understand how this occurs, researchers must learn what information is being extracted from incoming signals, and so need to find characteristics that differentiate odorants from each other. In other senses, this is typically a physical aspect of the stimulus that varies on a continuum, such as sound frequency or light wavelength<sup>1</sup>. No such linear aspect has been found in odorants. As olfaction is a chemical sense, one nonlinear yet potentially-defining attribute is odorant chemical structure. Attempts to organize odorants by chemical structure have had mixed results as such attributes have not historically correlated with odorant strength or quality<sup>2-4</sup>, though recent breakthroughs have linked odorant structure relationships to brain activity patterns<sup>5,6</sup>. Odorants can be grouped by nonlinear percept descriptions in humans (e.g. fishy versus fruity odorants)<sup>7,8</sup>, yet these verbal classifications are not attainable in animal research. In order to study olfactory classifications in animal models such as mice, researchers must use behavioral tests to assess animal reactions to odorants. Animal studies have found a potentially-useful dimension to olfactory stimuli: innate odorant valence.

In psychology, valence defines “likeability”, with positive valence signifying attractiveness and negative valence signifying aversiveness<sup>9</sup>. Behavioral tests have converted valence into a measurable attribute based on the simple hypothesis that animals move towards something they like and move away from something they do not like<sup>10</sup>. These tests have been successfully used to study many aspects of behaviors, such as drug-seeking<sup>10,11</sup>. These tests are also used to study innate olfactory responses - animals display innate attraction to conspecific odors and food, and innate aversion to predator odors and rot<sup>12,13,18,20-26</sup>. Odorant valence research

has identified certain stimuli which cause innate responses and an olfaction-responsive amygdalar region (CoA) that may mediate such responses<sup>14-17</sup>. Further, some suggest valence is topographically-mapped onto the olfactory bulb<sup>18</sup> and the CoA<sup>16,17</sup>, though research on the latter point is inconsistent<sup>19</sup>. However, tests beyond a small pool of strong, well-studied stimuli are rare<sup>12,13,18,20-25</sup>, and it is not yet clear whether innate responses can be elicited outside this specific, ethologically-relevant stimulus pool. Assaying innate responses across many odorants is essential to understand if innate valence is a linear quality shared by all odorants or a categorical one shared by few.

One roadblock to large scale olfactory valence screens is reliance on troublesome assays. While conceptually simple, innate olfactory valence tests are low-throughput, taking anywhere from three and twenty-five minutes per animal<sup>18,20-25</sup>. Tests also have several inherent issues, as they lack methods of stimulus control and require potentially-stressful human-interaction. Assays are not standardized, with aspects including assay time, apparatus, and analysis varying between studies – this variability makes inter-study comparison of results difficult and use of such assays for discovery questionable. It is not yet known whether and how variation in apparatus, assay, or analysis affect measured innate olfactory valence. Two groups have attempted improvements upon the typical innate olfactory valence apparatus and assay<sup>17,26</sup>, providing an opportunity to study how varying test attributes can affect results and ultimate conclusions.

In order to determine the extent to which variations in apparatuses, assays, and analyses change the measured innate responses to olfactory stimuli, we tested an odorant panel of known valence in a typical two-choice test as well as two improved assays. Inter-assay comparison revealed inconsistent differences in valence strength, temporal dynamics, and valence conclusion, indicating that assay and apparatus affect data. Data was also highly variable within and between assays, and this variability was not explained by any extracted measure of mouse behavior. Raw



data did not reflect the processed data's conclusions, suggesting that data requires processing to achieve significance. Raw data also revealed that behavioral differences occur over minutes and that attractive and aversive odors elicit similar initial responses, despite the expectation that innate responses occur rapidly. Overall, this data suggests that current innate olfactory valence tests are not robust enough to be used for exploration, and that the position-as-response assumption these tests rely on is flawed – tests must be redesigned and standardized to capture informative data on immediate odorant responses.

## RESULTS

### 2.1 Olfactory valence strength and sign varies with assay and apparatus

A troubling aspect of innate olfactory valence research is the absence of apparatus and assay standardization. Given the field's lack of standardization, one would hypothesize that innate olfactory valence measures are minimally impacted by testing variation, yet this has not been confirmed. In order to assess the extent to which innate valence test variation changes measured responses to olfactory stimuli, we assayed the same odors with a typical valence test as well as two attempted improvements<sup>17,26</sup>. To represent commonly-used valence assays, a modified version of the usual olfactory valence test was used (hereafter "Two-Choice") (Figure 2.1a). Aspects from previously-published assays were kept while minimizing odorant diffusion by maximally enclosing compartments and providing a slight vacuum pull. In the Two-Choice test, mice were placed in the test chamber for a 15-minute habituation period followed by a 10-minute odor-exposure test using odorant and water control. We also tested two new olfactory assays which attempt to control odorant diffusion. The first assays mice in an open, symmetrical four-quadrant chamber where air is pumped into each quadrant; odorant is isolated to one quadrant by an "air curtain" created by balanced airflow in and vacuum pull out of the chamber (hereafter "Four-Quadrant test") (Figure 2.1c). In the Four-Quadrant test, mice were habituated in the test chamber for 15 minutes followed by a 15-minute odor-exposure test. The second new assay uses a small plexiglass box with airflow in through a nose cone and out a vacuum port on the opposite wall; a pre-defined computer program delivers odors without human interaction, and mouse investigation is assayed by detecting nose pokes into the nose cone via beam break (hereafter "PROBES"<sup>26</sup>) (Figure 2.1e). Mice were habituated in the test chamber for 15 minutes, followed by a 15-minute odorant test. Mice exhibited expected responses to strong positive

controls and no response to control in all three tests (Figure 2.1b,d,f), indicating that all were functional in our hands.

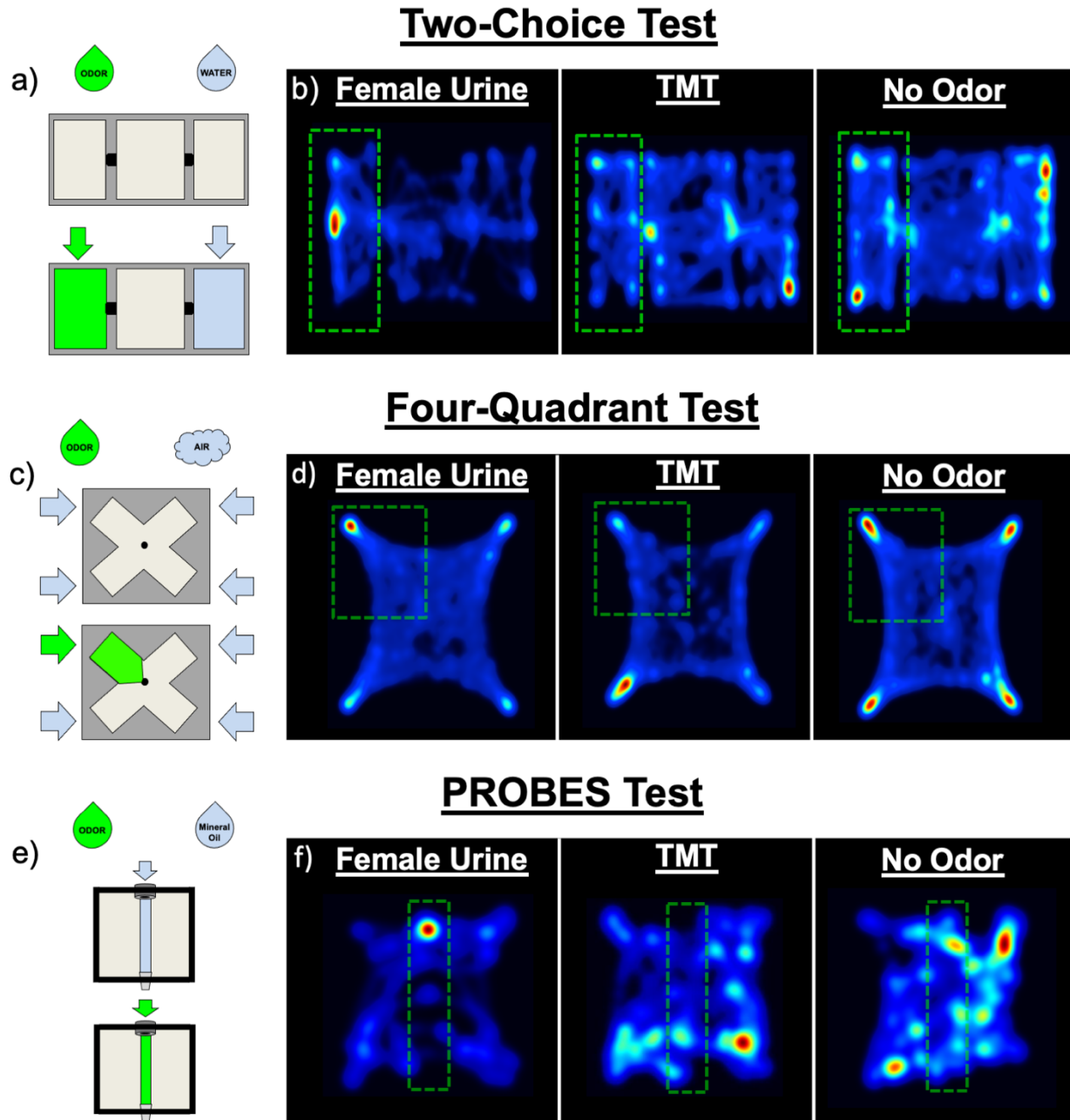








**Figure 2.1.** Tests used for innate olfactory valence comparison.

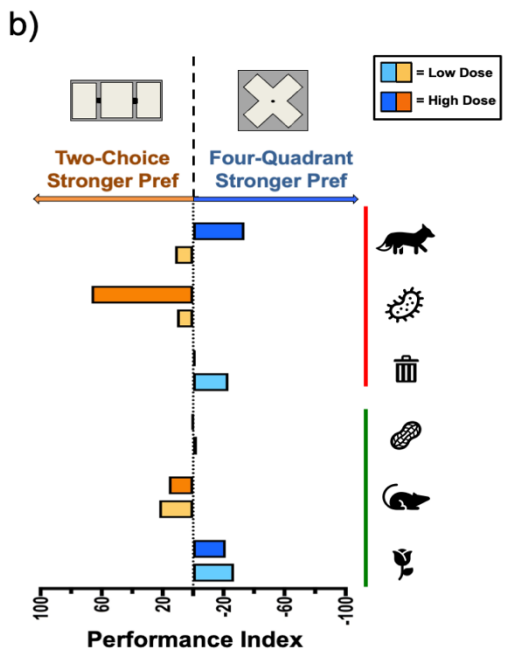
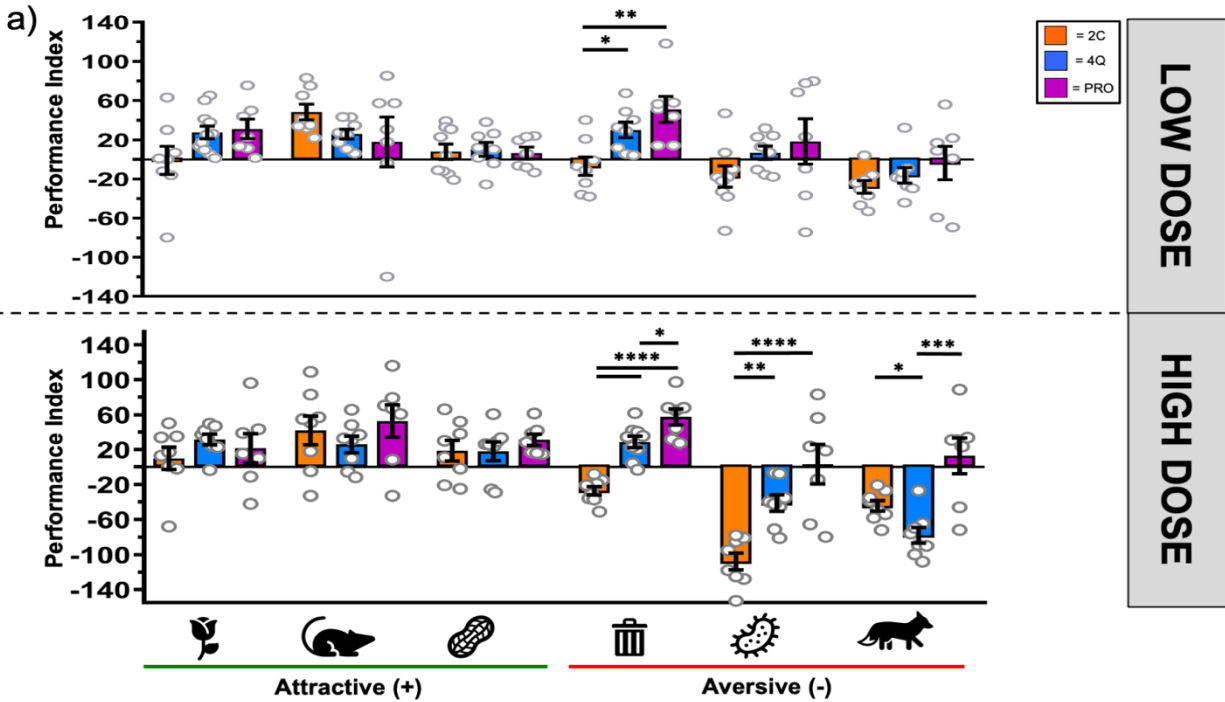
**a**, Schematic for Two-Choice test. **b**, Positive (left, middle) and negative (right) controls for Two-Choice apparatus. **c**, Schematic for Four-Quadrant test. **d**, Positive (left, middle) and negative (right) controls for Four-Quadrant apparatus. **e**, Schematic for PROBES test. **f**, Positive (left, middle) and negative (right) controls for PROBES apparatus.

To compare measured valences within the Two-Choice, Four-Quadrant, and PROBES tests, we used an odor/odorant (hereafter odorant) panel containing six well-studied odorants for which valence has been established, including three attractive stimuli (2-phenylethanol<sup>17,20</sup>, female urine<sup>18,26,27</sup>, peanut oil<sup>17,18</sup>) and three aversive stimuli (2-methylbutyric acid<sup>18,20,26</sup>, isopentylamine<sup>17,18,20,23</sup>, TMT<sup>17,18,20,28,29</sup>) (Table 2.1). We tested all odorants at a previously-cited low dose<sup>17</sup> (1 $\mu$ L pure) and a high dose determined by publication<sup>18,20,23,26-29</sup> or dose-response curve when necessary (5, 20 or 50 $\mu$ L, data not shown) in order to unveil any dose-dependent effects. One roadblock to inter-assay comparison is variation between analyses; to allow for direct comparison between all tests, we converted all assays to one standardized formula (see Methods).

**Table 2.1. Odorants used in innate olfactory valence comparison.**

<b>Odor</b>	<b>Published Valence</b>	<b>Symbol</b>
<b>2-Phenylethanol (2PE)</b>	Attractive	
<b>Female Urine (FU)</b>	Attractive	
<b>Peanut Oil (PO)</b>	Attractive	
<b>2-Methylbutyric Acid (2MB)</b>	Aversive	
<b>Isopentylamine (IPA)</b>	Aversive	
<b>2,4,5-Trimethyl-thiazoline (TMT)</b>	Aversive	

Lack of standardization suggests that varying ones methods does not markedly affect acquired data. Direct inter-assay comparison of measured odorant responses shows substantial differences in response strength at matched doses (Figure 2.2a), indicating that the apparatus and test choice does have a considerable impact on assay outcome. These differences occur in nearly all odorant-dose combinations, revealing that the testing methods' effects are extensive. We see that differences across odors are inconsistent, such that one assay does not consistently elicit a stronger animal reaction to tested odors, suggesting that data variation is not due to basic test effectiveness. Instead, the relationship between assays appears to be odor-dependent, such that certain odors have a more robust effect in the Two-Choice test (ISO) while others are more robust in the Four-Quadrant test (2PE, PO, 2MB, TMT) or the PROBES test (FU) (Figure 2.2a-b). The inter-assay differences are largely consistent between doses, indicating that data effects are not random but instead involve specific properties of each odorant. Interestingly, an unexpected attraction is seen to 2MB in the Four-Quadrant assay and low-dose ISO in the PROBES assay (Figure 2.2a-b), indicating that apparatus and assay choice can affect both data strength and odorant valence conclusions (Figure 2.2c). Altogether, inter-assay comparison reveals that assay and apparatus can change strength and sign of innate odorant valence results, and that lack of standardization currently makes inter-study comparison not feasible.



		Valence			
		Published	Two-Choice	Four-Quadrant	PROBES
2PE	LOW	+	N	++	++
	HIGH	+	+	++	+
FU	LOW	+	+++	++	+
	HIGH	+	++	++	+++
PO	LOW	+	+	+	++
	HIGH	+	+	+	+
2MB	LOW	-	-	++	+++
	HIGH	-	--	++	+++
ISO	LOW	-	-	+	+
	HIGH	-	---	---	N
TMT	LOW	-	--	-	N
	HIGH	-	---	---	+

**Figure 2.2. Innate olfactory valence results and conclusions change across apparatuses.**

**a**, Comparison between odorant valences to matching odorants and doses in Four-Quadrant, Two-Choice, and PROBES tests. Kruskal-Wallis test,  $n=6-8$ . Significant  $p$ -values are as follows: Low Dose - 2MB (Two-Choice versus Four-Quadrant,  $p=.010$ ; Two-Choice versus PROBES,  $p=.007$ ). High Dose - 2MB (Two-Choice versus Four-Quadrant,  $p<.0001$ ; Four-Quadrant versus PROBES,  $p=.025$ , Two-Choice versus PROBES,  $p<.0001$ ); ISO (Two-Choice versus Four-Quadrant,  $p=.009$ ; Two-Choice versus PROBES,  $p<.0001$ ); TMT (Two-Choice versus Four-Quadrant,  $p=.033$ ; Four-Quadrant versus PROBES,  $p=.0008$ ). **b**, Summary of A for Two-Choice and Four-Quadrant apparatuses. **c**, Conclusions from A, compared to published literature. Each symbol represents  $\pm 20$  Performance Index.

## 2.2 Olfactory valence temporal dynamics vary with assay and apparatus

Another difference between olfactory valence tests is assay length, which can span from three to over twenty minutes long. Indeed, the Two-Choice, Four-Quadrant, and PROBES test times range widely (ten, fifteen, and less than five minutes, respectively). As mouse reactions to odorants likely change over time, perhaps the variability between assays is driven by test length differences. If so, we would expect to see similar response trajectories between tests even if their end results diverge. In order to compare the temporal dynamics of valence across tests, all assays' data were re-analyzed to visualize behavior in one-minute-or-less increments (see Methods). For each ~minute, all mice within one odorant/apparatus group were assessed as being in the odorant quadrant more or less than chance, and the number of mice in the quadrant more than chance was used to calculate that odor, apparatus, and ~minute's "percentage different from chance" value (Figure 2.3a). Two-Choice and Four-Quadrant tests for high dose odorants were plotted together as they had more similar assay length (Figure 2.3b), and the short PROBES test was plotted individually and compared to the other tests visually (Figure 2.3c). Temporal dynamics were largely inconsistent between all assays, suggesting that valence differences did not stem from disparate assay lengths. For example, ISO elicited a slowly-decaying attraction in the Four-Quadrant test yet a sustained avoidance in the Two-Choice test. TMT elicited an initial and belated attraction in the Two-Choice test, whereas the Four-Quadrant test revealed slight initial attraction then consistent avoidance. Interestingly, 2MB showed similar, mirrored temporal dynamics between the Four-Quadrant and Two-Choice tests despite showing inverse valences (Figure 2.3b), and PROBES showed different 2MB temporal dynamics than the Four-Quadrant test despite having the same conclusion (Figure 2.3c). Certain odorants such as female urine did not show temporal differences between tests (Figure 2.3b-c), indicating that temporal

inconsistencies are not ubiquitous but instead are odorant-specific. Overall, inter-assay comparison shows that assay length differences do not explain disparate valence strengths and conclusions between tests – instead, comparison reveals temporal dynamics as another source of inter-assay variation.



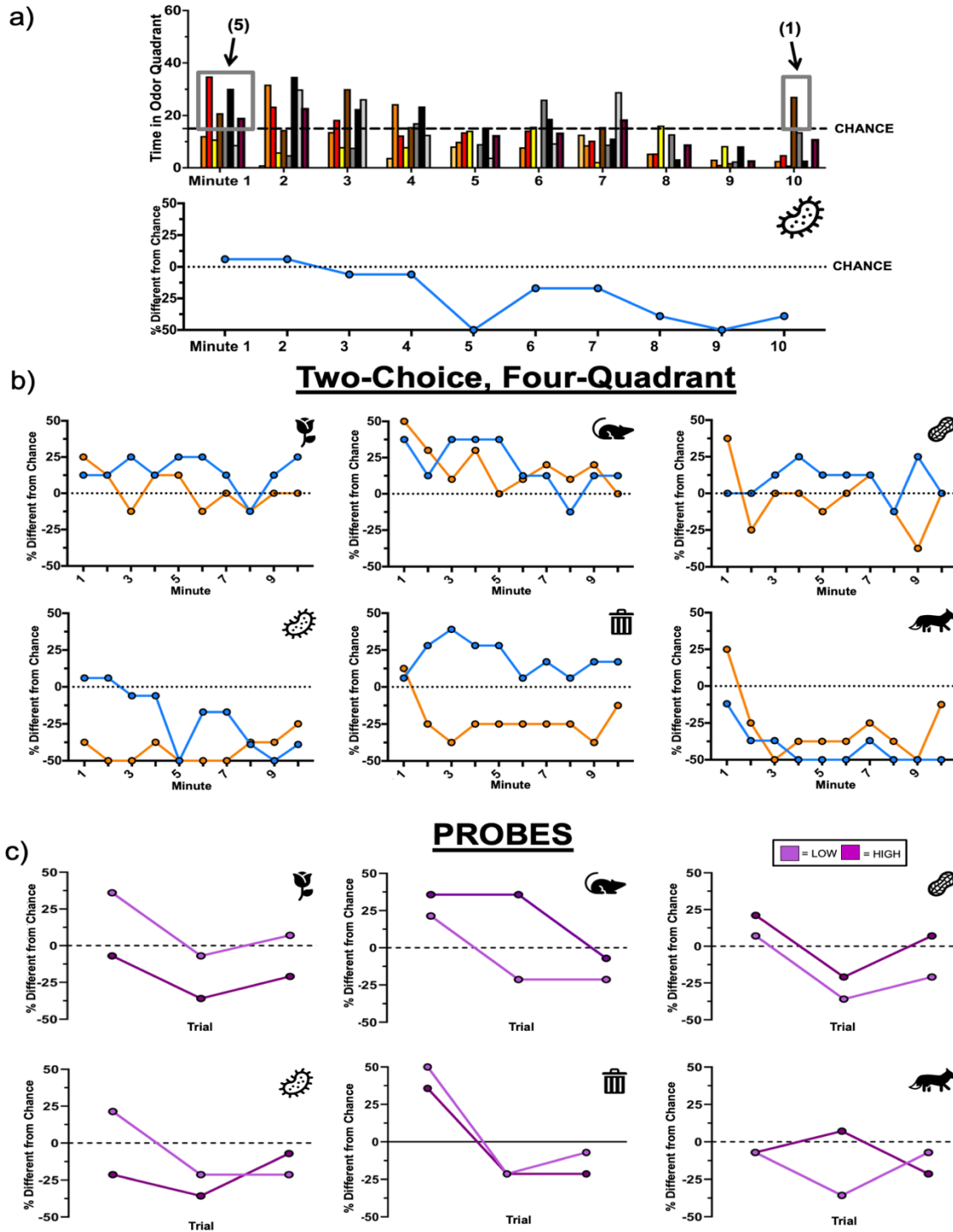


**Figure 2.3. Innate olfactory valence temporal dynamics changes across apparatuses.**

**a**, Example of how temporal dynamics are condensed into one metric. For each apparatus, a chance level is set based on the size of the assay's odorant stream and arena. The percentage of mice over that cutoff is then converted to a percent from chance measure based on the behavior of the whole experimental group. **b**, Temporal dynamics for Four-Quadrant and Two-Choice assays' high dose tests are plotted together for the ease of comparison. **c**, Temporal dynamics for PROBES tests at high dose (dark purple) and low dose (light purple). PROBES data is charted alone given the test's unique short length.

### **2.3 Other mouse tracking parameters do not explain mouse valence variability**

Innate olfactory valence behavior is variable, both between and within assays (Figure 2.2a). This intra-assay variation makes using assays for exploration unlikely as data spread may mask any middling or weak valence effect – it also calls into question the robustness of the method itself. Identifying the cause or correlating markers of this behavioral spread would potentially enable its reduction through early detection of outliers or removal of spread origin. Disparate responses are ubiquitous across odors and doses, suggesting that the source is likely not situation-specific and instead comes from the animals themselves. To look for possible identifying correlates of valence behavior abnormality, several measures were taken from Four-Quadrant and Two-Choice habituation data and compared to a z-score-like measure of data spread, “difference score” (Figure 2.4a, see Methods). Measures tested include latency (time taken to initially contact odorant quadrant), habituation spatial bias (strength of attraction for one location in apparatus), and a variety of movement-related attributes (e.g., average speed). Correlation analysis revealed no significant relationship between any variables and difference score, either when data is combined or split by apparatus (Figure 2.4b-d; odorant quadrant spatial bias, distance, and percent immobility not shown). However, habituation spatial bias trends towards significance, potentially indicating an obscured relationship (Figure 2.4d; See Figure 2.5). Plotting all variables in principal component space revealed no clustering according to difference score value (Figure 2.4e, left) or direction (Figure 2.4e, right), suggesting that combining measures was not more informative. No easily-measurable metric correlates with odorant response variability, so more powerful forms of analysis will be needed to identify sources or correlates of behavioral abnormality. As it stands, assays are too variable to be used for substantial discovery.

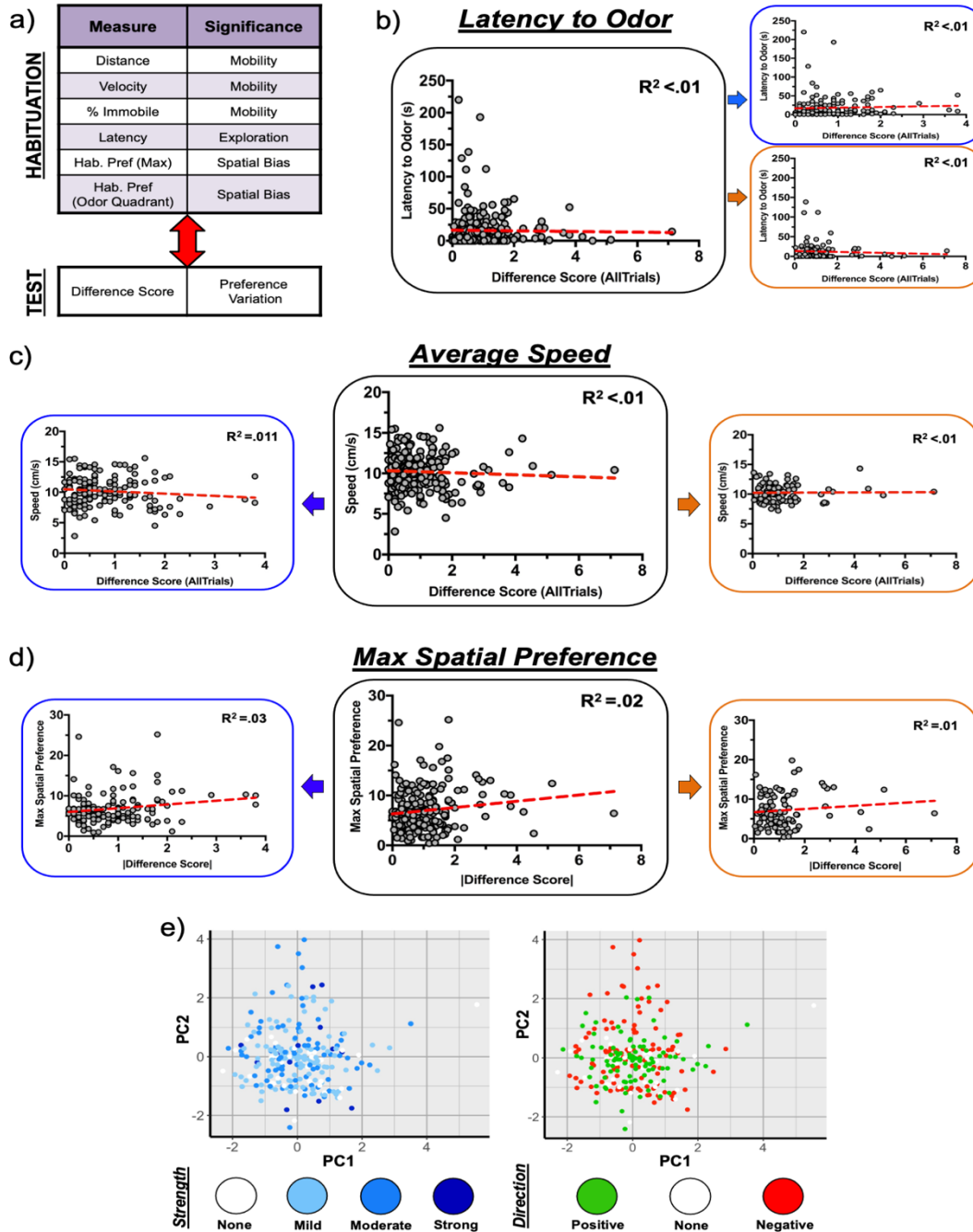


**Figure 2.4. Behavioral variability in olfactory valence unexplained by tracking-derived parameters.**

**a.** Schematic of experiment. Six behavioral variables extracted from habituation or pre-odorant encounter and one valence variability measure extracted from odorant exposure trials are cross-correlated to look for relationships between animals and experimental outcome. **b.** Correlation between latency and difference score. Four-Quadrant data (top-right,  $p=.072$ ,  $R^2<.01$ ), Two-Choice data (bottom-right,  $p=.353$ ,  $R^2<.01$ ), and combined data (left,  $p=.160$ ,  $R^2<.01$ ) is shown. **c.** Correlation between average speed and difference score. Four-Quadrant data (left,  $p=.340$ ,  $R^2=.011$ ), Two-Choice data (right,  $p=.522$ ,  $R^2<.01$ ), and combined data (middle,  $p=.195$ ,  $R^2<.01$ ) is shown. **d.** Correlation between % immobility and difference score. Four-Quadrant data (left,  $p=.066$ ,  $R^2<.01$ ), Two-Choice data (right,  $p=.271$ ,  $R^2<.01$ ), and combined data (middle,  $p=.955$ ,  $R^2=.021$ ) is shown. **e.** Principal Component Analysis of habituation parameters, with strength (left) and direction (right) information overlaid onto individual points. Strength cutoffs: 0-.25 = “None”, .25-1 = “Mild”, 1-2 = “Moderate”, >2 = “Strong”. Direction cutoffs: <(-.25) = “Negative”, (-.25) - (+.25) = “None”, >(+.25) = “Positive”.

## 2.4 Spatial bias relationship with odorant valence varies between assays

An inherent problem with using a location-based valence measure is spatial bias. Many factors ranging from stress level<sup>30,31</sup> to first point of entry<sup>32,33</sup> can influence a mouse's spatial location, so some level of spatial bias is typically unavoidable. As such, the animal's location conveys the combination of at least two types of preference, confounding the measure and masking valuable data. In conditioned place preference (CPP), perhaps the most common location-based preference assay, it is standard practice to measure spatial bias prior to testing and then subtract out bias afterwards<sup>10,11,32,33</sup>. While there is no consensus about how to handle spatial bias in innate olfactory valence behavior, most have adopted some version of the CPP method, normalizing by deducting spatial bias from overall behavior<sup>18,20-25</sup>.

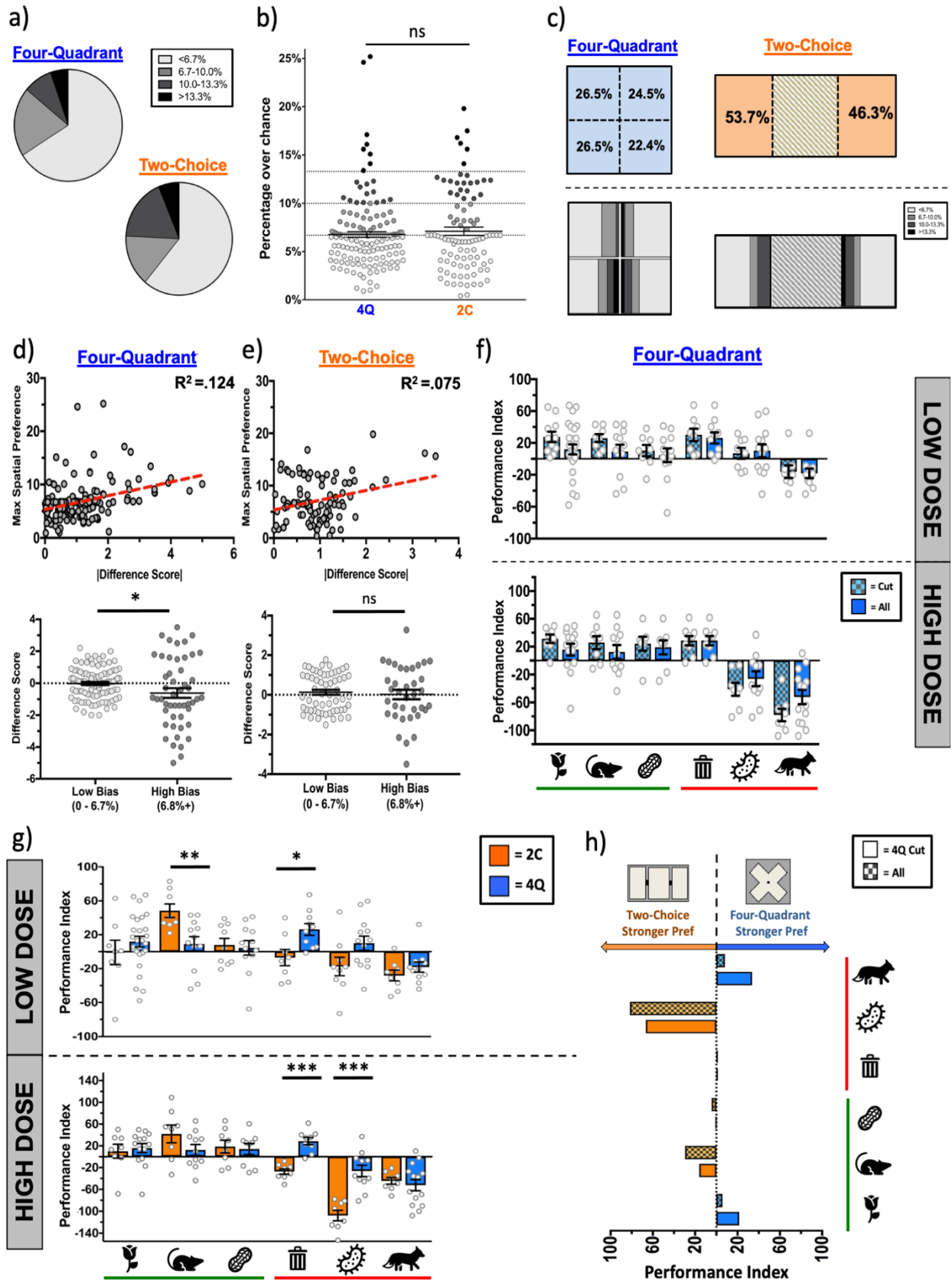
The Four-Quadrant test employs a different tactic, using a pre-defined cutoff to identify animals with low, "acceptable" levels of spatial bias and excluding all animals above the threshold<sup>17</sup>. This method is interesting, as it treats spatial bias not as a subtractable variable but as an indicator of behavioral abnormality. If and how spatial bias interacts with olfactory valence is not understood. Data from Figure 2.4d suggests a potential relationship between the two variables. Interestingly, this relationship appears to be stronger in the Four-Quadrant test, suggesting that assay type can affect sources of data abnormality and so drive inter- and intra-assay variability. Understanding the relationship between assay and behavioral variability is essential for strengthening data through proper methods or uncovering insurmountable assay issues. To start, we assessed the distribution of spatial bias across apparatuses – habituation (odorless) trials were binned for "low", "medium", "strong" or "extreme" levels of bias or plotted without processing. Spatial bias was not significantly different between apparatuses (Figure 2.5a-b), suggesting that its existence is not assay-specific. Spatial bias data appears as

one continuous population in both apparatuses (Figure 2.5b) and does not appear to be stronger in any one location in the apparatuses, indicating that bias is not occurring from an external source (Figure 2.5c). Instead, spatial bias occurs on a continuum and does so similarly across apparatuses.

Is spatial bias a marker of behavioral abnormality in either assay? To assess the relationship between spatial bias and odorant valence, bias was plotted against difference score. In the Two-Choice assay, spatial bias and difference score are not correlated (Figure 2.5e, above), and difference scores are not different between animals above and below the spatial bias cutoff (Figure 2.5e, below). In contrast, in the Four-Quadrant apparatus spatial bias and difference score are significantly correlated (Figure 2.5d, above), with higher spatial bias leading to lower difference scores (Figure 2.5d, below). This suggests that a relationship between spatial bias and odorant valence exists, yet it manifests in an apparatus-specific manner. To further explore this relationship, data including (“All”) and excluding (“Cut”) animals outside of the spatial bias cutoff were compared for each apparatus. A clear decrease in Four-Quadrant valence in most odorant categories occurs when including spatially-biased animals (Figure 2.5f), while no such trend is seen using Two-Choice animals (data not shown). Including spatially-biased animals lowers Four-Quadrant valence while leaving Two-Choice valence largely unaffected (Figure 2.5g-h), solidifying spatial bias’s differing significance in each assay. Overall, these results reveal that assay choice can affect intra-assay as well as inter-assay variability.

**Figure 2.5. Relationship between spatial bias and odorant valence varies between assays.**

**a-b**, For each animal, the strongest spatial bias during habituation is recorded and compared between assays. A depicts total data plotted in pie charts. Chi-square test,  $p=.074$ . B depicts raw values. Mann-Whitney U Test,  $p=.908$ . **c**, For each animal, quadrant identity (top) or strength (bottom) of peak habituation spatial bias is plotted and compared within test. Neither percentage (Four-Quadrant: Chi-square test,  $p=.856$ ; Two-Choice: Binomial Test,  $p=.538$ ) nor binned bias strength (Four-Quadrant: Chi-square test,  $p=.249$ ; Two-Choice: Chi-square test,  $p=.422$ ) significantly differs between quadrants. **d-e**, Assessment of apparatus-specific spatial bias-odorant valence relationship. Top, correlation between max spatial bias and absolute difference score within each apparatus. Left, Four-Quadrant: Spearman's Rho,  $R^2=.124$ ,  $p<.0001$ . Right, Two-Choice: Spearman's Rho,  $R^2=.075$ ,  $p=.503$ . Bottom, Comparison of difference scores from low and high spatial bias trials. Left, Four-Quadrant: Mann-Whitney U test,  $p=.031$ . Right, Two-Choice: Mann-Whitney U test,  $p=.909$ .  $N=149$  (Four-Quadrant), 94 (Two-Choice). **f**, Comparison between Four-Quadrant odorant valence determined with and without use of  $<6.7\%$  spatial bias cutoff ("Cut" and "All", respectively). All groups were compared with unpaired t-tests unless otherwise stated. P-values are: Low Dose (Upper) - 2PE ( $p=.147$ ), FU ( $p=.154$ ), PO ( $p=.636$ ), 2MB ( $p=.723$ ), ISO ( $p=.798$ ), TMT ( $p=.840$ ). High Dose (Lower) - 2PE (Mann-Whitney U Test,  $p=.231$ ), FU ( $p=.357$ ), PO ( $p=.727$ ), 2MB ( $p>.999$ ), ISO ( $p=.324$ ), TMT ( $p=.105$ ). **g**, Comparison between Two-Choice and Four-Quadrant Assay results, without application of a spatial bias cutoff. All groups were compared with unpaired t-tests unless otherwise stated. P-values are: Low Dose (Upper) - 2PE ( $p=.362$ ), FU ( $p=.005$ ), PO ( $p=.783$ ), 2MB ( $p=.011$ ), ISO ( $p=.054$ ), TMT ( $p=.283$ ). High Dose (Lower) - 2PE (Mann-Whitney U Test,  $p=.868$ ), FU ( $p=.123$ ), PO ( $p=.774$ ), 2MB ( $p<.0001$ ), ISO ( $p<.0001$ ), TMT ( $p=.588$ ). **h**, Summary of valence strength data in G and 2.2a.



## **2.5 Raw investigation time does not reflect inter-odor differences or valence conclusions**

In an optimal behavioral assay, measures should be logical and behavioral differences should be readily apparent. However, few labs use raw investigation time to measure odorant responses, instead filtering valence results through several normalization steps that turn unimpressive raw data into significant differences<sup>17,18,20-26</sup>. If olfactory valence measures are robust, behavioral differences should be apparent within the raw data. Innate olfactory valence tests are also quite long, ranging from three to twenty-five minutes<sup>18,20-25</sup>. Given that innate behavioral responses are automatic and do not require memory access<sup>12-14</sup>, they likely occur much more rapidly than the typical valence assay time – we expect that a robust measure should reflect the quick nature of innate behavioral responses. In order to determine if raw data reveals strong and swift reactions, raw time spent in the Two-Choice or Four-Quadrant odorant chamber was compared across odorants for several time cutoffs. Time spans analyzed include short cutoffs (30 seconds, one minute), and longer times (three, five, and 12 minutes). Most odorants and doses are attractive within the first minute regardless of assay (Figure 2.6a-b, upper), even in odorants with reported<sup>17,18,20,23,26,28,29</sup> and personally-quantified negative or neutral valence. This indicates that valence is not accurately captured in the beginning of odorant response assays, and that place preference assay data does not match anticipated innate behavior timing. As tested time spans lengthen, investigation times move towards or below baseline (neutral valence) across all odorants, with few odors moving significantly below baseline (becoming aversive) (Figure 2.6a-b, lower). Even at the longest time spans assayed, raw data did not fully capture odorant valence in any assay or dose. This indicates that raw investigation time is only able to accurately capture the most robust behavioral differences (e.g., female urine), and so data typically requires normalization to reach significance. Differences between odorants were also compared to assess raw investigation data's ability to accurately portray inter-odorant relationships (Figure 2.6c-d).



Throughout the test, response to nearly every odorant is indistinguishable across dose and assay. As in Figure 2.6a-b, only the odorants with the strongest behavioral responses (female urine and ISO in the Two-Choice Test; female urine and TMT in the Four-Quadrant test) can be detected, further validating that only the most extreme differences can be distinguished using raw investigation time. Overall, this data calls into question the validity of the entire position-as-reaction hypothesis upon which current assays are based. A measure that is heavily variable within and between assays, does not function in the expected timeframe, and requires transformation to reach significance is not suitable for discovery. Overall, these data suggest that another measure is needed to improve upon the flawed one currently in use, and so allow fruitful research of innate olfactory valence to continue.

**Figure 2.6. Raw time does not reflect behavioral differences of innate olfactory valence assays.**

**a**, Raw time spent in the odorant quadrant in low dose (light orange) and high dose (dark orange) tests of the Two-Choice assay. Dotted line represents chance value, as determined by the size of quadrant and the length of time assayed. values were compared versus this chance percentage by Binomial test. P-values are as follows:

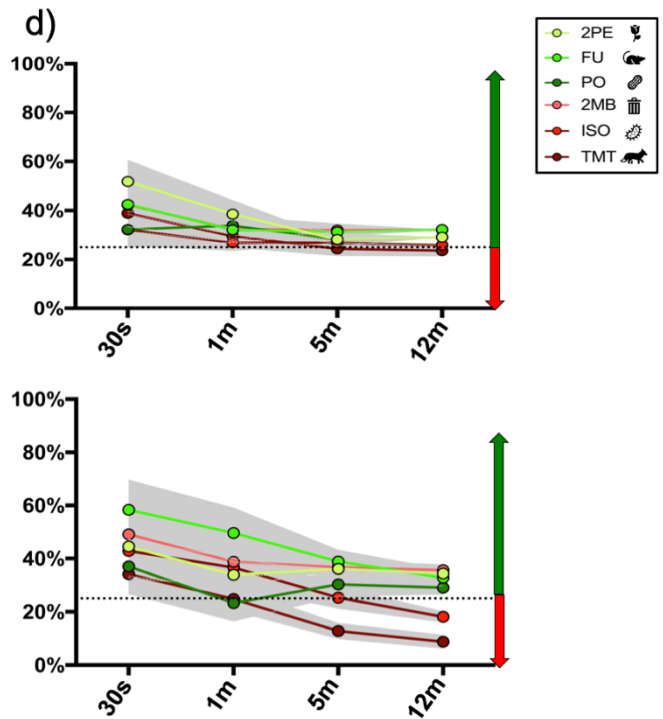
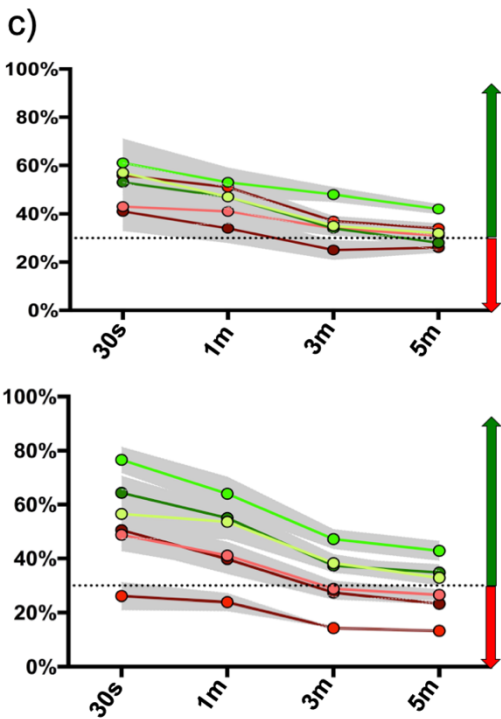
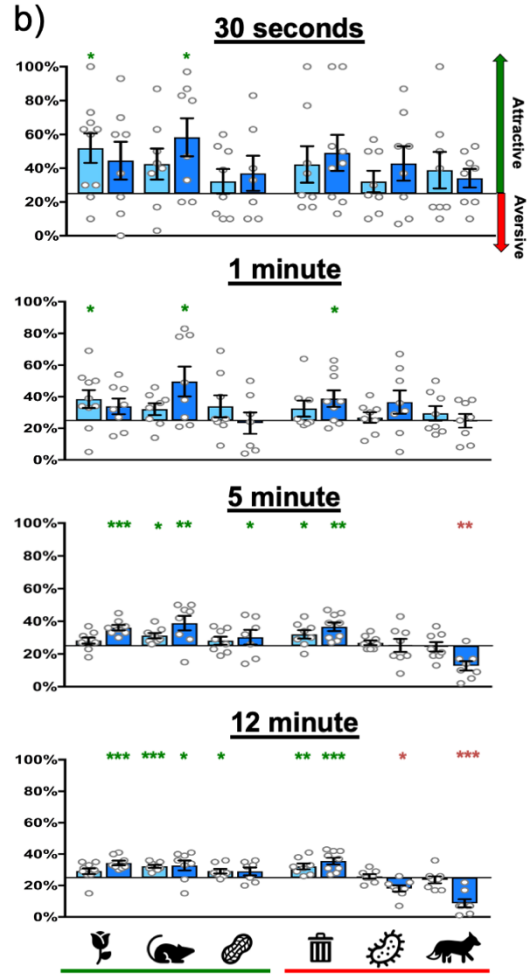
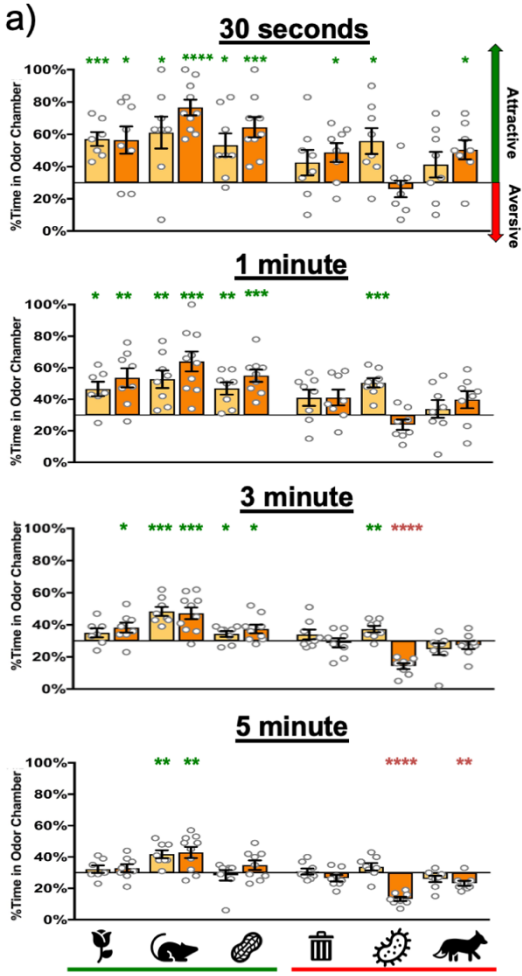
30 Seconds (upper): Low Dose - 2PE (p=.0007), FU (p=.016), PO (p=.014), 2MB (p=.157), ISO (p=.015), TMT (p=.199). High Dose - 2PE (p=.017), FU (p<.0001), PO (p=.0006), 2MB (p=.015), ISO (p=.473), TMT (p=.011). One minute (upper middle): Low Dose - 2PE (p=.011), FU (p=.005), PO (p=.003), 2MB (p=.07), ISO (p=.0002), TMT (p=.515). High Dose - 2PE (p=.006), FU (p=.0004), PO (p=.0002), 2MB (p=.063), ISO (p=.106), TMT (p=.114). Three minutes (lower middle): Low Dose - 2PE (p=.128), FU (p=.0003), PO (p=.049), 2MB (p=.233), ISO (p=.009), TMT (p=.196). High Dose - 2PE (p=.030), FU (p=.001), PO (p=.025), 2MB (p=.680), ISO (p<.0001), TMT (p=.330). Five minutes (bottom): Low Dose - 2PE (p=.377), FU (p=.0021), PO (p=.807), 2MB (p=.706), ISO (p=.158), TMT (p=.085). High Dose - 2PE (p=.291), FU (p=.006), PO (p=.15), 2MB (p=.128), ISO (p<.0001), TMT (p=.004).

**b**, Raw time spent in the odorant quadrant in low dose (light blue) and high dose (dark blue) tests of the Four-Quadrant assay. Dotted line represents chance value, as determined by the size of quadrant and the length of time assayed. values were compared versus this chance percentage by Binomial test. P-values are as follows:

30 Seconds (upper): Low Dose - 2PE (p=.013), FU (p=.098), PO (p=.360), 2MB (p=.155), ISO (p=.300), TMT (p=.240). High Dose - 2PE (p=.120), FU (p=.020), PO (p=.290), 2MB (p=.053), ISO (p=.120), TMT (p=.140). One minute (upper middle): Low Dose - 2PE (p=.041), FU (p=.096), PO (p=.809), 2MB (p=.184), ISO (p=.590), TMT (p=.360). High Dose - 2PE (p=.116), FU (p=.040), PO (p=.809), 2MB (p=.031), ISO (p=.158), TMT (p=.956). Five minutes (lower middle): Low Dose - 2PE (p=.118), FU (p=.016), PO (p=.246), 2MB (p=.030), ISO (p=.239), TMT (p=.884). High Dose - 2PE (p=.0003), FU (p=.006), PO (p=.284), 2MB (p=.002), ISO (p=.951), TMT (p=.004). Twelve minutes (bottom): Low Dose - 2PE (p=.050), FU (p=.0001), PO (p=.028), 2MB (p=.006), ISO (p=.539), TMT (p=.554). High Dose - 2PE (p=.0004), FU (p=.045), PO (p=.156), 2MB (p=.001), ISO (p=.011), TMT (p=.0004).

**c**, Condensed low dose (upper) and high dose (lower) raw data for Two-Choice assay. Colors indicate odorant (see key in upper right), lines indicate average time spent in odorant quadrant, and grey indicates standard deviation of time spent in odorant quadrant.

**d**, Condensed low dose (upper) and high dose (lower) raw data for Four-Quadrant assay. Colors indicate odorant (see key in upper right), lines indicate average time spent in odorant quadrant, and grey indicates standard deviation of time spent in odorant quadrant.



## DISCUSSION

Innate olfactory valence is considered a fundamental attribute of some and perhaps all odorants<sup>12,13,17,18,20-26</sup>, so high-throughput and rigorous assays are needed to assess valence of the potentially millions of odorants that exist. Here, we show that the current innate olfactory valence assays and the position-as-reaction hypothesis they rely on are inherently flawed. Apparatus and test have a substantial effect on resulting data, impacting measured valence strength, direction, and time. This indicates that assay and apparatus standardization is critical for interpretable olfactory valence data moving forward. Yet, data also showed high intra-assay variability despite identical housing, handling, and testing conditions for animals, suggesting deeper issues. While behavioral data is often variable, the level seen shows that technical and/or biological factors are influencing assay outcome. In all innate olfactory valence assays, effects rely on transformation to appear robust and take minutes to appear, further suggesting that how researchers assess valence needs to be revised. Indeed, though innate olfactory responses likely occur in seconds<sup>12-14</sup>, mouse investigation of aversive and attractive stimuli remains similar for nearly a minute. It must be noted that biological factors such as internal state may also contribute to data variability by affecting behavior, odorant perception, or even odorant sensation<sup>34-36</sup>. However, our data shows that technical factors are apparent in innate olfactory assays, and the test form itself must be changed before such interfering biological factors and valence as a whole can be effectively researched.

### *The effects of apparatuses on behavioral assays*

Behavioral apparatus shape and rough size are typically standardized to maximally equalize both subject and stimuli, particularly where tests involve free movement. In studies of arena shape's effect on behavior, global changes to shape have been shown to affect both rodent

navigation paths<sup>37,38</sup> and interaction with objects within the arena<sup>39</sup>. Arena size can also affect animal behavior, with a greater space leading to different, anxiety-based behavior in mice<sup>30,31</sup>. As the innate olfactory valence apparatuses used by the field have unstandardized shapes and sizes, this likely contributes to the inter-assay variability we have shown.

Different arena size and shape likely also affects odorant dynamics. Odorant plume movement is turbulent, with one location's odorant concentration varying between seconds and affected by the environment<sup>40,41</sup>. Though the Four-Quadrant and PROBES setups exert more control over odorant application than the traditional Two-Chamber apparatus, odorant movement is either not tested (Four-Quadrant<sup>17</sup>) or tested with only a handful of odorants (PROBES<sup>26</sup>). Further, PROBES odorant tests indicate that odorant dynamics fluctuate with odorant identity, even in a controlled environment. Odorant movement throughout arenas and tubing, and the contribution of molecular structure to that movement, has been ignored in innate olfactory valence studies. Indeed, the ability to visualize odorant plumes was generated merely five years ago<sup>41</sup> and is currently only used in odorant navigation research<sup>41-43</sup>. Until innate odorant valence studies are willing and able to adopt similar techniques, odorant delivery should be normalized as much as possible. This may look like a head-fixed apparatus<sup>44</sup> (stressful but structured), or an odorant applicator such as an olfactometer (preferred but more complicated)<sup>44,45</sup>. An additional benefit to direct odorant application would be equal and precisely-timed odorant sampling, which is impossible to control in all current assay setups aside from PROBES.

### ***Flaws with the position-as-reaction hypothesis in odorant tests, and potential alternatives***

The typical innate olfactory valence assay is at least five minutes long and behavioral effects take minutes to manifest, raising logical and technical concerns. The deepest flaw with innate olfactory valence tests' long assay times is that they are not on a neural timescale.

Olfactory percepts take seconds to generate<sup>46-48</sup> as do automatic reactions to stimuli<sup>12-14</sup>. Why would an innate response to an odorant take minutes to manifest? While mouse movement may add some seconds to the expected time of a strong response, this cannot account for the similarity seen between positively and negatively-valenced odors within one minute of stimulus contact. Even if long-term effects are informative, a neural timescale is necessary to meaningfully connect odorant valence to olfactory coding. The long time-scale of current odorant valence assays suggests that position is not an accurate or fruitful measure. New assays with quicker timescales are needed to push such studies forward. Shortening assays may also lower data variability, as mice become less active and habituate to odorants over longer periods of time<sup>49,50</sup>. We note that, while place preference assays are not optimal for innate odorant valence research, they remain useful for studies of learned behaviors (e.g. drug-seeking)<sup>10,32,33</sup>.

Study of more fine-grained and immediate physical reactions to stimuli, as opposed to mere proximity, is now becoming possible and may provide a path forward. Behavioral responses such as risk assessment<sup>25</sup> and freezing<sup>51</sup> have been used to describe ethologically-relevant pheromonal stimuli in past studies, though this method is subjective. New tools such as MoSeq<sup>52</sup> allow for unbiased, computer-generated identification of repeated behavioral “modules”. In addition, animal body position analysis, which allows for estimation of relative limb, torso, head, and tail position, may provide a useful blend of behavioral definitions and unbiased methods (e.g., tail position after odorant sampling). One intriguing study allows tracking of mouse facial reactions to stimuli<sup>54</sup>, which are well-known to reflect pain state<sup>55</sup> and are reported to convey various emotions such as disgust, fear, and pleasure<sup>54</sup>. If paired with controlled odorant application, body and facial expressions may provide better temporal and behavioral resolution than former innate olfactory valence measures.

Despite the critical technical concerns described here, the driving question still remains: can we use innate olfactory valence to group odorants? The concept of widespread innate odorant valence is a hypothesis that is currently being questioned. Odorants that elicit automatic and well-documented responses are often pheromone-adjacent, coming from conspecific and predator sources<sup>12,13,18,20,22-25</sup>. It is possible that most odorants do not elicit an automatic response, but instead are assigned meaning after interaction. Alternatively, global innate odorant valence may be so plastic that measurement is incredibly difficult. Odorant responses in the brain are malleable over time<sup>56</sup>, vary depending on the olfactory context of presentation<sup>20,57</sup>, and are modulated by early-life experience<sup>58</sup> - olfactory responses may also be affected by state as seen in the pheromone system<sup>59,60</sup>. To differentiate between these possibilities, we first must find a robust assay for future investigation. Generating new methods of assaying responses to odorants will be informative and are necessary to understanding how the brain makes sense of the olfactory world around us.

## MATERIALS AND METHODS

### Mice

All mice were c57BL/6J, 9-11 weeks, and males. Mice were group-housed with a PVC tube, handled in and out of tubes for three days prior to testing, and single-housed the day of testing. Mice were habituated in the assay room with water bottles and food for three to four hours prior to testing. Mice were tested between 6pm-2am. Mice were only tested once in the Four-Quadrant and Two-Choice test, to ensure minimal impacts of experience on data. Mice were tested multiple times in the PROBES assay, as the assay was extremely brief – these mice were additionally habituated to handling and red light between testing days. Between three and six mice were tested within a single testing session. All tests were done under red light. Mice were transferred into testing arenas by PVC tube to ensure minimal stress. Six to eight mice were tested per odorant dose, identity, and assay.

### Odorants

Odorants and doses were chosen based on previous publications. 2PE, 2MB, and ISO were purchased (Sigma) and used within one year. Unrefined, gourmet peanut oil was bought from the grocery store and used within one year. TMT of 97% purity was purchased (BioSRQ) and stored at 4°C until use. Female urine was collected fresh, combined from three BalbC females, and stored on ice until use. Odorant doses are chosen based on previous publications or personal dose-response curves (data not shown). Low doses consisted of 1µL for all odorants, while high doses consisted of 5µL (TMT), 20µL (PO, ISO, and 2PE), or 50µL (female urine and 2MB). Odorants were transferred and stored in clean sandwich bags outside of the testing room. All odorant vials, pipette tips, and Kimwipes (Kimtech) were double-sealed in sandwich bags outside of the testing room after use. Each apparatus was cleaned with 70% ethanol and a



deodorizer and flushed with clean air for 15 minutes between experiments. All tests that occurred within one day used the same odorant.

### **Four-Quadrant Test**

The Four-Quadrant test was built as previously described<sup>17</sup> and run as previously described with minor modifications. Briefly, mice were placed into the testing apparatus as close to the center as possible. Mice were allowed to explore the air-filled chamber for 15 minutes – ten minutes of this habituation period was recorded by mounted overhead camera to later assess spatial bias. Next, odorant was applied to a Kimwipe (Kimtech Sciences) and placed into an odorant vial connected to air flow. Mice were given 15 minutes to explore the chamber, and exploration was recorded. To note, we kept the first two minutes of testing, which differs than what was previously described. Only mice with spatial bias less than 6.7% were included in standard comparisons (Figure 2.1-2.3, 2.6), but all mice were included in certain tests (Figure 2.4, 2.5). Note that this percentage is slightly changed from the published cutoff of 5.1%.

### **Two-Choice Test**

The Two-Choice test was designed to ensure minimal odorant diffusion between chambers. The test apparatus is a 27.5” by 16.5” polypropylene chamber with three compartments, one slightly larger neutral compartment in the center and two equally-sized odorant compartments at left and right. In an attempt to prevent odorant movement out of odorant compartments, each is maximally enclosed with only a small hole connecting to the central chamber, and small electronic fans that provided a slight, quiet vacuum pull were connected to each odorant chamber. A lid was placed on the apparatus to ensure minimal odorant movement up and out of the chamber. Clean filter paper was taped in both odorant compartments prior to habituation – paper was placed ten inches high to avoid animals moving the odorant

source. Assays were filmed by mounted overhead camera. Mice were placed in the central chamber and given 15 minutes to habituate, and the last five minutes were used to establish spatial bias. Equal amounts of odorant and water control were pipetted simultaneously onto opposite odorant chambers' filter papers. Odorant chamber location was pseudo-randomized, with location typically alternating expect for when animals exhibited visible spatial biases during habituation; if strong spatial biases were detected by eye, odorant chamber location was chosen based on odorant identity (opposite of preferred chamber if attractive, same as preferred chamber if aversive). All mice were included in data analysis.

### **PROBES Test**

The PROBES was built and run as previously described<sup>17</sup> with some modifications. Briefly, PROBES was run with a simple, self-generated code that allowed for alternating between control (mineral oil) and odorant exposure. Odorants were placed in odorant vials filled with mineral oil to allow for a 5mL headspace. Odorants were rapidly connected to and removed from air flow using the assay code. Mice were placed into the PROBES arena on the assay day as close to the center as possible. Mice were allowed to explore the air-filled chamber for five minute, then were run through a testing program where mineral oil control alternated with odorant. The testing program was as follows:

- 1) (20 seconds air, 20 seconds mineral oil) x 4.
- 2) (20 seconds mineral oil, 20 seconds low-dose odor) x 4.
- 3) (20 seconds mineral oil, 20 seconds high-dose odor) x 4.
- 4) Repeat steps 1-3.

Interaction with the odorant was detected by beam break. The infrared beam was placed in the nose cone near to the odorant source, such that nose pokes led to beam breaks, and any infrared

beam interruption was detected by the assay code. Mice were tested every-other day for three days, with attractive odorants tested first to minimize experience effects. Testing groups were as follows: PO, FU, ISO (group 1); 2PE, 2MB, TMT (group 2). All mice were included in data analysis.

### **Measures and Statistics**

For all behavioral analysis, Ethovision software was used to create representative heatmaps (Figure 2.1) and extract measures from videos (Figure 2.2-2.6). For Figure 2.2, each assay was converted into Performance Index for comparison. Performance Index was calculated as previously described<sup>17</sup> with modifications, by using the following formulas:

$$\frac{(((\text{Percentage time in odorant quadrant during assay}) - (\text{chance percentage in odorant quadrant}))/ .3)) * 100 = \text{Odorant Performance Index.}}$$

$$\frac{(((\text{Percentage time in odorant quadrant during habituation}) - (\text{chance percentage in odorant quadrant}))/ .3)) * 100 = \text{Habituation Performance Index.}}$$

$$\text{Odorant Performance Index} - \text{Habituation Performance Index} = \underline{\text{Performance Index.}}$$

Chance percentages were assessed by determining the size of the arena. We note that the scales between the Four-Quadrant and Two-Choice/PROBES tests are slightly different as they have a 25% versus 30% odor quadrant size respectively, which makes the *percentage of time in odor quadrant* for Four Quadrant data slightly mismatched (off by ~+16PI); however, as linearizing the data to equalize *percentage of time in odor quadrant* data would then cause a mismatch in the *percentage of time in odor quadrant difference from chance* data, Performance Index was used for comparison as stated above without further transformation. For PROBES, combined mineral

oil data across the first three trials were used as habituation, and combined odorant exposure across the first three trials was used for odorant data.

Difference score (Figure 2.4-2.5) was generated by assessing z-score, with mean and standard deviation reassessed after tested datapoint removal. Percent difference from chance (Figure 2.3) was calculated by determining the chance percentage time in odorant quadrant within each time (Four-Quadrant, Two-Choice) or trial (PROBES) bin, then determining how many mice were above the chance threshold. This number of mice over chance was converted into a percentage (out of total mice) and plotted. For PROBES, only the first three odorant trials are shown in Figure 2.3. All measures other than difference score were calculated using the habituation period (Figure 2.4). Latency was determined as the time difference between the start of habituation trial and the animal entering into the odorant quadrant. Average speed was determined by Ethovision and measured in centimeters per seconds. Percent immobility was determined by Ethovision and measured as percentage of habituation trial. Average distance to odorant was determined by Ethovision and measured in centimeters. Max habituation preference was defined as the strongest bias exhibited for any quadrant (Four-Quadrant), chamber (Two-Chamber), or side of odorant stream (PROBES). Odorant quadrant preference was defined as the bias for the odorant quadrant, chamber, or stream. For raw time analysis (Figure 2.6), times were adjusted so quantification began when animals entered into the odorant quadrant.

All data is represented as mean +/- standard error of mean (S.E.M.) unless otherwise stated. All statistics were completed using GraphPad Prism 6.0 software. Unless otherwise stated, the Shapiro-Wilkinson normality test was used to determine the nature of the data's distribution. For normally-distributed comparisons, a student's t-test (2 groups) or one-way ANOVA (3 groups) was used to evaluate significance. For non-normally distributed

comparisons, the non-parametric Mann-Whitney U test (2 groups) or Kruskal-Wallis test (3 groups) was used to evaluate significance. For comparisons to an expected value, the Binomial test (2 groups) or Chi-Square test (3+ groups) was used. In Figure 2.5, one outlier was removed from each dataset using Grubbs Method. Spearman's Rho was used to assess significance of all correlations.

Chapter 2, in part, is a reprint of material that is currently being prepared for publication. Koblesky, Norah; Taylor; Sandy; Gutierrez, Zachary; Stowers, Lisa. "Sources of Variation in Innate Olfactory Valence Tests". The dissertation author was the primary investigator and author of this paper.

## REFERENCES

1. Squire, L., Berg, D., Bloom, F. E., du Lac, S., Ghosh, A., & Spitzer, N. C. (2013). *Fundamental Neuroscience*, Fourth Edition. Academic Press.
2. Arctander, S. (1960). *Perfume and Flavor Materials of Natural Origin*.
3. Poivet, E., Peterlin, Z., Tahirova, N., Xu, L., Altomare, C., Paria, A., Zou, D. J., & Firestein, S. (2016). Applying medicinal chemistry strategies to understand odorant discrimination. *Nature communications*, 7, 11157.
4. Keller, A., Gerkin, R. C., Guan, Y., Dhurandhar, A., Turu, G., Szalai, B., Mainland, J. D., Ihara, Y., Yu, C. W., Wolfinger, R., Vens, C., Schietgat, L., De Grave, K., Norel, R., DREAM Olfaction Prediction Consortium, Stolovitzky, G., Cecchi, G. A., Vosshall, L. B., & Meyer, P. (2017). Predicting human olfactory perception from chemical features of odor molecules. *Science (New York, N.Y.)*, 355(6327), 820–826.
5. Schaffer, E. S., Stettler, D. D., Kato, D., Choi, G. B., Axel, R., & Abbott, L. F. (2018). Odor Perception on the Two Sides of the Brain: Consistency Despite Randomness. *Neuron*, 98(4), 736–742.
6. Pashkovski, S. L., Iurilli, G., Brann, D., Chicharro, D., Drummey, K., Franks, K. M., Panzeri, S., & Datta, S. R. (2020). Structure and flexibility in cortical representations of odour space. *Nature*, 583(7815), 253–258.
7. Dravnieks, A. (1985). *Atlas of Odor Character Profiles* ASTM International, 354 pp
8. Chastrette M., Elmouaffek A., P. Sauvegrain P. (1988). A multidimensional statistical study of similarities between 74 notes used in perfumery. *Chem. Senses*, 13, 295–305.
9. Frijda, N. (1986). *The Emotions*. Cambridge(UK): Cambridge University Press. p. 207
10. Prus, A. J., James, J. R., & Rosecrans, J. A. (2009). Conditioned Place Preference. In J. J. Buccafusco (Ed.), *Methods of Behavior Analysis in Neuroscience*. (2nd ed.). CRC Press/Taylor & Francis.
11. Tzschentke T. M. (1998). Measuring reward with the conditioned place preference paradigm: a comprehensive review of drug effects, recent progress and new issues. *Progress in neurobiology*, 56(6), 613–672.
12. Li, Q., & Liberles, S. D. (2015). Aversion and attraction through olfaction. *Current biology : CB*, 25(3), R120–R129.
13. Stowers, L., & Kuo, T. H. (2015). Mammalian pheromones: emerging properties and mechanisms of detection. *Current opinion in neurobiology*, 34, 103–109.

14. Blanchard, D. C., & Blanchard, R. J. (1972). Innate and conditioned reactions to threat in rats with amygdaloid lesions. *Journal of comparative and physiological psychology*, *81*(2), 281–290.
15. Slotnick B. M. (1985). Olfactory discrimination in rats with anterior amygdala lesions. *Behavioral neuroscience*, *99*(5), 956–963
16. Sosulski, D. L., Bloom, M. L., Cutforth, T., Axel, R., & Datta, S. R. (2011). Distinct representations of olfactory information in different cortical centres. *Nature*, *472*(7342), 213–216.
17. Root, C. M., Denny, C. A., Hen, R., & Axel, R. (2014). The participation of cortical amygdala in innate, odour-driven behaviour. *Nature*, *515*(7526), 269–273.
18. Kobayakawa, K., Kobayakawa, R., Matsumoto, H., Oka, Y., Imai, T., Ikawa, M., Okabe, M., Ikeda, T., Itohara, S., Kikusui, T., Mori, K., & Sakano, H. (2007). Innate versus learned odour processing in the mouse olfactory bulb. *Nature*, *450*(7169), 503–508.
19. Iurilli, G., & Datta, S. R. (2017). Population Coding in an Innately Relevant Olfactory Area. *Neuron*, *93*(5), 1180–1197.
20. Saraiva, L. R., Kondoh, K., Ye, X., Yoon, K. H., Hernandez, M., & Buck, L. B. (2016). Combinatorial effects of odorants on mouse behavior. *Proceedings of the National Academy of Sciences of the United States of America*, *113*(23), E3300–E3306.
21. Dewan, A., Pacifico, R., Zhan, R., Rinberg, D., & Bozza, T. (2013). Non-redundant coding of aversive odours in the main olfactory pathway. *Nature*, *497*(7450), 486–489.
22. Pérez-Gómez, A., Bleymehl, K., Stein, B., Pyrski, M., Birnbaumer, L., Munger, S. D., Leinders-Zufall, T., Zufall, F., & Chamero, P. (2015). Innate Predator Odor Aversion Driven by Parallel Olfactory Subsystems that Converge in the Ventromedial Hypothalamus. *Current biology : CB*, *25*(10), 1340–1346.
23. Ferrero, D. M., Lemon, J. K., Fluegge, D., Pashkovski, S. L., Korzan, W. J., Datta, S. R., Spehr, M., Fendt, M., & Liberles, S. D. (2011). Detection and avoidance of a carnivore odor by prey. *Proceedings of the National Academy of Sciences of the United States of America*, *108*(27), 11235–11240.
24. Li, Q., Korzan, W. J., Ferrero, D. M., Chang, R. B., Roy, D. S., Buchi, M., Lemon, J. K., Kaur, A. W., Stowers, L., Fendt, M., & Liberles, S. D. (2013). Synchronous evolution of an odor biosynthesis pathway and behavioral response. *Current biology : CB*, *23*(1), 11–20.
25. Papes, F., Logan, D. W., & Stowers, L. (2010). The vomeronasal organ mediates interspecies defensive behaviors through detection of protein pheromone homologs. *Cell*, *141*(4), 692–703.

26. Qiu, Q., Scott, A., Scheerer, H., Sapkota, N., Lee, D. K., Ma, L., & Yu, C. R. (2014). Automated analyses of innate olfactory behaviors in rodents. *PloS one*, *9*(4), e93468.
27. Nyby, J., Wysocki, C. J., Whitney, G., & Dizinno, G. (1977). Pheromonal regulation of male mouse ultrasonic courtship (*Mus musculus*). *Animal behaviour*, *25*(2), 333–341.
28. Wallace, K. J., & Rosen, J. B. (2000). Predator odor as an unconditioned fear stimulus in rats: elicitation of freezing by trimethylthiazoline, a component of fox feces. *Behavioral neuroscience*, *114*(5), 912–922.
29. Rosen, J. B., Asok, A., & Chakraborty, T. (2015). The smell of fear: innate threat of 2,5-dihydro-2,4,5-trimethylthiazoline, a single molecule component of a predator odor. *Frontiers in neuroscience*, *9*, 292.
30. Denenberg V. H. (1969). Open-field behavior in the rat: what does it mean?. *Annals of the New York Academy of Sciences*, *159*(3), 852–859.
31. Archer J. (1973). Tests for emotionality in rats and mice: a review. *Animal behaviour*, *21*(2), 205–235.
32. Simkevich, M. J., Campbell, R. R., & White, A. O. (2020). Examining Cocaine Conditioning Place Preference in Mice. *Bio-protocol*, *10*(8), e3595.
33. Cunningham, C. L., & Shields, C. N. (2018). Effects of multi-modal cues on conditioned place preference in C57BL/6J and DBA/2J mice. *Psychopharmacology*, *235*(12), 3535–3543.
34. Stowers, L., & Liberles, S. D. (2016). State-dependent responses to sex pheromones in mouse. *Current opinion in neurobiology*, *38*, 74–79.
35. Tan, S., & Stowers, L. (2020). Bespoke behavior: mechanisms that modulate pheromone-triggered behavior. *Current opinion in neurobiology*, *64*, 143–150.
36. McIntyre, J. C., Thiebaud, N., McGann, J. P., Komiyama, T., & Rothermel, M. (2017). Neuromodulation in Chemosensory Pathways. *Chemical senses*, *42*(5), 375–379.
37. Ben-Yehoshua, D., Yaski, O., & Eilam, D. (2011). Spatial behavior: the impact of global and local geometry. *Animal cognition*, *14*(3), 341–350.
38. Yaski, O., Portugali, J., & Eilam, D. (2011). Arena geometry and path shape: when rats travel in straight or in circuitous paths? *Behavioural brain research*, *225*(2), 449–454.
39. Kalueff, A. V., Keisala, T., Minasyan, A., Kuuslahti, M., & Tuohimaa, P. (2006). Temporal stability of novelty exploration in mice exposed to different open field tests. *Behavioural processes*, *72*(1), 104–112.



40. Pannunzi, M., & Nowotny, T. (2019). Odor Stimuli: Not Just Chemical Identity. *Frontiers in physiology*, *10*, 1428.
41. Connor, E.G., McHugh, M.K. & Crimaldi, J.P. (2018). Quantification of airborne odor plumes using planar laser-induced fluorescence. *Exp Fluids* *59*, 137.
42. Gumaste, A., Coronas-Samano, G., Hengeniuss, J., Axman, R., Connor, E. G., Baker, K. L., Ermentrout, B., Crimaldi, J. P., & Verhagen, J. V. (2020). A Comparison between Mouse, *In Silico*, and Robot Odor Plume Navigation Reveals Advantages of Mouse Odor Tracking. *eNeuro*, *7*(1), ENEURO.0212-19.2019.
43. Victor, J. D., Boie, S. D., Connor, E. G., Crimaldi, J. P., Ermentrout, G. B., & Nagel, K. I. (2019). Olfactory Navigation and the Receptor Nonlinearity. *The Journal of neuroscience : the official journal of the Society for Neuroscience*, *39*(19), 3713–3727.
44. Han, Z., Zhang, X., Zhu, J., Chen, Y., & Li, C. T. (2018). High-Throughput Automatic Training System for Odor-Based Learned Behaviors in Head-Fixed Mice. *Frontiers in neural circuits*, *12*, 15.
45. Findley, T. M., Wyrick, D. G., Cramer, J. L., Brown, M. A., Holcomb, B., Attey, R., Yeh, D., Monasevitch, E., Nouboussi, N., Cullen, I., Songco, J. O., King, J. F., Ahmadian, Y., & Smear, M. C. (2021). Sniff-synchronized, gradient-guided olfactory search by freely moving mice. *eLife*, *10*, e58523.
46. Smear, M., Shusterman, R., O'Connor, R., Bozza, T., & Rinberg, D. (2011). Perception of sniff phase in mouse olfaction. *Nature*, *479*(7373), 397–400.
47. Spors H, Wachowiak M, Cohen LB, Friedrich RW (2006) Temporal dynamics and latency patterns of receptor neuron input to the olfactory bulb. *J Neurosci* *26*: 1247–1259.
48. Haddad R, Lanjuin A, Madisen L, Zeng H, Murthy VN, et al. (2013) Olfactory cortical neurons read out a relative time code in the olfactory bulb. *Nat Neurosci* *16*: 949–957.
49. Arbuckle, E. P., Smith, G. D., Gomez, M. C., & Lugo, J. N. (2015). Testing for odor discrimination and habituation in mice. *Journal of visualized experiments : JoVE*, (99), e52615.
50. Linster, C., Henry, L., Kadohisa, M., & Wilson, D. A. (2007). Synaptic adaptation and odor-background segmentation. *Neurobiology of learning and memory*, *87*(3).
51. Wallace, K. J., & Rosen, J. B. (2001). Neurotoxic lesions of the lateral nucleus of the amygdala decrease conditioned fear but not unconditioned fear of a predator odor: comparison with electrolytic lesions. *The Journal of neuroscience : the official journal of the Society for Neuroscience*, *21*(10), 3619–3627.

52. Wiltschko, A. B., Johnson, M. J., Iurilli, G., Peterson, R. E., Katon, J. M., Pashkovski, S. L., Abraira, V. E., Adams, R. P., & Datta, S. R. (2015). Mapping Sub-Second Structure in Mouse Behavior. *Neuron*, *88*(6), 1121–1135.
53. Pereira, T. D., Shaevitz, J. W., & Murthy, M. (2020). Quantifying behavior to understand the brain. *Nature neuroscience*, *23*(12), 1537–1549.
54. Dolensek, N., Gehrlach, D. A., Klein, A. S., & Gogolla, N. (2020). Facial expressions of emotion states and their neuronal correlates in mice. *Science (New York, N.Y.)*, *368*(6486), 89–94.
55. Langford, D. J., Bailey, A. L., Chanda, M. L., Clarke, S. E., Drummond, T. E., Echols, S., Glick, S., Ingrao, J., Klassen-Ross, T., Lacroix-Fralish, M. L., Matsumiya, L., Sorge, R. E., Sotocinal, S. G., Tabaka, J. M., Wong, D., van den Maagdenberg, A. M., Ferrari, M. D., Craig, K. D., & Mogil, J. S. (2010). Coding of facial expressions of pain in the laboratory mouse. *Nature methods*, *7*(6), 447–449.
56. Schoonover, C. E., Ohashi, S. N., Axel, R., & Fink, A. (2021). Representational drift in primary olfactory cortex. *Nature*, *594*(7864), 541–546.
57. Qiu, Q., Wu, Y., Ma, L., & Yu, C. R. (2021). Encoding innately recognized odors via a generalized population code. *Current biology : CB*, *31*(9), 1813–1825.
58. Qiu, Q., Wu, Y., Ma, L., Xu, W., Hills, M., Jr, Ramalingam, V., & Yu, C. R. (2021). Acquisition of innate odor preference depends on spontaneous and experiential activities during critical period. *eLife*, *10*, e60546.
59. Dey, S., Chamero, P., Pru, J. K., Chien, M. S., Ibarra-Soria, X., Spencer, K. R., Logan, D. W., Matsunami, H., Peluso, J. J., & Stowers, L. (2015). Cyclic Regulation of Sensory Perception by a Female Hormone Alters Behavior. *Cell*, *161*(6), 1334–1344.
60. Nakahara, T. S., Camargo, A. P., Magalhães, P., Souza, M., Ribeiro, P. G., Martins-Netto, P. H., Carvalho, V., José, J., & Papes, F. (2020). Peripheral oxytocin injection modulates vomeronasal sensory activity and reduces pup-directed aggression in male mice. *Scientific reports*, *10*(1), 19943.